

CHARACTERIZATION OF GROUNDWATER AND SURFACE WATER  
INTERACTION IN KIRMIR STREAM USING THERMAL REMOTE SENSING  
AND IN-STREAM MEASUREMENTS

A THESIS SUBMITTED TO  
THE GRADUATE SCHOOL OF NATURAL AND APPLIED SCIENCES  
OF  
MIDDLE EAST TECHNICAL UNIVERSITY

BY

DİLGE VARLI

IN PARTIAL FULFILLMENT OF THE REQUIREMENTS  
FOR  
THE DEGREE OF MASTER OF SCIENCE  
IN  
GEOLOGICAL ENGINEERING

MAY 2016



Approval of the thesis:

**CHARACTERIZATION OF GROUNDWATER AND SURFACE WATER  
INTERACTION IN KIRMİR STREAM USING THERMAL REMOTE  
SENSING AND IN-STREAM MEASUREMENTS**

submitted by **DİLGE VARLI** in partial fulfillment of the requirements for the degree of **Master of Science in Geological Engineering Department, Middle East Technical University** by,

Prof. Dr. Gülbin Dural Ünver  
Dean, Graduate School of **Natural and Applied Sciences**

\_\_\_\_\_

Prof. Dr. Erdin Bozkurt,  
Head of Department, **Geological Engineering**

\_\_\_\_\_

Assoc. Prof. Dr. Koray K. Yılmaz,  
Supervisor, Geological Engineering Dept., METU

\_\_\_\_\_

**Examining Committee Members:**

Prof. Dr. Hasan Yazıcıgil  
Geological Engineering Dept., METU

\_\_\_\_\_

Assoc. Prof. Dr. Koray K. Yılmaz  
Geological Engineering Dept., METU

\_\_\_\_\_

Prof. Dr. M. Zeki Çamur  
Geological Engineering Dept., METU

\_\_\_\_\_

Prof. Dr. M. Lütfi Süzen  
Geological Engineering Dept., METU

\_\_\_\_\_

Prof. Dr. Mehmet Ekmekçi  
Hydrogeological Engineering Dept., Hacettepe University

\_\_\_\_\_

**Date:** 02/05/2016

**I hereby declare that all information in this document has been obtained and presented in accordance with academic rules and ethical conduct. I also declare that, as required by these rules and conduct, I have fully cited and referenced all material and results that are not original to this work.**

Name, Last name: DİLGE VARLI

Signature :



## **ABSTRACT**

### **CHARACTERIZATION OF GROUNDWATER AND SURFACE WATER INTERACTION IN KIRMİR STREAM USING THERMAL REMOTE SENSING AND IN-STREAM MEASUREMENTS**

Varlı, Dilge

M. S., Department of Geological Engineering

Supervisor: Assoc. Prof. Dr. Koray K. Yılmaz

May 2016, 163 pages

Effective management of water resources requires understanding and quantification of interaction between groundwater and surface water bodies. The exchange processes have recently received increasing attention because also they have important influences on ecological status of watersheds. The purpose of this study was to characterize the interaction between surface water - groundwater in Kirmir stream - a controlled stream nearby Kızılcahamam, Ankara, Turkey. At the first stage, stream reaches with interaction of groundwater – surface water potential were identified using geological information. Then, thermal remote sensing was utilized to further pinpoint the potential locations in which interaction could occur at a smaller scale. Nested piezometers were installed in identified locations to observe the variations in vertical hydraulic gradient over time. Discharge measurements were performed to understand the gains and losses in stream discharge. Streambed

temperature measurements were taken at two different depths for a period of time using temperature loggers to calculate the vertical fluid fluxes through the streambed at various locations. Basic water quality field parameters (temperature, electrical conductivity, total dissolved solid amount, dissolved oxygen, pH and oxidation - reduction potential) were measured. Water samples were taken from both stream and piezometers and these samples were analyzed for major anion concentrations. Chloride mass balance was performed to find the contribution of groundwater and chloride concentrations were associated with the geology of the area. This hierarchical, multi-scale methodology provided an efficient and effective way to determine the locations and the direction of groundwater and surface water exchange processes within the study area.

Keywords: Groundwater - stream interaction, in-stream measurements, thermal remote sensing, field parameters, major anion concentrations

## ÖZ

# YERALTISUYU VE YÜZEY SUYU ETKİLEŞİMİNİN KIRMİR NEHRİ BOYUNCA TERMAL UZAKTAN ALGILAMA VE NEHİR İÇİ ÖLÇÜMLER İLE BELİRLENMESİ

Varlı, Dilge

Yüksek Lisans, Jeoloji Mühendisliği

Tez Yöneticisi: Doç. Dr. Koray K. Yılmaz

Mayıs 2016, 163 Sayfa

Su kaynaklarının etkili bir şekilde yönetilmesi yeraltısuyu ve yüzey suyu arasındaki etkileşimin anlaşılması ve miktarının belirlenmesini gerektirir. Yeraltısuyu ve yüzey suyu arasındaki etkileşim havzalar üzerinde ekolojik açıdan da önemli etkilere sahip olduğu için son zamanlarda giderek artan bir önem kazanmıştır. Bu çalışmanın amacı Kızılcahamam, Ankara yakınında bulunan ve kontrol altında olan Kirmir nehri üzerinde yüzey suyu ve yeraltısuyu arasındaki etkileşimi karakterize etmektir. Kirmir nehri ve yeraltı suyu arasındaki etkileşim, su kalitesi arazi parametreleri, ana anyon derişimleri, nehir içinden ve uzaktan algılama ile alınan ölçümler kullanılarak araştırılmıştır. İlk etapta, jeolojik bilgiler kullanılarak nehrin yeraltısuyu ve yüzey suyu etkileşimine uygun kısmı saptanmış ve termal uzaktan algılama ile etkileşimin görüldüğü olası lokasyonlar küçük ölçekte belirlenmiştir. Düşey hidrolik eğimin zamanla olan değişimini gözlemleyebilmek için belirlenen potansiyel beslenim

yerlerine yan yana piezometreler yerleştirilmiştir ve nehirdeki su kazanım ve kayıplarını görebilmek için debi ölçümleri alınmıştır. Nehir yatağında farklı derinliklere yerleştirilen sıcaklık ölçerler ile düşey akımda zamanla gözlenen değişimlerin miktarı farklı likasyonlar için belirlenmiştir. Çalışma alanı boyunca sıcaklık, elektriksel iletkenlik, çözünmüş katı madde miktarı, çözünmüş oksijen miktarı, yükseltgenme-indirgenme potansiyeli gibi su kalitesini gösteren arazi parametreleri ölçülmüş ve nehir içinden ve piezometrelerden su örnekleri alınıp ana anyon derişimleri belirlenmiştir. Bütün bu parametreler ve ana anyon derişimleri yeraltı suyu ve Kirmir nehrinin kimyasal etkileşimi açısından değerlendirilmiş ve klor kütle dengesi uygulanarak, yeraltı suyunun nehre katkısı araştırılmıştır. Son olarak da, çalışma alanında ölçülen klor miktarları jeoloji ile ilişkilendirilmiştir. Bu hierarşik, çok ölçekli metodoloji çalışma alanında yeraltı suyu ve yüzey suyu arasında gözlenen etkileşimin lokasyonlarının ve yönünün saptanmasını sağlamıştır.

Anahtar Kelimeler: Yeraltısu - nehir etkileşimi, nehir içi ölçümler, termal uzaktan algılama, arazi parametreleri, ana anyon derişimi

*To My Beloved Family*

## ACKNOWLEDGEMENTS

I would like to express my thankfulness to my supervisor Assoc. Prof. Dr. Koray K. Yılmaz for his patience, support, guidance and criticism. He always supported, guided and motivated me to complete my research. Without his knowledge and directives, I was not able to complete it. He is a great advisor for a person who is just at the beginning of the academia.

I would like to thank Prof. Dr. Hasan Yazıcıgil for his kind and caring attitudes. I am really thankful to him for providing me a place to carry on my studies throughout this long journey and treating me like I am one of his graduate students. Also, I want to express my gratitude to Prof. Dr. Zeki Çamur for guiding me with his knowledge. He always made suggestions and was ready to help without hesitation. Last but not least I would like to thank Prof. Dr. Mehmet Lütü Süzen for his support and helps.

One of my greatest gratitudes goes to Scientific and Technological Research Council of Turkey (TÜBİTAK) for their scholarship (2210-C) they provided. Seeing me worthy of this scholarship motivated me to complete my research in a better way.

I am also grateful to Asia Minor Mining (AMM) for facilities they provided. Especially Cansu Kahraman, Tevfik Kaan Düz, İsa Alanka, Ali Sırrı Köseoğlu were always ready to help.

My thankfulness goes to Hydrochemistry Laboratory of Hacettepe University for their help in the analysis of my data.

My appreciation belongs to my colleagues at the hydrogeology laboratory, Çidem Argunhan, Ayşe Peksezer Sayıt and Hatice Kılıç. They are beyond roommates that a person can have. They were incredibly supportive and always helped me without

hesitation. Hatice Kılıç and Ecenur Ceyhan become one of the most important people in my life. During this period, we have established a strong bond of friendship which I wish to last for my entire life. They made my journey more colorful and meaningful. Without their kindness, helps, friendship and supportive attitudes, I was not able to finish my research. Ayşe Peksezer Sayit was always ready to help me during my hard periods. She motivated me with her knowledge and experiences. Çidem Argunhan always did her best to help me in any situation.

I am grateful to Deniz Atilla for his supports for any time. He is the best listener that I have ever met. His different perspective and personality made the life more understandable. I feel very lucky to have him as a dear friend.

Also, I am thankful to Yasemin Öztumur for her enduring encouragement and supports. She was always ready to help when I needed.

My deepest gratitude goes to my dearest friends Buse Altay, Ecem Balkan and Burak Gönenç who always supported and encouraged me. I cannot think any moment that I do not share with them. They are making my life more beautiful, meaningful and entertaining. They are my second family and I am grateful to them for their contributions to my life. Buse Altay was always like a sister to me. We grew up together and I think that we still have a long journey together. I cannot think my life without Burak Gönenç and Ecem Balkan. I know that these three people will always be there.

I am deeply grateful to my dear family. My sister, Ekin always brought heat to my life and made it more colorful. I am grateful for her supports and encouragements in any time. Especially my mom and dad provided me all opportunities during my entire life. They are the best thing that ever happened to me. I am thankful to the perspective that they bring into my life. They always did their best to educate and improve myself. I cannot express my gratefulness for them. My wish for any person is to have such parents.

## TABLE OF CONTENTS

ABSTRACT .....	v
ÖZ.....	vii
ACKNOWLEDGEMENTS .....	x
TABLE OF CONTENTS.....	xii
LIST OF TABLES .....	xvi
LIST OF FIGURES .....	xviii

### CHAPTERS

1. INTRODUCTION.....	1
1.1. Importance of Groundwater and Surface Water Interaction.....	1
1.2. Objective.....	3
1.3. Approach.....	4
2. BACKGROUND LITERATURE.....	5
2.1. Groundwater Interactions with Streams .....	5
2.2. Measuring the Exchange of Water Between Surface Water and Groundwater.....	9
2.2.1. Non-thermal Methods for Measuring the Exchange of Water Between Surface Water and Groundwater.....	9
2.2.1.1. Environmental Tracers - Solute Mass Balances .....	10
2.2.2. Heat as a Groundwater Tracer .....	13
2.2.2.1. Temperature Time Series Methods.....	14



2.3. Chemistry of Natural Waters.....	19
2.3.1. Chemical Interactions of Groundwater and Streams .....	20
2.3.2. The Hyporheic Zone .....	23
3. DESCRIPTION OF THE STUDY AREA.....	25
3.1. Physiography .....	25
3.2. Previous Studies .....	27
3.3. Climate.....	28
3.4. Surface Water Resources .....	29
3.5. Geology.....	30
3.5.1. Regional Geology.....	30
3.5.2. Local Geology .....	31
3.5.2.1. Basement Volcanics .....	35
3.5.2.2. Çeltikçi Formation.....	35
3.5.2.2.1. Bostantepe Unit .....	35
3.5.2.2.2. Lower Çavuşlar Unit.....	35
3.5.2.2.3. Upper Çavuşlar Unit .....	36
3.5.2.2.4. Abacı Unit .....	36
3.5.2.2.5. Kocalar Unit .....	37
3.5.2.2.6. Aktepe Unit .....	37
3.5.2.2.7. Bezci Unit .....	37
3.5.2.3. Plio-Quaternary Units.....	37
3.5.2.4. Quaternary Alluvial Deposits .....	38
3.5.2.5. Structural Geology .....	38
3.5.2.5.1. Paleo-high Fault .....	38

3.5.2.5.2.	Thrust Faults .....	39
3.5.2.5.3.	Normal Faults.....	39
3.5.2.5.4.	Kocalar Monocline.....	39
3.5.2.5.5.	Peyikler Front.....	40
3.5.2.5.6.	Folding.....	40
3.5.2.5.7.	Bedding.....	40
3.6.	Hydrogeology.....	40
4.	METHODS .....	43
4.1.	Measurement of Water Skin Temperatures Using Thermal Camera .....	43
4.2.	Nested Piezometers .....	47
4.3.	Stream Discharge Measurements .....	54
4.4.	Water Flux Calculations .....	57
4.4.1.	Streambed Temperature Measurements .....	57
4.4.2.	Calculation of Water Flux .....	60
4.5.	Measurement of Water Quality Field Parameters .....	62
4.5.1.	Major Anions .....	65
5.	RESULTS AND DISCUSSIONS .....	67
5.1.	Water Skin Temperatures Using Thermal Camera .....	67
5.2.	Hydraulic Head and Vertical Hydraulic Gradient Values .....	73
5.3.	Temporal Changes in Discharge Measurements.....	92
5.4.	Groundwater Discharge .....	96
5.4.1.	Temperature Data - VFLUX.....	96
5.4.2.	Vertical Fluid Flux Values - VFLUX.....	103

5.4.2.1. Calculation of Vertical Hydraulic Conductivity of the streambed .....	111
5.4.3. Solute Mass Balance .....	114
5.5. Chemical Interactions of Groundwater - Stream Water and Indications of Water Quality .....	119
5.5.1. Water Quality Field Parameters .....	119
5.5.1.1. Temperature Measurements.....	120
5.5.1.2. Electrical Conductivity (EC) Measurements .....	128
5.5.1.3. The pH and Redox Environment .....	130
5.5.2. Major Anion Hydrochemistry .....	133
6. CONCLUSIONS AND RECOMMENDATIONS .....	147
REFERENCES .....	155

## LIST OF TABLES

### TABLES

Table 1: Length of piezometers, depth of piezometers in the streambed and depth to screen middle of each piezometer for each installation location. ....	49
Table 2: Streambed temperature measurement periods.....	59
Table 3: A sample input temperature time series data collected from a single streambed vertical profile. ....	62
Table 4: Total head values, VHG values and flow directions in S1-P, S2-P and S3-P. ....	76
Table 5: Total head values, VHG values and flow directions in S4-P, S6-P and S7-P. ....	81
Table 6: Total head, surface water level, VHG values and flow directions in S9-P..	82
Table 7: Total head, VHG values and flow directions in S10-P-B.....	83
Table 8: Mean, minimum and maximum VHG values for each monitoring location. ....	84
Table 9 : Discharge values in each measurement location. ....	94
Table 10 : Difference between discharge values of consecutive measurement locations (negative (positive) values indicate decreasing (increasing) discharge downstream).....	94
Table 11: Minimum, maximum streambed temperature values and their differences in monitoring sites S3-P, S4-P and S16-D for each measurement period.....	97
Table 12 : Minimum and maximum flux values for each time interval in each site. ....	103
Table 13: Maximum and minimum flux values in S16-D for each segment.....	108

Table 14: Vertical Hydraulic Conductivity values in location S3-P. ....	112
Table 15: Geometric means of vertical hydraulic gradient values in S3-P and S4-P for each flux measurement dates. ....	112
Table 16: Vertical hydraulic conductivity values in location S4-P. ....	113
Table 17 : Chloride concentrations and discharge values in sampling locations. ....	115
Table 18: Mean, maximum and minimum values of water quality field parameters measured from surface water in summer and winter seasons. ....	121
Table 19: Mean, maximum and minimum values of water quality field parameters measured from nested piezometers in summer season. ....	122
Table 20: Major anion concentrations of water samples taken from piezometers and surface water at selected monitoring locations (Us: upstream, Pz: piezometer, Dn: Downstream). ....	134
Table 21: Chloride concentrations (mg/L) in sampling locations. ....	138
Table 22: Chloride concentrations (mg/L) and the interacted geological units of wells around the study area. ....	138
Table 23: Chloride concentrations (mg/L) and the interacted geological units of fountain around the study area. ....	139

## LIST OF FIGURES

### FIGURES

Figure 1: Groundwater flows to a stream. ....	6
Figure 2: Three basic interaction types between groundwater and a stream. a) Gaining Stream. b) Losing Stream. c) Groundwater flows in and out through stream d) Disconnected Stream.....	8
Figure 3: Conceptual model of how groundwater inflow can be quantified from the change in concentration in stream from upstream to downstream. ....	12
Figure 4: The difference in amplitude and shift in phase in the diurnal temperature signal in the streambed at various depths (Hatch et al., 2006).....	15
Figure 5: Hyporheic Zone (Buss et al., 2009).....	24
Figure 6: Regional view of the study area. ....	26
Figure 7: Position of monitoring locations in the study area. ....	27
Figure 8: Regional geology of the area – Galatian Volcanic Province (Rojay, 2013) .....	31
Figure 9: Generalized columnar section in the local geology (AMM,2015).....	32
Figure 10: Geological map of the study area (AMM, 2015). ....	33
Figure 11 : Application of thermal remote sensing by Optris IR Camera PI160 in the study area. There is a thermal camera and a visible camera mounted on the platform. ....	46
Figure 12: Optris IR Camera Software window .....	47
Figure 13: a) Perforated section, tip and head of the piezometer used in the study. b) Installation of an piezometer by sledge hammer in the field. ....	50
Figure 14: Drawing of nested piezometers in site S1-P in terms of their sizes. ....	51

Figure 15: a) Nested piezometers and measurement of height of the piezometer above ground b) Measurement of water levels inside the nested piezometers by Solinst TLC Meter. ....	52
Figure 16: Hydraulic and elevation heads in the nested piezometers. ....	53
Figure 17: Measurement of discharge by FP111 Globe Water Flow Probe in monitoring location S17-D. ....	56
Figure 18: Preparation and installation of i-buttons. ....	59
Figure 19: Measurement of water quality field parameters for stream water in the field. ....	63
Figure 20: Purging of deep piezometer in S4-P site for measurement of water quality field parameters. ....	64
Figure 21: Chloride sampling monitoring locations through the study area. ....	66
Figure 22: Some of water samples taken for major anion analysis. ....	66
Figure 23: Mixing of two different waters in S9-P. ....	68
Figure 24: TIR and visible images taken from S10-P-B. ....	69
Figure 25: The interface of cold and warm water in S10-P-B. ....	70
Figure 26: TIR and visible images taken from S15. ....	71
Figure 27 : TIR and visible images taken from S17-D. ....	72
Figure 28: Sites having losing, both gaining - losing and gaining characters. ....	74
Figure 29: Water level change in time at the losing reach of the study area (S1-P, S2-P and S3-P). ....	75
Figure 30: Water level change in S4-P, S6-P, S7-P, S9-P and S10-P-B. ....	79
Figure 31: Vertical hydraulic gradient change in S1-P, S2-P and S3-P in time. ....	85
Figure 32: Vertical hydraulic gradient change in S4-P, S6-P, S7-P, S9-P and S10-P-B in time. ....	87

Figure 33: The variation in streambed elevation throughout the monitoring locations in the study area.....	92
Figure 34 : Discharge variation in time for each measurement location. ....	93
Figure 35: a) Streambed temperature variations in S3-P at depths of 5 cm and 20 cm during 12.03.2015 – 26.03.2015 measurement period. b) Streambed temperature variations in S4-P at depths of 5 cm and 20 cm during 12.03.2015 – 26.03.2015 measurement period. c) Streambed temperature variations in S16-D at depths of 5 cm and 20 cm during 12.03.2015 – 27.04.2015 measurement period. ....	99
Figure 36: Streambed temperature variations in each location at depths of 5 cm and 15 cm during 10.07.2015 - 03.08.2015 measurement period. ....	100
Figure 37: Streambed temperature variations in S4-P and S16-D at depths of 5 cm and 15 cm during 03.09.2015 – 14.09.2015 measurement period. ....	101
Figure 38 : Vertical flux variations in S3-P and S4-P calculated using temperature variations at depths of 5 cm and 20 cm during 12.03.2015 – 26.03.2015 measurement period.....	104
Figure 39: Vertical flux variations in each location at depths of 5 cm and 15 cm during 10.07.2015 - 03.08.2015 measurement period.....	105
Figure 40 : Vertical flux variations in S4-P and S16-D at depths of 5 cm and 15 cm during 03.09.2015 – 14.09.2015 measurement period. ....	106
Figure 41 : Segments of whole temperature and flux data in S16-D for measurement period March – April. ....	108
Figure 42: Temperature variation in streambed and flux values for segments 1 and 2 in S16-D during March - April 2015 measurement period.....	109
Figure 43: Temperature variation in streambed and flux values for segments 3 and 4 in S16-D during March - April 2015 measurement period.....	110
Figure 44: Chloride sampling monitoring locations through the study area. ....	114
Figure 45 : Box plots of water quality field parameter for stream water. ....	123



Figure 46: Change in water quality field parameters through monitoring locations for stream water and water samples taken from piezometers.....	125
Figure 47: Normalized electrical conductivity change in each site during measurement period.....	128
Figure 48: Major anion concentrations throughout the selected sampling locations. ....	135
Figure 49: Change in total anion concentrations throughout the selected sampling locations .....	137
Figure 50: Position of wells in the geological map (AMM, 2015).....	141
Figure 51: Position of fountains in the geological map (AMM, 2015). ....	142



## **CHAPTER 1**

### **INTRODUCTION**

#### **1.1. Importance of Groundwater and Surface Water Interaction**

In the past, especially prior to 1990s, groundwater and surface water were considered as separate resources although they are hydraulically connected with each other. Development, management and protection of water resources have gained an increasing importance in recent years. For example, Water Framework Directive (WFD) developed by European Union (EU) revealed as a result of increasing threat of pollution and increasing demand for cleaner water resources such as rivers, lakes and reaches. It specifically aims the protection of all waters (surface water, groundwater and coastal waters), achievement good status of all waters (quantitative and chemical status), management of water bodies based on river basins or catchments and involvement of public under one piece of environmental statute. Competing demands for water resources within and between human communities and natural systems necessitates competent, scientifically-based management (Kikuchi et al., 2012). Moreover, WFD outlines an approach about management of water resources by focusing on interaction between groundwater bodies, groundwater dependent terrestrial ecosystems and surface water bodies. Therefore, groundwater and surface water interaction is becoming the subject of increasing attention as more emphasis is placed on integrated water resources management. Management of one component of the hydrologic system, such as a stream or an

aquifer, is only partly effective because each hydrologic component is in continuous interaction with other components (Winter et al., 1998). Many surface water bodies such as springs, wetlands, lakes, and estuaries are partially or wholly dependent on interactions with groundwater. Especially, rivers and lakes generally have strong baseflow component in the dry seasons.

The interaction between groundwater and surface water means the exchange of water masses between these resources. The chemical and microbiological characteristics of surface water and groundwater are different from each other. Therefore, exchange of water causes significant modifications in physical, chemical, biological, and energetic properties of groundwater, surface water and hyporheic zone in which mixing occurs. Various processes like transportation, degradation, transformation, precipitation or sorption occurring in the transition zone affect the water quality of this zone because chemical, biological and physical properties of groundwater and surface water are indeed different (Kalbus et al., 2006). In other words, interaction between groundwater and surface water affect the quantity and quality of each other, pollution of one of them can degrade the other. Determination the amount of contaminant movement or waste load to surface waters is required to meet the water quality standards. Winter et al. (1998) indicate that considering the contribution of groundwater in the estimation of waste load may be a better approach. In some cases, water quality standards can be met by reducing contaminant loads carried by groundwater to streams. Also, water exchange between groundwater and surface water creates a habitat near the interface. This contributes the diversity of ecological community and affects the aquatic environment. Understanding and quantifying physical processes and ecological implications of groundwater and surface water interaction is becoming an important subject in hydrogeological and river ecological studies (Schmidt et al., 2006). According to ecologist, hydrogeochemists, and hydrologists interactions between surface water and groundwater play in important role in stream ecosystem. For the protection of water resources it is vital to comprehend the significance of the effects of exchange processes between these two sources. Groundwater and surface water ecosystems are considered as linked

components of a hydrologic continuum; therefore, this causes related sustainability issues (Sophocleous, 2002).

Additional to integrated water management and water quality issues, understanding interaction between groundwater and surface water is essential for water supply. Due to various reasons like environmental concerns and difficulty of finding suitable sites, constructing reservoirs for surface storage of water is becoming a challenging process day by day. Instead of constructing surface storage reservoirs, an aquifer system can be used to store water temporarily. One of the factors that should be taken into consideration in such projects is the groundwater-surface water interaction. Winter et al (1998) explains that in aquifer systems where water is stored temporarily, the characteristics and extent of interactions between groundwater and surface water influence the success of such integrated use projects. Furthermore, excessive usage of one of them can affect the other. For example, if groundwater is pumped excessively, this can cause the depletion of surface water.

As integrated management and sustainability of water resources become more important, interaction of groundwater and surface water has also gained an increasing attention due to its impacts on environment. Exchange processes have significant effects on groundwater, surface water and ecology as mentioned. Consequently, to achieve an effective water resources management, an understanding the interconnections between surface water and groundwater is essential.

## **1.2. Objective**

The primary objective of this study is to characterize the groundwater and surface water interaction by identifying the spatial and temporal hydrological pathways along a small reach of Kirmir Stream near Çeltikçi town, which is in the vicinity of Kızılcahamam, in the Central Anatolian Region of Turkey. In particular, to investigate whether the adjacent aquifer systems in the region provide a source of water to Kimir Stream along flowpaths and if so from which geological units this groundwater affected and how it influences the chemistry of stream.

### **1.3. Approach**

To achieve this goal, a variety of methods was combined. Groundwater discharge zones were quantified by temperature – based groundwater flux measurements and the stream water and shallow groundwater quality were analyzed to detect the source of water feeding the Kirmir Stream. The objective was accomplished by applying a field based study to approximately 2 km reach of Kirmir Stream. The scientific approach of this thesis is defined as follows:

- [1] Detecting the groundwater discharge zones above and along streambank by the help of remote sensing measurements collected with handheld thermal infrared (TIR) camera. Therefore, an understanding about the study area was obtained and next steps were planned.
- [2] Installation of nested piezometers into specific locations to observe the direction of flow and to identify the gaining and losing reaches within the study area.
- [3] Quantification of vertical flow flux in losing and gaining reaches of the study area continuously by using temperature based equations.
- [4] Measurement of water quality field parameters for both stream water and shallow groundwater. Evaluating the whole data in terms of exchange processes to find a relation between stream water and groundwater.
- [5] Quantifying the amount of major anion concentrations in stream water and shallow groundwater to make an interpretation between them and finding groundwater contribution by using mass balance equations.
- [6] Evaluation of all above findings together and finally characterizing the groundwater and surface water interaction in the study

## CHAPTER 2

### BACKGROUND LITERATURE

#### 2.1. Groundwater Interactions with Streams

As mentioned before, groundwater and surface water are linked components of hydrologic continuum. Groundwater is present in nearly all landscapes and interacts with surface water. Therefore, they affect the quality and quantity of each other. The exchange processes between groundwater and surface water bodies are complex because they are controlled by many factors such as geology, geomorphology, topography, climate, and position of surface water body and water table with respect to each other (Sophocleous, 2002; Winter, 1999). Stream channel orientation and stream channel geometry are important factors affecting exchange processes between groundwater and a stream (Woessner, 2000). Groundwater flow systems affect the degree of interaction and chemistry. They develop in association with the physical framework which is determined by the setting of land (Younger, 2007). There are three types of flow systems which are local, intermediate and regional (Figure 1) (Tóth, 1963). Groundwater flows from groundwater recharge areas to groundwater discharge areas. Local groundwater flow systems occur near the surface and characterized by high degree of interaction. Winter et al. (1998) states that in the uppermost part where the unconfined aquifer is located, length of flow paths range between tens to hundreds of feet and residence times correspond to days to a few days.

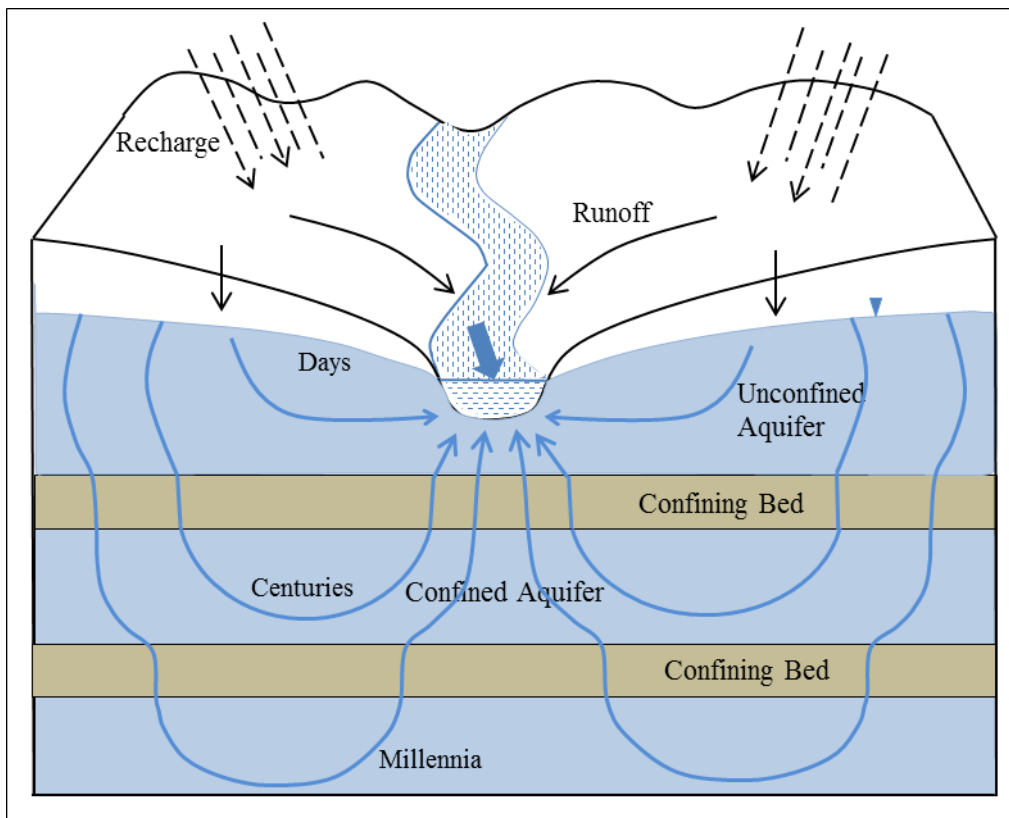


Figure 1: Groundwater flows to a stream.

A local groundwater system occurs between a topographic high and adjacent topographic low. Because of proximity to the ground surface (therefore, closer to the atmosphere also), dissolved oxygen amount is high in local flow systems and they are open to chemical pollutants resulting from human activity. These pollutants can be nutrients such as nitrate and phosphates. Intermediate flow systems include several topographic lows between recharge and discharge areas. They generally occur within confined aquifers. Therefore, they are separated from a local flow system by a confining layer. Because their interaction with the atmosphere is cut by a confining layer, they have relatively low dissolved oxygen concentration. Their travel times can reach up to centuries. Regional groundwater flow systems are characterized by the longest and the deepest flow paths. Residence times can last for millennia. This long residence time causes the interaction of groundwater with



surrounding environment resulting in high amount of total dissolved solids in the water. Groundwater flow is affected from the topography (Fan et al., 2007). Winter (1999) superficially explained the effect of topography in regional flow systems and said that topographically low areas are groundwater discharge areas where the groundwater moves upward while topographically high areas are groundwater recharge areas where the groundwater flows downward.

The interaction processes between groundwater and streams occur in three basic ways (Figure 2). Streams can gain water from the adjacent groundwater system through the streambed and these kind of streams are named as gaining streams (Figure 2a). Conversely, groundwater can gain water from a stream and these streams are known as losing streams (Figure 2b). Lastly, a stream can do both, that is, it may gain water in some reaches and may lose its water in the other reaches (Figure 2c). If a stream is a gaining stream, its stream water head is lower than the water table. When the stream water head becomes higher than the water table, stream feeds the groundwater, that is, it becomes a losing stream. Also, gaining streams and losing streams can be defined as groundwater effluent and surface water influent respectively. In losing stream shown in Figure 2b, groundwater is connected to the stream by a continuous saturated zone. However, groundwater can also be disconnected from the losing stream by an unsaturated zone. In this case, the water table can bulge towards the stream depending on the relationship between the rate of lateral groundwater flow and the rate of recharge through the unsaturated zone (when the lateral groundwater flow rate becomes lower than the recharge rate) (Winter et al., 1998; Winter, 1983). These streams are named as disconnected streams and can be seen in Figure 2d.

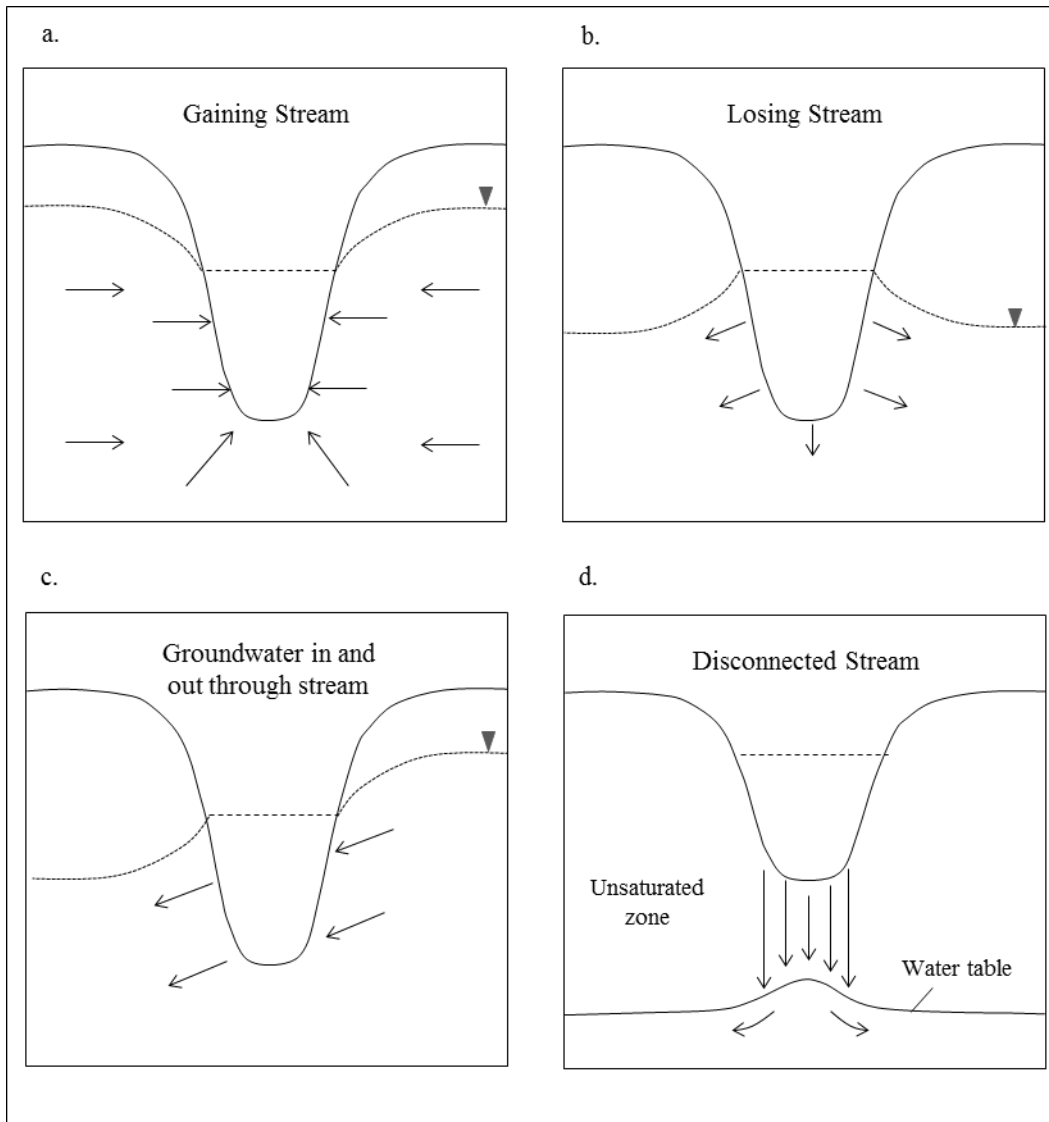


Figure 2: Three basic interaction types between groundwater and a stream. a) Gaining Stream. b) Losing Stream. c) Groundwater flows in and out through stream d) Disconnected Stream

## **2.2. Measuring the Exchange of Water Between Surface Water and Groundwater**

Estimates of groundwater flux to streams facilitate conjunctive management of connected aquifers and streams and it is crucial to characterize the exchange processes between them. A variety of techniques were defined to identify and quantify this interaction. They can be applied to groundwater, streams and hyporheic zone. Choosing an appropriate method depends on the purpose of the study, temporal and spatial scales, limitations and uncertainties (Kalbus et al., 2006).

### **2.2.1. Non-thermal Methods for Measuring the Exchange of Water Between Surface Water and Groundwater**

The most common technique to quantify exchange fluxes through groundwater – stream interface is to use hydraulic gradient. Hydraulic head can be found by measuring water levels inside the piezometers which are at two different depths through streambed. From hydraulic heads, hydraulic gradient values are obtained and then Darcy's equation is solved to calculate flux values using an appropriate hydraulic conductivity:

$$q = -K \frac{dh}{dl} \quad (1)$$

Where, K is hydraulic conductivity and  $\frac{dh}{dl}$  is hydraulic gradient.

According to Kalbus et al. (2006), hydraulic conductivity can be estimated by grain size analysis, permeameter tests, slug and bail tests and pumping tests.

Furthermore, seepage meters provide direct measurement of exchange fluxes (Lee, 1977). This method consists of a bottomless cylinder having a deflated plastic bag attached to it. It is installed into streambed and plastic bag collects the water moving

from groundwater to stream. By using the volume of the collected water, the cross section area of the cylinder and collection period seepage flux is calculated. For reverse conditions in which stream feeds groundwater, a known water volume is filled to the plastic bag and then bottomless cylinder is installed to the streambed. Lastly, using volume loss stream contribution to groundwater is calculated (Rosenberry et al., 2008). Seepage meters are easy to use and inexpensive. According to Kalbus et al. (2006), they should be installed in many locations to obtain representative flux values. Another method which can be used to quantify exchange fluxes is dilution gauging. Dilution gauging is performed by using a chemical tracer. A solute is added at known rate in upstream of stream and dilution is measured in downstream. This is used to find the streambed fluxes (Constantz et al., 2003; Rosenberry et al., 2008).

#### **2.2.1.1. Environmental Tracers - Solute Mass Balances**

Water level and chemical composition in surface water bodies such as streams, lakes etc. are controlled by input and output. Generally, concentration of dissolved ions occurring in groundwater is higher than concentration of dissolved ions in natural river water. As groundwater joins the stream, electrical conductivity and conservative ions (non-reactive) such as chloride show an increase towards downstream and contribution of groundwater to a stream can be quantified by using this increase. Using the environmental tracers to quantify groundwater discharge to streams is more advantageous than physically based methods because they can offer more accurate information on the spatial distribution with less resources (Cook, 2013).

Chemical methods that are used to estimate groundwater discharge can be applied in time domain or in spatial domain. For methods based on time domain, stream water chemistry is measured over time at a single location so that how groundwater discharge has varied temporally is estimated (e.g. Sklash & Farvolden, 1979). Also, environmental tracers can be used to estimate the residence time of water in

subsurface. According to Cook (2013), a tracer concentration is measured at one point in time so that changes in concentrations are obtained. By comparing them with rainfall concentrations, key parameters defining the distribution of travel times are solved. In addition, he emphasizes that the residence time distribution of water discharging to stream change along the stream length and different residence time distributions obtained from a single location may be used to convert them into a single broad distribution. On the contrary, water chemistry is measured at different locations along the stream in the concept of the methods which are based on spatial domain. Groundwater inflow varies spatially and this causes the changes in stream water chemistry from point to point. Interpretation of downstream changes in water chemistry provides the quantification of groundwater inflow.

Environmental tracer approach was used in many studies to estimate groundwater inflow. Tracer studies were taken into consideration in high-gradient stream systems affected from advection, dispersion, groundwater inflow, and exchange processes between channel and subsurface water (Wagner & Harvey, 1997). The spatial and temporal variability of groundwater - surface water interaction was investigated by mass balance calculations (Unland et al., 2013). A chloride dilution experiment was performed to quantify groundwater components of water balance in a proglacial moraine (Langston et al., 2013). A tracer injection was applied to determine the mine drainage inflows in Little Cottonwood Creek, Utah (Kimball et al., 2001). Furthermore, tritium data from outflow waters of river basins were used to find the average residence times in the river basins (Michel, 1992). Several tracers were used in several studies, such as chloride (Cartwright et al., 2011; Meredith et al., 2009), helium (Gardner et al., 2011) and radon (Cartwright et al., 2011; Ellins et al., 1990; Mullinger et al., 2007; Peterso et al., 2010; Smith et al., 2010; Wu et al., 2004). These studies can be given as examples in which tracer approach is used to understand the groundwater inflow. Also, various tracers can be used in such studies, as in the conceptual model given in Figure 3. In this model, there are three components which are stream upstream, stream downstream and groundwater.  $Q_1$ ,  $Q_2$  and  $Q_{gw}$  represents the flow upstream, flow downstream and groundwater inflow.

C1, C2 and C3 are used to infer the concentration of conservative ion in upstream, downstream and groundwater concentration.

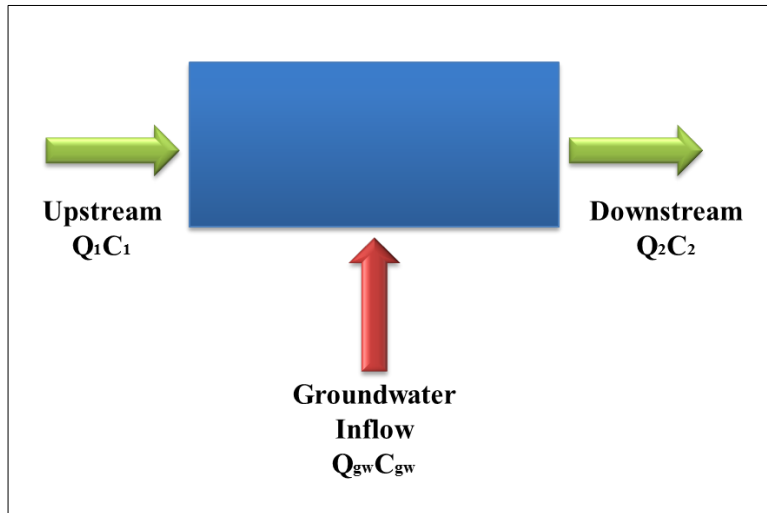


Figure 3: Conceptual model of how groundwater inflow can be quantified from the change in concentration in stream from upstream to downstream.

When evaporation is ignored, water balance can be written as:

$$Q_1 + Q_{gw} = Q_2 \quad (2)$$

The solute mass balance becomes as:

$$Q_1c_1 + Q_{gw}c_{gw} = Q_2c_2 \quad (3)$$

Then, groundwater inflow is calculated by the following formula:

$$Q_{gw} = \frac{Q_2C_2 - Q_1C_1}{C_{gw}} \quad (4)$$

Using this formula, groundwater inflow can be calculated along a length of stream if concentration measurements are performed along the stream.

Mass balance assumes that the system is at steady state when the measurements are taken. If the stream has the contributions of tributaries, then they must be sampled and involved in the mass balance as well. It is assumed that the input concentrations of groundwater do not show variations in time. This method works best when the stream and groundwater concentrations are significant. By the help of this method, the chemical composition of groundwater discharging to stream can be calculated. If the obtained results are compared with the chemical compositions of adjacent aquifer systems, it can be understood that from which aquifer inflow into the stream occur.

### **2.2.2. Heat as a Groundwater Tracer**

Temperatures of groundwater and streams are different from each other. Groundwater temperatures are relatively constant throughout the year, on the other hand stream temperatures vary daily and seasonally (Kalbus et al., 2006). Stream temperatures are affected from the exchange processes between stream and groundwater, because as water moves between stream and nearby groundwater through adjacent sediments, it carries measureable amounts of heat together with it. In the environment, temperature changes occur naturally as a result of heat flow. Heat flow cannot be quantified directly but it can be obtained by measuring temperature changes and multiplying it with the physical properties of the material. Therefore, temperature fluctuations at the streambed provide signals for tracing the groundwater - stream exchanges.

The fundamentals of using heat as a groundwater tracer were first developed in 1960s. Naturally occurring heat flow can be used as a tracer for groundwater movement and exchange flow (Stallman, 1963, 1965; Suzuki, 1960). Suzuki (1960) measured groundwater temperatures to predict the water flux through saturated sediments:

$$\frac{\partial T}{\partial t} = \kappa_e \frac{\partial^2 T}{\partial z^2} - \frac{nv_f}{\gamma} \frac{\partial T}{\partial z} \quad (5)$$

where T is temperature of the soil, t is time,  $\kappa_e$  is effective thermal diffusivity, z is depth,  $\gamma$  is  $c_s \rho_s / c_w \rho_w$  (specific heat of the soil / specific heat of water), n is porosity and  $v_f$  is the vertical fluid velocity.

#### **2.2.2.1. Temperature Time Series Methods**

The fluxes of groundwater-stream interface can be quantified by measuring the streambed temperatures at different depths. Gaining reaches of streams have relatively stable streambed temperatures and damped diurnal variations, while losing reaches demonstrate highly variable streambed and surface water temperatures (Winter et al., 1998). Because surface water is heated and cooled at the surface, downward moving water causes a deeper penetration of cyclic temperature changes, whereas upward moving water leads to less penetration of cyclic temperature changes since the upwelling groundwater has a relatively constant temperature (Stonestrom et al., 2003). Temperature measurements can be performed at various depths in the streambed for a period of time, so that temperature profiles for different depths are obtained (Figure 4). From temperature profiles, vertical flux values through the stream – groundwater interface can be calculated using the difference in phase and amplitude.



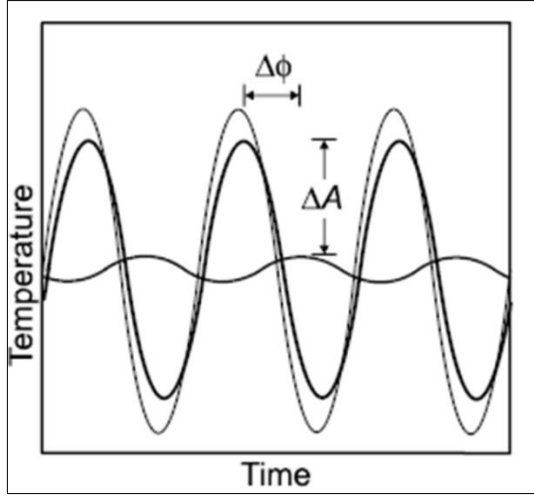


Figure 4: The difference in amplitude and shift in phase in the diurnal temperature signal in the streambed at various depths (Hatch et al., 2006).

A solution for equation (5) was developed to find the vertical flux (Goto et al., 2005):

$$T(z, t) = A \exp\left(\frac{vz}{2\kappa_e} - \frac{z}{2\kappa_e} \sqrt{\frac{\alpha + v^2}{2}}\right) \cos\left(\frac{2\pi t}{P} - \frac{z}{2\kappa_e} \sqrt{\frac{\alpha - v^2}{2}}\right) \quad (6)$$

where A is amplitude of temperature variations,  $\kappa_e$  is effective thermal diffusivity, P is the temperature variation period,  $\alpha = \sqrt{v^4 + (8\pi \kappa_e / P)^2}$ , v which is penetration of thermal front which is proportional to the fluid velocity,  $v_f$ .

The first part of equation (6) represents the differences in the amplitude of temperature variations (damping of them) with depth throughout the streambed and the second part represents the shift in phase with depth (Hatch et al., 2006). Hatch et al. (2006) solved equation (6) using amplitude ratio ( $A_r$ ) of variations in temperature

values at two different depths and phase shift ( $\Delta\phi$ , the time delay between the different depths):

$$A_r = \exp \left\{ \frac{1}{2\kappa_{e,d}\kappa_{e,s}} \left[ v (z_d \kappa_{e,s} - z_s \kappa_{e,d}) - \left( z_d \kappa_{e,s} \sqrt{\frac{\alpha_d + v^2}{2}} - z_s \kappa_{e,d} \sqrt{\frac{\alpha_s + v^2}{2}} \right) \right] \right\} \quad (7)$$

where s and d represent the effective properties at two different depths as shallow and deep respectively. If the effective properties are the same then the equation becomes:

$$A_r = \exp \left\{ \frac{\Delta z}{2\kappa_e} \left( v - \sqrt{\frac{\alpha + v^2}{2}} \right) \right\} \quad (8)$$

where  $\Delta z$  refers the distance between the measurement points.

Also, phase shift was developed between two measurement points:

$$\Delta\phi = \frac{P}{4\pi} \left( \frac{z_d}{\kappa_{e,d}} \sqrt{\frac{\alpha_d - v^2}{2}} - \frac{z_s}{\kappa_{e,s}} \sqrt{\frac{\alpha_s - v^2}{2}} \right) \quad (9)$$

If effective sediment properties are the same again, then:

$$\Delta\phi = \frac{P\Delta z}{4\pi\kappa_e} \sqrt{\frac{\alpha - v^2}{2}} \quad (10)$$

As final step, equations (8) and (10) can be used to obtain q:

$$q \frac{c_w \rho_w}{c_s \rho_s} = \frac{2\kappa_e}{\Delta z} \ln A_r + \sqrt{\frac{\alpha + v^2}{2}} \quad (11)$$

$$q \frac{c_w \rho_w}{c_s \rho_s} = \sqrt{\alpha - 2 \left( \frac{\Delta\phi 4\pi\kappa_e}{P\Delta z} \right)^2} \quad (12)$$

Vertical water flux, q, is present in both sides of the equations (11) and (12). It is involved by both  $v$  which is equal to  $\left( q \frac{c_w \rho_w}{c_s \rho_s} \right)$  and  $\alpha$ . Due to this, both equations should be solved iteratively.

Hatch et al. (2006) emphasized that these equations are mostly suitable for thermal conditions within a semi – infinite half space which has the upper part of the streambed (one dimension). This method can be made suitable for two or three dimensions. For more complex systems having irregular upper boundary, more numerical analysis are required. However, this approach works best for simple geometry and properties.

This approach is based on the quantification of phase and amplitude changes of temperature variations between two different depths. When amplitude ratio is taken into account, this time series method provides reliable flux values between -5 to 3

m/day. When phase shift is valid, values between -10 m/day and 10 m/day are the reliable flux values.

In addition to Hatch et al. (2006), Kerry et al. (2007) also created a solution based on the temperature time series approach:

$$q = \sqrt{\left(\left(\frac{c_s \rho_s \Delta Z}{\Delta \phi c_w \rho_w}\right)^2 - \left(\frac{4\pi \Delta \phi K}{P \Delta Z c_w \rho_w}\right)^2\right)} \quad (13)$$

Time series thermal methods were used in previous studies for various purposes. As mentioned earlier Kerry et al. (2007) used them to find the temporal and spatial streambed fluxes. Also, they were used to examine spatial and temporal variabilities in hydraulic conductivity values (Hatch et al., 2010). By time series methods, the effect of field conditions on flux values was investigated (Lautz, 2010). Also, the variation in groundwater flux values in the area which is under the control of small dams were investigated (Fanelli et al., 2008; Gordon et al., 2012). Time series methods provide an easy way for collection of data and this method is insensitive to streambed scour and sedimentation.

In addition to these, heat was used as a tool to characterize the groundwater – stream interactions in various studies (Anderson, 2005; Becker et al., 2004; Conant, 2004; Jim Constantz, 1998; Cranswick et al., 2014; Duque et al., 2015; Kurylyk et al., 2015; Lee et al., 2013; Schmidt et al., 2006). In the study performed by Conant (2004), streambed temperatures and piezometer data were combined. From piezometers, flux estimates were found using Darcy’s law. After that, streambed temperature measurements and flux estimates were combined to develop a simple mathematical relationship. The purpose here was to use this mathematical relationship to find the flux values by only using temperature data. Thereby, flux values were estimated at so many locations without a need of installation of piezometers and slug tests. This is an easy way that saves time and money.

### 2.3. Chemistry of Natural Waters

Water is a highly reactive substance so it contains dissolved solids, liquids, gases, inorganic - organic molecules, organisms etc. Physical and chemical characteristics of natural waters are controlled by mainly the lithology of the geological strata where the water is in contact with, residence time of water in that strata and environmental conditions (Candela et al., 2009). A small number of substances which are major ions have the main effect in the chemical composition of water. They have the greatest concentrations; generally greater than 1.0 mg/L (Nikanorov et al., 2009). Also, minor constituents are available in natural waters and they are present at concentrations in the range of 0.01mg/L and 1.0 mg/L. Additional to major and minor ions in water, the ions having concentrations less than 0.01 mg/L are named as trace ions. Generally, major constituents in water are  $\text{Ca}^{2+}$ ,  $\text{Na}^+$ ,  $\text{Mg}^{2+}$ ,  $\text{K}^+$  as positive charged ions (cations) and  $\text{Cl}^-$ ,  $\text{F}^-$ ,  $\text{HCO}_3^-$ ,  $\text{SO}_4^{2-}$ ,  $\text{NO}_3^-$ ,  $\text{NO}_2^-$ , as negative charged ions (anions). Weathering of rocks and soils, solutes from the atmosphere, chemical reactions existing in the surrounding environment determine the chemistry of natural waters.

Surface water chemistry is controlled by several factors such as climate, vegetation, geology, aquatic environment etc. (Meybeck, 2003). Chemistry of streams can be defined in terms of dissolved, suspended and deposited materials. Streams carry dissolved ions that they receive from ground water and surface runoff. These dissolved ions can include  $\text{HCO}_3^-$ ,  $\text{Ca}^{2+}$ ,  $\text{SO}_4^{2-}$ ,  $\text{H}_4\text{SiO}_4$ ,  $\text{Cl}^-$ ,  $\text{Na}^+$ ,  $\text{Mg}^{2+}$ ,  $\text{K}^+$ ,  $\text{PO}_4^{3-}$  etc. Most of these ions come from the interaction of rainwater with the soil and rock when it reaches the surface. The other constituents such as  $\text{SO}_4^{2-}$ ,  $\text{Cl}^-$  are provided by weathering. Total dissolved solid amount in streams is much higher than the concentration of rain water due to the dissolution of deposition particles and weathering of minerals. Additionally, small rock fragments and minerals produced in weathering reactions exist in streams.

Nearly all groundwater originates from rain and snowmelt infiltrating through the soil into flow systems. Chemistry of groundwater is determined by the composition

of water which enters the groundwater reservoir and the reactions with surrounding environment. Although the minerals are not soluble generally, their solubility are affected from the presence of  $\text{CO}_2$ . As the water infiltrates through the soil, large amounts of acid is produced. Soil is degraded by microorganisms using dissolved oxygen available in the water infiltrating through soil. As a result of this process, carbonic acid ( $\text{H}_2\text{CO}_3$ ) is produced. Occurrence of carbonic acid leads to the decrease in pH. Therefore,  $\text{H}_2\text{CO}_3$  is derived from the reaction of  $\text{CO}_2$  and  $\text{H}_2\text{O}$ . After the production of carbonic acid, mineral weathering reactions occur and the most abundant anion, bicarbonate ion ( $\text{HCO}_3^-$ ) is formed. As new water comes with infiltration of rain or snowmelt, biogeochemical processes offers a supply of acidity. In addition to formation of carbonic acid, the reaction between the oxygen and pyrite provides acidity. As groundwater moves through subsurface, its total dissolved solid amounts increase because it contacts with the surrounding environment. Generally, shallow groundwater systems have lower ion concentrations with respect to deeper systems. If short contact times between water and minerals in shallow groundwater flow paths are effective, the dissolved-solids concentration in the water becomes low also. In such settings, limited chemical changes occur before ground water feeds the streams.

### **2.3.1. Chemical Interactions of Groundwater and Streams**

Groundwater and surface water can not be thought as separate sources because they affect the quality and quantity of each other as mentioned in section 1.1. Exchange processes between streams and groundwater affect the chemistry of both. Streams gain water from groundwater and chemistry of stream is influenced depending on which geological strata this groundwater interacted and length of time that the groundwater is in contact with this stratum. Same thing is valid for groundwater. In losing streams – stream chemistry causes the changes in the groundwater chemistry depending on the ions that the stream has. The exchange processes between groundwater and stream carry the chemicals between these two sources (Winter et al., 1998). These chemicals cause changes in the amounts of carbon, oxygen,

nitrogen etc. Winter et al. (1998) summarized the several biological and chemical reactions affecting the transport of chemicals in groundwater and surface water. Some of them are acid-base reactions, mineral precipitation and dissolution, sorption and ion exchange, oxidation – reduction reactions.

#### *Acid – Base Reactions*

These reactions are about the exchange of hydrogen ions ( $H^+$ ) through the solutes available in the water. Therefore, concentrations of dissolved chemicals change because of the changes in the concentration of hydrogen ions in the water.

#### *Mineral Precipitation and Dissolution*

As a result of precipitation reactions, formation of minerals from ions, which are dissolved in water, occur. A common example for this is the precipitation of iron. Iron occurs mainly in groundwater seeps and springs and iron dissolves when it contacts with the groundwater. When dissolved iron in groundwater interacts with oxygen rich surface water such as streams, a solid material iron hydroxide precipitates. In addition to precipitation of minerals, dissolution of them is also observed. For instance, calcium and bicarbonate ions are released from calcite when it dissolves. Therefore, these reactions points the existance of exchange processes between groundwater and surface water.

#### *Ion Exchange Processes*

Ions tend to be attached to the surfaces of solid materials due to their electrical charges. Solutes existing in groundwater or streams can sorbed to an aquifer or streambed. This process is named as sorption. The reverse process indicating the release of sorbed minerals from solid surfaces to the water are called as desorption. Ion exchange means the replacemet of the ions attached to the solid surfaces by the ions existing in water. For instance, calcium and magnesium are replaced by sodium on the solid surface. Therefore, as the amounts of calcium and magnesium decrease,

the amount of sodium increases in the water. The reverse occurs when saltwater enters to the aquifer.

### Oxidation – Reduction Reactions

Chemical reactions based on the transfer of electrons from one ion to another are called as oxidation – reduction reactions or redox reactions. When the iron dissolved in the water which is oxygen depleted, interacts with the water including dissolved oxygen, the oxygen and the iron react with each other. As a result of this reaction, iron loses electrons and becomes oxidized while the oxygen gains electrons and becomes reduced. Generally, oxygen depleted and rich environments are groundwater and surface water (i.e. streams) respectively. When two sources mix with each other, oxidation – reduction reactions can take place.

Chemistry is very important to detect the groundwater and stream interactions. As explained in section 2.3, their chemistry are different. Water quality provides valuable information about the interaction between adjacent aquifer system and stream. For example, electrical conductivity which is directly related with the total dissolved solid amount in water, pH indicating the hydrogen ion transfer, dissolved oxygen amount giving information about the dissolved oxygen concentration in groundwater and stream, oxidation – reduction potential are different for these two water resources. Mixing of them causes significant variations in these water quality parameters. Therefore, chemical tracers (chloride, radon, etc.) and chemical analysis (such as water quality field parameters, analysis of major ion chemistry and stable isotopes) were frequently used in the literature to understand and quantify the exchange processes (Harrington et al., 2002; McCallum et al., 2012; Soulsby et al., 2007; Yang et al., 2012). Soulsby et al. (2007) analyzed groundwater and stream water samples in terms of chloride and alkalinity. They emphasized that under baselow conditions alkalinity is highly variable depending on geology and chloride concentrations of stream depend on the contribution of groundwater as well.



### **2.3.2. The Hyporheic Zone**

After the connection between groundwater and surface water is accepted, the focus has become the understanding the interface between these two sources. Interaction between groundwater and surface water takes place across a transition zone which is known as hyporheic zone (Figure 5). Hyporheic zone can be defined as subsurface region of streams, rivers, lakes, seas etc. in which interaction of groundwater and surface water occurs (Valett et al., 1993). The water within a hyporheic flowpath is a mixture of stream and subsurface waters. Each of the waters contribute dissolved gase, solutes and colloidal materials. Also, it is an active, heterogeneous, dynamic region between groundwater and stream and influenced from stream flow, hydrogeology and bedforms (Boulton et al., 1998; Fraser et al., 1998). In this region, additional to the exchange of water, the exchange of nutrients and organic matters also occur. Boulton et al. (1998) point that subsurface water moving in upward direction carries nutrients to streams and downwelling stream water provides dissolved oxygen and organic materials to groundwater. The boundaries of hyporheic zone varies in time and space, its extent can change from centimeters to hundreds of meters depending on the flow of stream water over surface variations such as flood plain (Boulton et al., 1998; Woessner, 2000).

The biogeochemistry of stream ecosystem is directly affected from the hyporheic zone (Bencala, 2000). Spatial and temporal distribution of microbial processes and concentrations of ions are all affected. Due to the capacity to hold significant amount of nutrients and contaminants, hyporheic zone gains an importance from ecologic point of view.

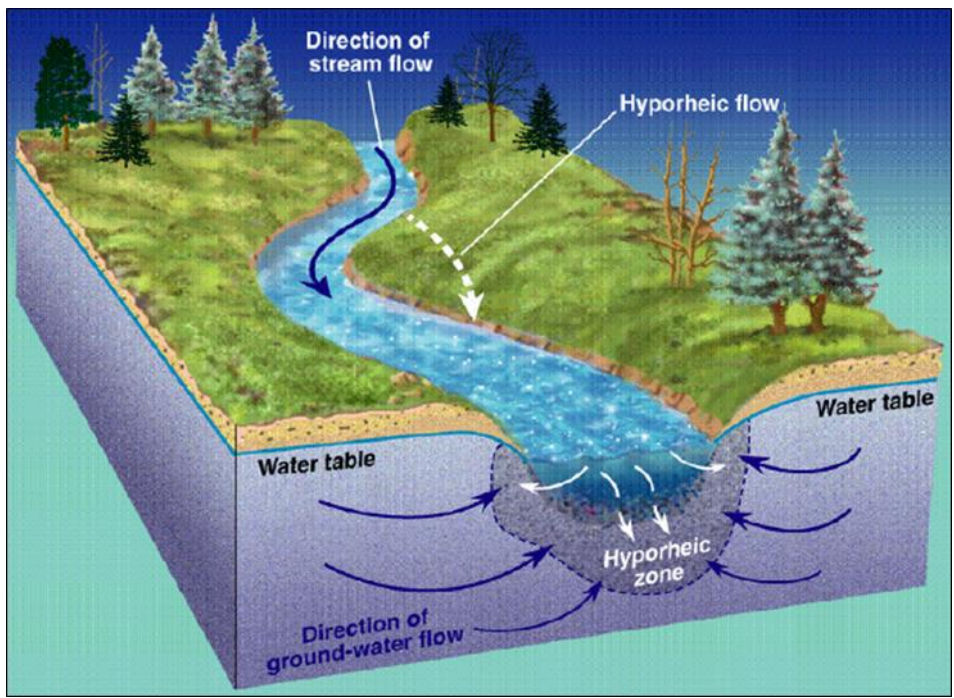


Figure 5: Hyporheic Zone (Buss et al., 2009).

## CHAPTER 3

### DESCRIPTION OF THE STUDY AREA

#### 3.1. Physiography

The study area is located in Central Anatolia covering an area between 32.583<sup>0</sup>-32.567<sup>0</sup> E longitude bands and 40.370<sup>0</sup>-40.362<sup>0</sup> N latitude bands. The study was carried out along a 2 km long reach of Kirmir Stream, near Çeltikçi town which is in the vicinity of Kızılcahamam (Figure 6). Kızılcahamam is situated 50 km northwest of the Ankara province. Access to the study area is provided with Ankara – İstanbul TEM motorway. The creeks that originate from piedmonts of Işık Hill and Çiçekliyayla Hill on the north of the Kızılcahamam flow toward south and join the Hamam Stream. This stream continues to flow in northeast-southwest direction in the vicinity of the Doğanözü village where it is named as Kirmir Stream. Kirmir Stream is controlled by important water structures which are Akyar Dam, Eğrekkaya Dam and Doğanözü Dam. These dams provide water to Ankara Metropolitan Municipality.

The study area is surrounded by a steep and rugged topography. The villages located near the study area are Doğanözü, Doymuşören, Kızılca, Mahkemeağcın, Demirciören, Değirmenönü, Çavuşlar, and Binkoz. Elevation ranges between 760 m and 780 m along Kirmir Stream. Along the floodplain of the Kirmir Stream, alluvial soil occurs and irrigated farming and forage areas are seen.

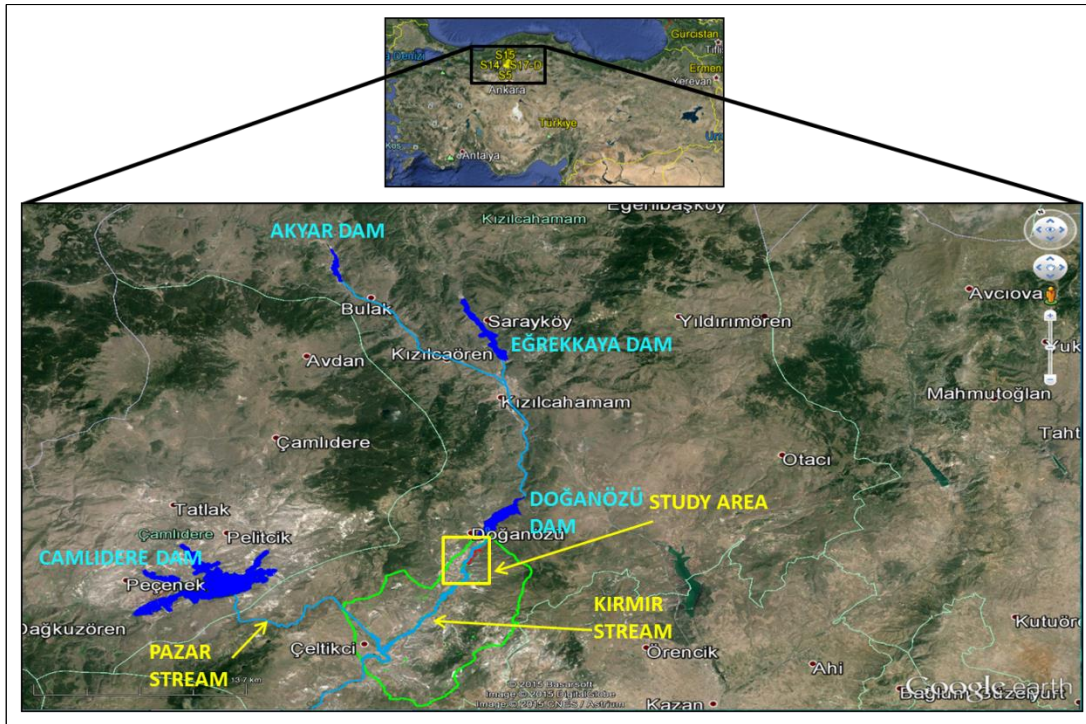


Figure 6: Regional view of the study area.

Along the study area, a total of 14 monitoring locations were identified to investigate groundwater - surface water interaction (Figure 7). Monitoring locations start from the downstream of Doğanözü Dam and they were named as S1-P, S2-P, S3-P, S4-P, S6-P, S7-P, S9-P, S10-P-B, S12-D, S13-D, S14, S15, S16-D and S17-D. Location names including P, D letters separately, indicate the stops where piezometers were installed and discharge measurements were performed respectively. In monitoring locations S3-P and S6-P, both piezometers were installed and discharge measurements were taken. S1-P is the most upstream and S17-D is the most downstream site of the study area and the exact distance between these locations is 2.1 km. As moving downstream within the study area, the number in the location name increases.



Figure 7: Position of monitoring locations in the study area.

### 3.2. Previous Studies

Limited hydrological and hydrogeological studies were performed near the study area in the past years. Geological maps of 1/100.000 and 1/25.000 have been created by General Directorate of Mineral Research and Exploration (MTA). However, detailed geologic studies about the area have been performed by Asia Minor Mining (2015) and Rojay (2013). Akarsu Engineering and Consultancy Co. Ltd prepared the planning report of the Doğanözü Dam which was constructed at the upstream of the Kirmir Stream by V. Regional Directorate of State Hydraulic Works. In addition to this study, three wells were drilled in the alluvium of the Pazar Stream to provide water to the Çeltikçi town by Bank of Provinces. The first hydrogeological study in the Çeltikçi region was performed within the scope the project “Hydrogeological Investigation and Characterization of the Çeltikçi Coal Basin” (Yazıcıgil et al., 2014). Monitoring and pumping well installations, aquifer tests, monitoring and



sampling of surface and groundwater have been conducted for this study. Also, latest study which is “The Development of Groundwater Flow Model, Dewatering Design Construction and Evaluation of Potential Impacts to Groundwater” about the region again conducted by Yazıcıgil et al. (2015). The latter is a follow up of the previous one. In addition to monitoring and sampling of groundwater, hydrogeological numerical model was constructed for dewatering for the coal mine which is planned to be constructed in following years.

### **3.3. Climate**

The study area which is in the Central Anatolian Region is characterized by the continental climate. Also, since the study area is close to the Black Sea Region, its moisture content is higher compared to the city of Ankara. According to Thorntwaite Climate Classification performed by Turkish State Meteorological Service (MGM), the climate of the area is classified as semi-arid and mesothermal. In this type of climate, summer months are hot and dry, winter months are cold and snowy. The majority of the total rainfall occurs in winter, spring and fall seasons in the area.

There are several meteorological stations close to the study area. Kızılcahamam meteorological station has long term and continuous data and hence, it gains more importance with respect to other stations. Also, Binkoz meteorological station was established by İKA Mining Inc. in the Binkoz village and it has collected meteorological data since 23 May 2013. In this station, average wind speed, average wind direction, air temperature (average, minimum and maximum), relative humidity (average, minimum and maximum), dew point temperature (average, minimum and maximum), barometric pressure (average, minimum and maximum), solar radiation (average, minimum and maximum), total rain and evapotranspiration values have been recorded for 10 minute intervals. According to long term precipitation measurements of Kızılcahamam station (1957-2014), December is the wettest and August is the driest months. Precipitation generally occurs between December and May, that is, in winter and spring months. July, August and September are the driest

months. Also, temperature values vary seasonally in the region. In summer, monthly average temperature values occur in the range between 20 - 25°C and maximum values can exceed 35°C. In winter months, monthly average temperature values vary between -2°C and 5°C. From October to May, temperatures may be under the freezing point. Especially, in months January and February temperatures may fall down to -15°C in the area.

### **3.4. Surface Water Resources**

The creeks that originate from piedmonts of Işık Hill and Çiçekliyayla Hill on the north of the Kızılcahamam flow toward south and join the Hamam Stream. This stream continues to flow in northeast-southwest direction in the vicinity of Doğanözü village where it is named as Kirmir Stream. The study area is located at the upstream part of the Kirmir Stream. Another important surface water unit near Çeltikçi town in the vicinity of Kızılcahamam is the Pazar Stream. It flows from the northern side of the Çeltikçi town toward south and joins Kirmir Stream. They have approximately 2000 km<sup>2</sup> catchment area near Çeltikçi town. Both Kirmir and Pazar Streams are controlled by important water structures. Kirmir Stream is controlled by 3 dams which are located at the upstream reaches of the study area. These are Akyar, Eğrekkaya and Doğanözü dams. Also, Pazar Stream is controlled by Çamlıdere Dam which is the largest water body with its 1226 hm<sup>3</sup> reservoir volume in the area. All dams are used for potable water supply by the Ankara Metropolitan Municipality.

Within the scope of the research conducted by Yazıcıgil et al. (2014) in Çeltikçi town, surface water monitoring points were determined along Kirmir Stream, Pazar Stream and the creeks which discharge into Kirmir Stream. In these monitoring points, monthly instantaneous flow rates have been measured. According to this research, stream flow was affected from the operation of dams. For example, after Eğrekkaya Dam started to hold water (1992), flow rates showed slight increase despite the significant amount of precipitation. Especially, with the operation of Akyar Dam (2001) and Doğanözü Dam (2012), decrease in flow rates became more

evident. Also, Yazıcıgil et al. (2015) stated that flow rates show seasonality. In spring months between February and May, flow rates increase because of snow melting. In summer months between June and September, generally lower flow rates are observed.

### **3.5. Geology**

#### **3.5.1. Regional Geology**

The study area is located on the southern margin of a volcanic terrain which is known as “Galatian Volcanic Province” (GVP) (Figure 8). GVP remains in between Cretaceous accretionary prism and North Anatolian Fault Zone (NAFZ). GVP is surrounded by the north of Cretaceous accretionary prism and to the south of seismogenic North Anatolian master Fault Zone, totally within Pontides, along the “Çeltikçi graben” (Öngür, 1977). These volcanic products were named as “Kızılcahamam volcanics” or “Köroğlu volcanics” (Türkecan et al., 1991). However, “Galatian Volcanic Province” is a more appropriate name in terms of tectonic setting (Toprak et al., 1996).

In the region, pre-Miocene aged rock units are pre-Triassic metamorphics, Triassic Complex, Jurassic-Cretaceous Atlantic type margin sequences, Upper Cretaceous-Paleogene ophiolitic mélange with Upper Cretaceous-Paleogene forearc volcano-sedimentary sequences and piggyback to peripheral Eocene basins (Koçyiğit et al., 2003). Miocene clastics and volcanics unconformably overlie these pre-Miocene units. Also, Miocene aged lavas and volcaniclastics of GVP are overlain by Miocene sequences. Lastly, Quaternary deposits unconformably overlie all the units.



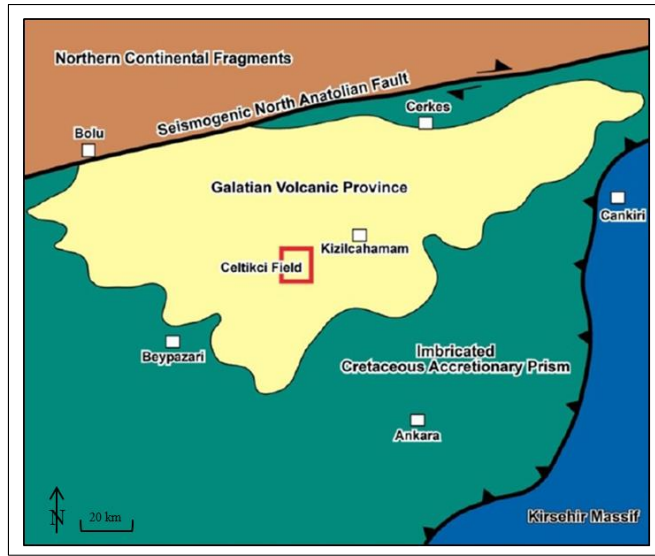


Figure 8: Regional geology of the area – Galatian Volcanic Province (Rojay, 2013)

### 3.5.2. Local Geology

The units exposed around the study area are classified as basement volcanics, Çeltikçi formation, Plio-Quaternary units, and Quaternary alluvium from bottom to top. Çeltikçi formation is divided into seven units. These are, from bottom to top, Bostantepe, Lower Çavuşlar, Upper Çavuşlar, Abacı, Kocalar, Aktepe and Bezci units (Figure 9). Çeltikçi group displays unconformable relationships in various parts of the Galatian Volcanic Province.

Study area only composes limited part of the entire area shown on Figure 10. Basement volcanics, Upper Çavuşlar unit, Kocalar unit, Plio-Quaternary units and Quaternary alluvial deposits are the only geological units that are observed in the study area.

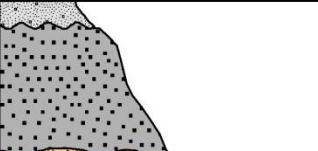


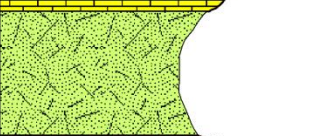

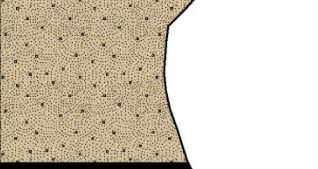

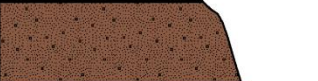


AGE	UNIT		THICKNESS (m)	LITHOLOGY	DESCRIPTION
	GROUP	FORMATION			
Quat.	Alluvium				Fluvial Deposits
Plio-Quaternary	Talus to fan deposits		>200		Fault-controlled continental deposits in the form of talus to alluvial fan.
Miocene	ÇELTIKÇI	Bezci	>60		Reddish to brown, thick bedded, continental clastics.
		Aktepe	~70		Cream to brown, moderately silicified limestone.
		Kocalar	170		Cream to light green, massive to faintly laminated claystone, mudstone and siltstone alternation.
		Abacı	40		Cream to light gray ignimbrite.
		Upper Çavuşlar	275		Cream to light green, massive claystone alternating with light brown to cream, well laminated bituminous shale.
		Coal (lignite) member			Coal (lignite) member
		Lower Çavuşlar	110		Dark brown, thin bedded, moderately to highly silicified claystone including immature coal seams and alternation of oolitic layers-varves.
	Bostantepe	70		Light gray to green sandstone and conglomerates with fragments derived from volcanic rocks.	
	Volcanic Basement	>400		Dark colored, massive, andesitic-basaltic lava flows and pyroclastics.	

Figure 9: Generalized columnar section in the local geology (AMM,2015)

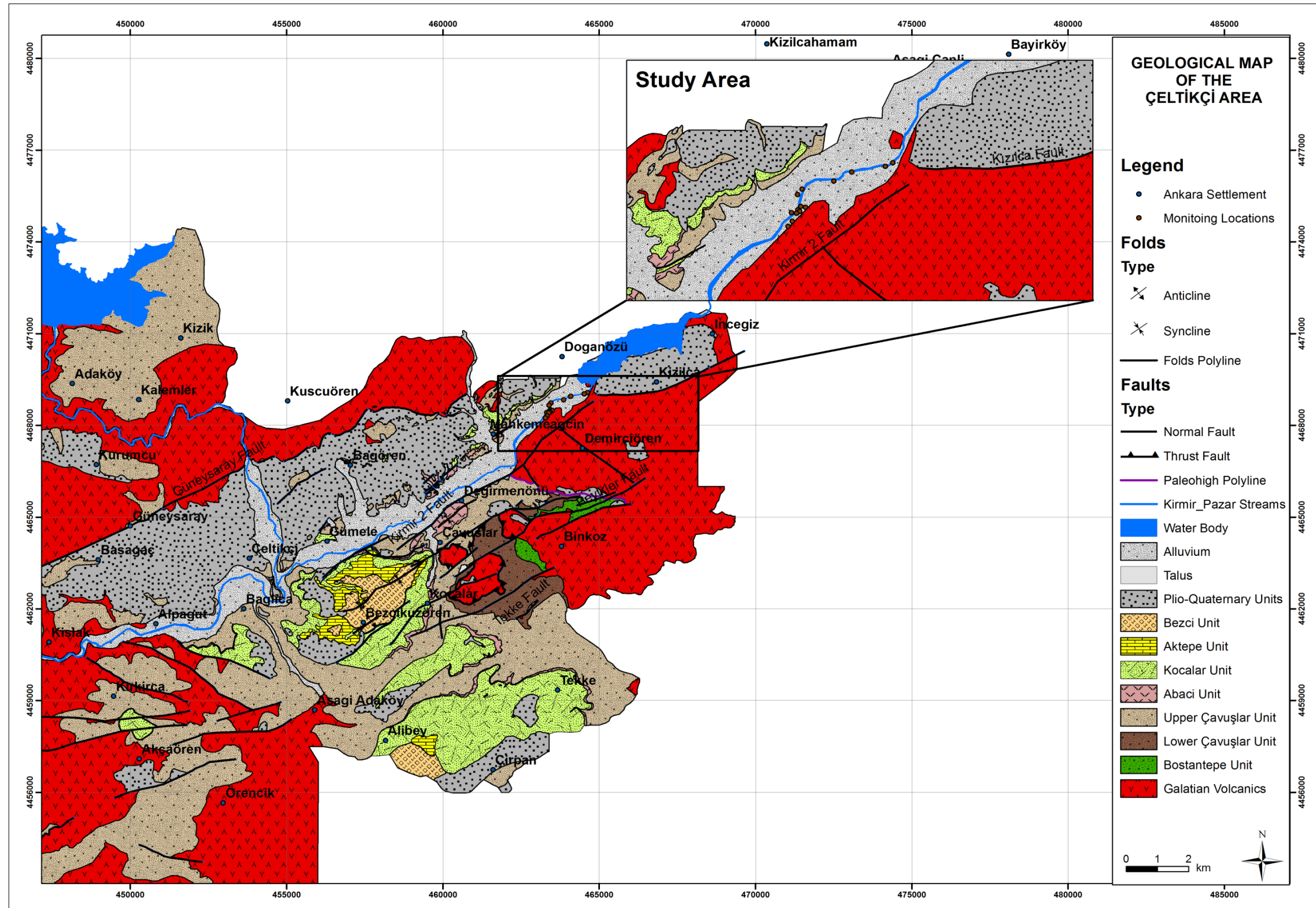


Figure 10: Geological map of the study area (AMM, 2015).



### **3.5.2.1. Basement Volcanics**

Volcanic rocks are the oldest units in the area and form the basement. They overlie pre-Miocene rocks unconformably and they are overlain by Çeltikçi formation. In some parts, Lower Çavuşlar unit overlies basement volcanics; however, in some parts Bostantepe unit overlies them. Lithologically, volcanic rocks composed of lava flows, tuffs, and pyroclastics of andesitic to andesitic-basaltic composition. Total thickness of this sequence is more than 400 m in the northern sectors of the Çeltikçi town along Pazar stream valley. The pyroclastics are jointed and highly porous media so groundwater is transmitted along them but they can not hold water (Rojay, 2013). The lavas mostly display impermeable horizons. However, in highly jointed parts, they show permeable characteristics.

### **3.5.2.2. Çeltikçi Formation**

#### **3.5.2.2.1. Bostantepe Unit**

Bostantepe unit is the lowermost member of the Çeltikçi formation. It is exposed as two large outcrops in the eastern side of the map. This member overlies the basement volcanics and underlies Lower Çavuşlar unit. Its thickness varies from place to place. In some parts, this unit shows thickness more than 100 m. Bostantepe unit is a large fan deposited at the basal part of the Çeltikçi group. It is characterized by fine to medium grained clastic sedimentary rocks. The dominant lithology is sandstones.

#### **3.5.2.2.2. Lower Çavuşlar Unit**

Lower Çavuşlar unit overlies Bostantepe and underlies Upper Çavuşlar unit. It is composed of alternating oolitic limestone, thin bedded immature coal seams and tuff layers, moderately to highly silicified chert layers from bottom to top. The silicified levels occur as lenses and layers of silica in the formation due to intense volcanic activity and faulting (Rojay, 2013). Therefore, the silica is present in the system as

primary (layers and lenses) and secondary (results of volcanism and faulting). Total thickness of this member is about 110 m.

#### **3.5.2.2.3. Upper Çavuşlar Unit**

Upper Çavuşlar unit conformably overlies Lower Çavuşlar unit and overlain by Abacı unit. This member is the most widespread unit in the area. Its total thickness is approximately 250 m. In Upper Çavuşlar unit, a coal member is observed. This member is composed of alternation of coal layers and marl. The thickness of it ranges approximately between 12.0 m to 27.5 m with an average of 21 m. In some places, the coal seam is exposed to the surface. Additional to coal seam and marl alternation, claystone and marl alternation is dominant lithology in Upper Çavuşlar formation.

As a whole, Çavuşlar unit is deposited in a lacustrine environment and evolved in swampy conditions collaborated with andesitic volcanism (Rojay, 2013).

#### **3.5.2.2.4. Abacı Unit**

This unit is a single ignimbrite (tuff) layer stratigraphically located in the middle of the Miocene lacustrine sequences between underlying Çavuşlar and overlying Kocalar units. Its thickness around the study area is about 40 m. This unit is composed two parts. First one is the lower, impervious, massive ignimbrite and the second one is the upper, compacted fine grained tuff layer. The lower part is made up of light to cream generally non-welded ignimbrite. Abacı unit overlies Çavuşlar unit (Upper Çavuşlar) with a sharp contact and gradational to overlying the Kocalar unit. Thick, green colored tuffaceous sandstone is deposited above Abacı unit. The upper contact is transitional part of this member to upper clastic sequence. Cross bedding can be observed within the sandstones.

#### **3.5.2.2.5. Kocalar Unit**

Kocalar unit conformably overlies Abacı and overlain by Aktepe units. The thickness of the unit is about 150 m. It includes beige-cream coloured mudrocks with sandstone beds and tuff layers. The upper part is dominated by beige-light gray to white coloured, thick bedded, highly porous limestones and dolomitic mudrocks with silica lenses of Aktepe unit (Rojay, 2013). Kocalar unit is deposited in a high silica compositional lacustrine environment.

#### **3.5.2.2.6. Aktepe Unit**

Aktepe unit conformably overlies Kocalar and underlies Bezci units. It is composed of beige-cream coloured carbonates at the bottom and continuous with beige-light gray to white colored, thick bedded, highly porous limestones-dolomitic mudrocks bearing silica nodules and lenses. Lithostratigraphically Aktepe member is correlative with the Upper Miocene limestones in Central Anatolia (Rojay, 2013).

#### **3.5.2.2.7. Bezci Unit**

This formation is the youngest unit of Çeltikçi formation. It conformably overlies Aktepe unit. On the other hand, its upper boundary is exposed to the erosion and has unconformable boundary with Plio-Quaternary units. Bezci unit is composed of pinkish red colored bedded clastic rocks. It is observed from highly elevated areas to river bottom. Sandstones-siltstones and conglomerates are common lithologies in this unit. Thin limestone layers are also observed in the sequence. Total thickness reaches up to 60 m.

#### **3.5.2.3. Plio-Quaternary Units**

Plio-Quaternary units and Bezci unit of formation are lithologically similar. Because of this they can easily be confused with each other. Plio-Quaternary units are

associated with faulting. They are talus to fan type deposits derived from the upthrown block and deposited over the downthrown blocks of the fault. They generally form a gentle topography. As in Bezci unit, these units are observed in highly elevated areas to recent river bottom. Sandstones-siltstones-conglomerates with some limnic-organic horizons are the common lithologies. Plio-Quaternary age is assigned to these units since they were deposited under the control of recent normal faulting in the region.

#### **3.5.2.4. Quaternary Alluvial Deposits**

Relatively old Quaternary units are elevated river terraces. These river terraces are composed of horizontally lying, well rounded, poorly sorted dominantly volcanic cobble bearing conglomerates. They are situated at 80 m above the Kirmir Stream unconformably on top of Plio-Quaternary clastics. Recent alluvial fans, recent alluvium, talus are the present day units deposited in the channels of the present day drainage system mainly along the Kirmir Stream and the margins of Kirmir Stream valley.

#### **3.5.2.5. Structural Geology**

Structures identified in the vicinity of the study area are Paleo-high fault, thrust faults, normal faults, Kocalar monocline, Peyikler front, folding and bedding.

##### **3.5.2.5.1. Paleo-high Fault**

Paleo-high fault represents the oldest structure in the area. This fault is observed in the 3.5 km southwest of Demirciören village (Figure 10). Paleo-high boundary constitutes the contact between the basal parts of the Çeltikçi formation and volcanic units. The boundary extends in E-W direction for a length of 4.34 km.



### **3.5.2.5.2. Thrust Faults**

Thrust faults and associated structures are common features in the area. Five large scale thrust faults mapped in the area can be seen in the geological map (Figure 10). Thrust faults which are of Early-Middle Miocene age cut Çeltikçi formation and, they are cut by normal faults which are of Plio-Quaternary age (AMM, 2015).

### **3.5.2.5.3. Normal Faults**

Most of the normal faults observed in the area are located in the southern part of the “Çeltikçi Graben” (Öngür, 1977). The major faults that shape the area are on southern block of the graben and are named as Kirmir 1, Kirmir 2, Karataş, Peyikler, Bezci 1, Bezci 2, Kocalar, Binkoz 1, Binkoz 2, Çavuşlar, Dumanlar, Tekke, Ortaca, Aladağ, Demirciören and Kızılca faults; also, Güneysaray, Bağören, Abacı and Mahkemeağacın faults are located over the northern block (Asia Minor Mining, 2015). Kirmir 1, Kirmir 2, Karataş, Peyikler, Bezci 1, Bezci 2, Binkoz 1, Binkoz 2, Dumanlar, Tekke, Ortaca, Aladağ, Kızılca, güneysaray, Bağören, Abacı and Mahkemeağacın faults strike NE-SW direction. On the other hand, Kocalar fault, Çavuşlar fault and Demirciören fault strike N-S, E-W and NW-SE directions respectively. Most of the normal faults are steeply dipping towards NW.

### **3.5.2.5.4. Kocalar Monocline**

Kocalar monocline which is trending almost in N-S direction is located between Kocalar and Çavuşlar villages and it divides the area into two distinct regions as the east and west. Two basic differences between these two regions are as follows (Asia Minor Mining, 2015):

- The eastern part is characterized by thrust faults and its associated structures. On the other hand, no thrusting is observed in the western part of the area.
- The oldest units are exposed in the eastern part and this points out uplift and erosion of younger units in this side of Kocalar monocline. However, the

western part includes the youngest units of Çeltikçi formation such as Aktepe and Bezci units.

#### **3.5.2.5.5. Peyikler Front**

A large scale overturned structure is observed in the area from Peyikler in the east to almost paleo-high boundary to the west (AMM, 2015). This structure is characterized by a southerly dipping steep, overturned and a northerly dipping, gentle, upright limbs. The southern part of the structure is totally elevated. Because of this, it is named as “front”. The front extends more than 3 km in NE-SW direction.

#### **3.5.2.5.6. Folding**

There are three folds in the area. They are all observed in the southern part of Kirmir Stream (Figure 10). All the axes of folds trend in NE-SW direction, they are parallel to the strike of thrust faults. All folding were developed in Çeltikçi formation.

#### **3.5.2.5.7. Bedding**

A total of 1027 measurements were analyzed by AMM (2015) and two dominant concentrations ( $322^{\circ}/17^{\circ}$  and  $170^{\circ}/13^{\circ}$ ) were identified. There is an almost symmetric and non-plunging folding in the area.

### **3.6. Hydrogeology**

The volcanic rocks consist of Miocene aged andesitic, andesitic-basaltic lavas and pyroclastics and they are exposed over large areas within and outside the study area. Along fractures and cracks occurring in these units, water is transported. They show the confined aquifer behavior in the area to the west of Kocalar monocline. Also, these units have free flow conditions at some locations in Kimir stream. In addition, volcanic units occurred at large areas on the eastern side of the Kocalar monocline

near the Binkoz village behave as an unconfined aquifer at this side (Yazıcıgil et al., 2015).

As explained in section 3.5.2, volcanics are overlain by Bostantepe units and Bostantepe units are overlain by Lower and Upper Çavuşlar units respectively. All these units carry water also. In the area on the western side of the Kocalar monocline, they behave as confined aquifer. Furthermore, in the area on the eastern and southern sides of the Kocalar monocline they show unconfined aquifer properties. Due to the sharp changes in the topography, free flow conditions are also observed. These units are overlain by the Abacı ignimbrite at the western side of the Kocalar fault. A massive silicified ignimbrite layers underlying the Abacı ignimbrites form an impervious layer over the Upper Çavuşlar units at the western side of the monocline and cause to develop a confined aquifer together with underlying volcanics. This aquifer system is known as lower aquifer system (Yazıcıgil et al., 2015).

In the western side of the Kocalar monocline, Kocalar units including mudrocks of having sandstones and tuffaceous layers, Aktepe units having limestones and dolomitic mudrocks, Bezci units consisting of sandstones and siltstones form an unconfined aquifer in a synclinal basin. This unconfined aquifer is defined as upper aquifer system (Yazıcıgil et al., 2015).

Quaternary aged alluvium occurring along Kirmir and Pazar streams forms an unconfined aquifer. However, because of its shallow thickness (20 m – 25 m) and limited spatial extent, this aquifer is a weak aquifer system (Yazıcıgil et al., 2015).



## CHAPTER 4

### METHODS

#### 4.1. Measurement of Water Skin Temperatures Using Thermal Camera

Each object emits a certain amount of radiation depending on its temperature, that is, when the temperature of the object changes, the intensity of the radiation changes. Thermal infrared radiation refers to electromagnetic waves with a wavelength between 3.5  $\mu\text{m}$  and 20  $\mu\text{m}$ . Thermal remote sensing deals with the thermal infrared (TIR) region of the electromagnetic (EM) spectrum and radiations emitted from surface of the target (Prakash, 2000). The intensity of infrared radiation emitted by each body depends on both temperature and the radiation features of the surface of the object. The emissivity is used as a constant factor describing the ability of the body to emit infrared energy compared to a black body of the same temperature. It ranges between 0 and 1. The emissivity of a black body and pure water is 1 and 0.96 respectively. By Stefan – Boltzman law the emissivity is explained as the ratio of the thermal radiation from a surface to the radiation from an ideal black surface at the same temperature. Stefan – Boltzman equation is:

$$M_R = \varepsilon\sigma T^4 \quad (14)$$

where  $M_R$  is total emitted radiation,  $\sigma$  is Stefan – Boltzman constant which is  $5.6697 \times 10^{-8} \text{ Wm}^{-2}\text{K}^{-4}$  and  $T$  is temperature.

The surrounding environment affect the precision of temperature measurements performed by thermal camera, because emitted radiation transmits temperature from both the stream itself and reflected radiation from the surrounding environment. Also, flowering plants lead to detection of lower temperatures than expected by affecting emissivity. Furthermore, suspended sediments in the surface water are the most common pollutants and their concentration and type influence the emissivity. Liu et al. (1987) measured the thermal emissivity of water while varying the suspended sediment concentration between zero and the significantly high values. They found that as sediment concentration increases, spectral emissivity decreases and occurs within 8 – 14  $\mu\text{m}$  waveband.

As mentioned, there exist a variety of methods to understand groundwater and surface water interaction. Application of traditional methods in the investigation of this concept could potentially need an intensive effort. Also, the effects of interaction can change spatially and temporally. Methods based on thermal and physical properties can provide an efficient characterization of the exchange processes. Groundwater has a predictable thermal signature and this can be used to locate groundwater discharge zones to surface water. One of the methods providing direct information is remote sensing measurements collected with thermal infrared (TIR) cameras. TIR data collection can quickly capture the discharge zones. Remotely sensed thermal images provide spatially distributed measurements of the radiant skin temperature of streams. For detection of groundwater discharge zones into the stream by a thermal camera, the hot (cold) spots during winter (summer) should be visible on the skin of the surface water.

At the beginning of the research, Kirmir Stream was investigated by thermal camera starting from upstream (Doğanözü Dam) to obtain a pre-perception about the area. With this investigation, potential groundwater discharge zones were tried to be captured by thermal camera and the broad extend of the study area was determined. The other field methods mentioned in following sections were applied after this investigation. In this study, Optris IR Camera PI160 having 160x120 resolution was

used to identify groundwater discharge zones in Kirmir Stream (Figure 11). At first, the software PI Connect was installed from the CD including the software application and the specific calibration data of the imager. After installation of the software, infrared imager can be connected into an USB port (USB 2.0) of the PC and live image of the camera can be seen inside a window on the PC screen. In the software window the following parts are available and all are shown in Figure 12:

1. An TIR image from the thermal camera.
2. Temperature profile showing the temperatures along maximum two lines at any size and position in the image.
3. Reference bar showing the scale of temperature within color palette.
4. Temperature of the measurement area. The measurement area can be rectangle, ellipse, polygon or curve optionally. This analyses the temperature depending on the measurement area. The temperature value can be seen both in the TIR image and the control displays.
5. Control displays showing the all temperature values in the areas like cold spots, hot spots, temperature at cursor, internal and chip temperature.
6. There exits a bar showing the defined temperature thresholds for both low (blue arrow) and high (red arrow) alarm value. The color of numbers within control varies to red and blue depending on whether the temperature value is below the low alarm value or above the high alarm value.
7. A histogram displays the distribution of temperature values.
8. Automatic and manual scaling of the palette.

9. Icon providing a quick access to image subtraction function.

10. Icon enabling switching between color palettes.

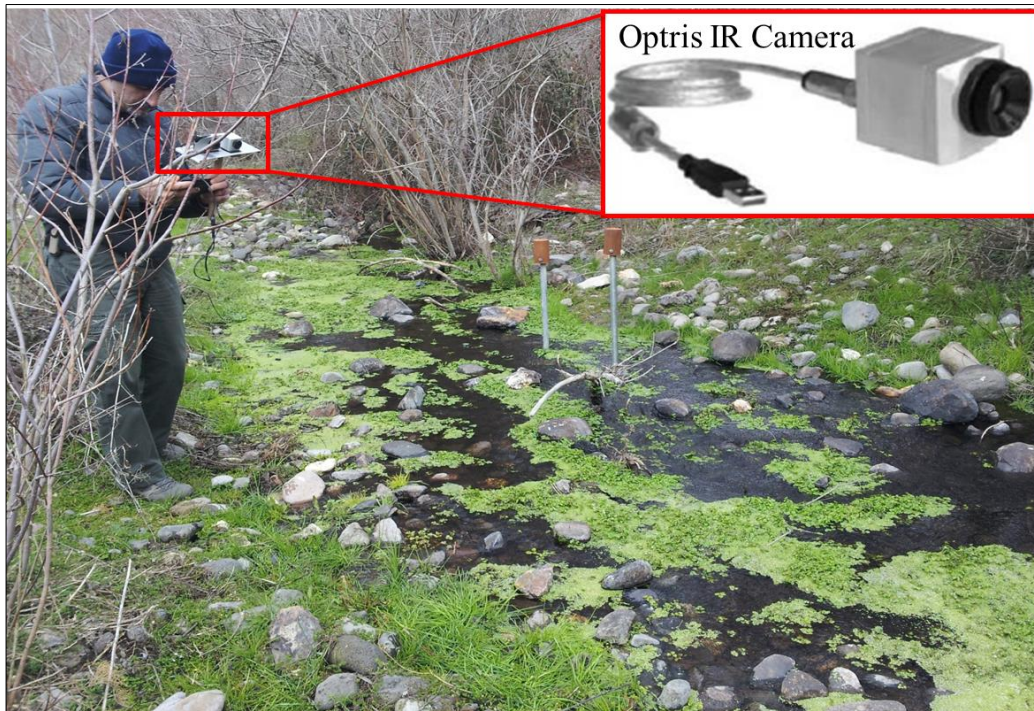


Figure 11 : Application of thermal remote sensing by Optris IR Camera PI160 in the study area. There is a thermal camera and a visible camera mounted on the platform.



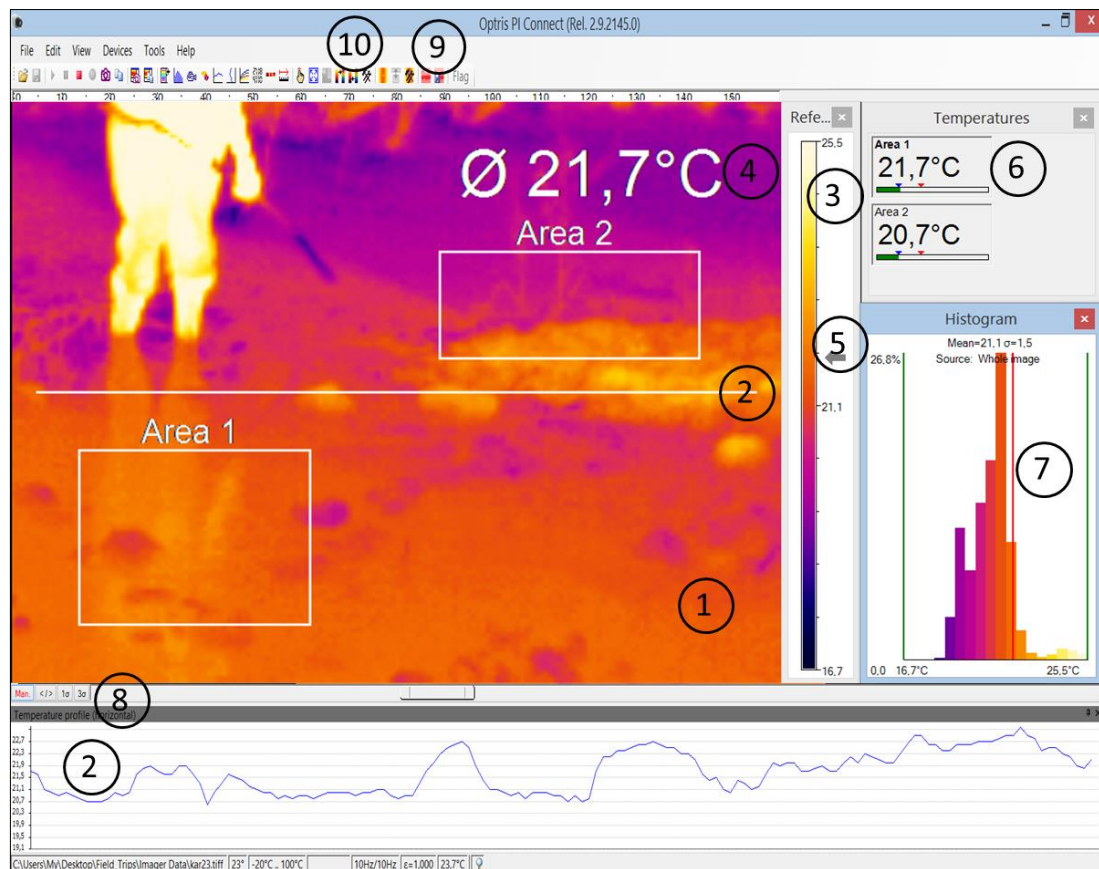


Figure 12: Optris IR Camera Software window

#### 4.2. Nested Piezometers

A total of 16 piezometers (7 piezometer nests and 2 separate piezometers) were installed using sledge hammer along the banks of the stream in order to obtain hydraulic gradient information (Figure 13b). Each piezometer consist of stainless steel pipe with 32 mm inner diameter, a perforated section and piezometer tip at the bottom (Figure 13a). The shallow piezometers have 185 cm length, but length of deep piezometers change between 270 cm to 285 cm depending on the locations. Shallow and deep piezometers installed in S1-P were schematically shown in Figure 14 as a reference. The sites where piezometers were installed in the study area, their lengths, installation depths in the streambed and the depth of screen center of each

piezometer are given in Table 1. Screen ranges and the length of tip of each piezometer are not the same. Depth to screen middle values in Table 1 were calculated by taking into account of each piezometer's own screen range and length of tip. All piezometers are in the hyporheic zone of the streambed.

First of all, in sites S4-P, S6-P, S7-P and S10-P-B shallow and deep piezometers were installed on 25<sup>th</sup> of September 2014 and 16<sup>th</sup> of October 2014 respectively. The sites S1-P, S2-P, S3-P and S9-P were defined as piezometer locations on the date 21<sup>th</sup> of November 2014 and piezometers were installed in these locations on the same date. In site S9-P, two deep piezometers were used, because this site is a pond which is full of reeds. These deep piezometers were placed at the opposing sides of this pond.

Water level measurements for all piezometers were performed between dates 16<sup>th</sup> of October 2014 and 19<sup>th</sup> of November 2015 biweekly by Solinst Model 107 TLC Meter (Figure 15b). It has 19 mm diameter probe which is attached to Solinst PVDF flat tape. This also measures temperature and conductivity (range of conductivity measurement is 0 – 80,000  $\mu\text{S}/\text{cm}$  and accuracy is 5%). Before measurement of conductivity, a two point calibration (1413 $\mu\text{S}/\text{cm}$  and 5000 $\mu\text{S}/\text{cm}$ ) is performed. On 16.01.2015 piezometers were purged to prevent a potential plugging. For this date, water level measurements were not taken.

Table 1: Length of piezometers, depth of piezometers in the streambed and depth to screen middle of each piezometer for each installation location.

<b>Site</b>	<b>Type</b>	<b>Length (cm)</b>	<b>Depth of Piezometer (cm)</b>	<b>Depth to Screen Middle (cm)</b>
S1-P	Deep	270	179	147
	Shallow	185	100	69
S2-P	Deep	270	182.5	150.5
	Shallow	185	97.5	66.5
S3-P	Deep	270	184	152
	Shallow	185	99.5	68.5
S4-P	Deep	280	198.5	162.5
	Shallow	185	102	56
S6-P	Deep	280	190.7	154.7
	Shallow	185	101	55
S7-P	Deep	280	192.5	156.5
	Shallow	185	100	54
S9-P	Deep	285	207	176
	Deep	285	177	146
S10-P-B	Deep	280	185.5	149.5
	Shallow	185	104.5	58.5

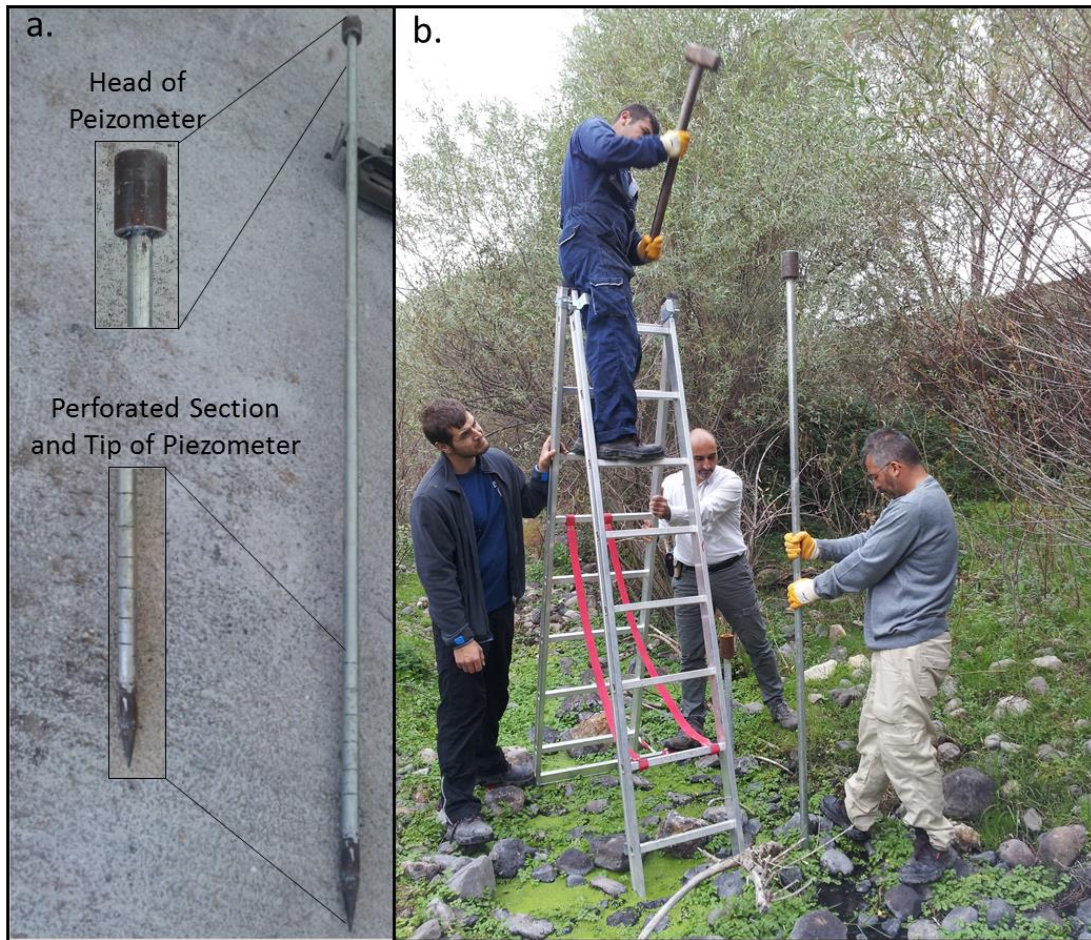


Figure 13: a) Perforated section, tip and head of the piezometer used in the study. b) Installation of an piezometer by sledge hammer in the field.

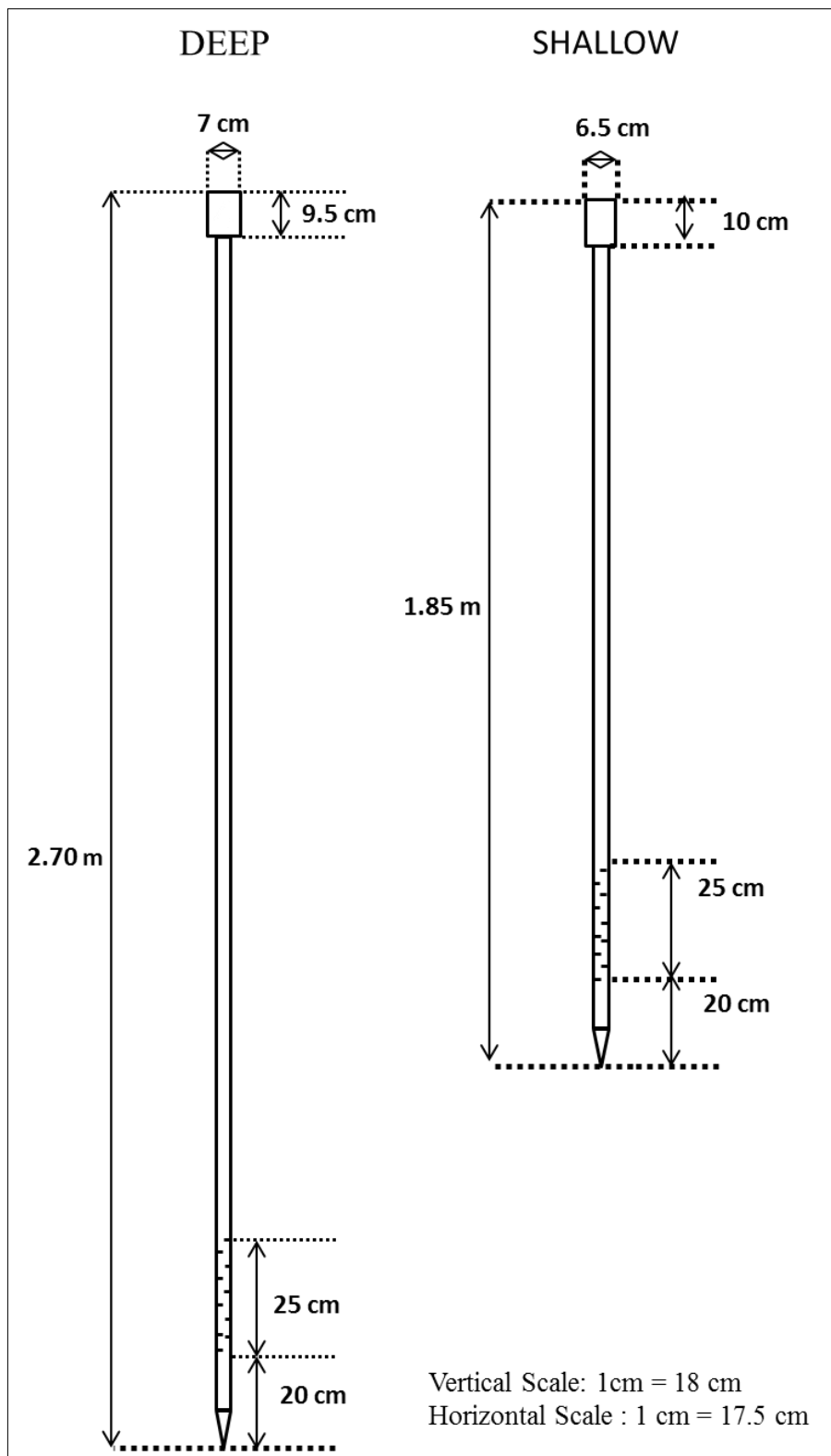


Figure 14: Drawing of nested piezometers in site S1-P in terms of their sizes.





Figure 15: a) Nested piezometers and measurement of height of the piezometer above ground b) Measurement of water levels inside the nested piezometers by Solinst TLC Meter.

Measuring the water level inside wells and piezometers installed in the fluvial plain is standard method to determine hydraulic head (Freeze & Cherry, 1979). A positive or negative value of the vertical hydraulic gradient indicates the direction of water flow within the streambed, that is, upwelling or downwelling (Schmidt et al., 2006). For this study, positive and negative VHG values indicate downwelling and upwelling movement respectively. Elevation of each piezometer location and depth to screen middle for each piezometer are known. Therefore, hydraulic head values and elevation head values were obtained using information of water level, elevation of installation location and depth to screen middle (Figure 16). Then, vertical

hydraulic gradient values were calculated using hydraulic head and elevation head. For nested piezometers the equation is as follows:

$$VHG = \frac{dh}{dl} \quad (15)$$

where VHG is the vertical hydraulic gradient,  $h$  is hydraulic head (m ) and  $l$  is elevation head (m).

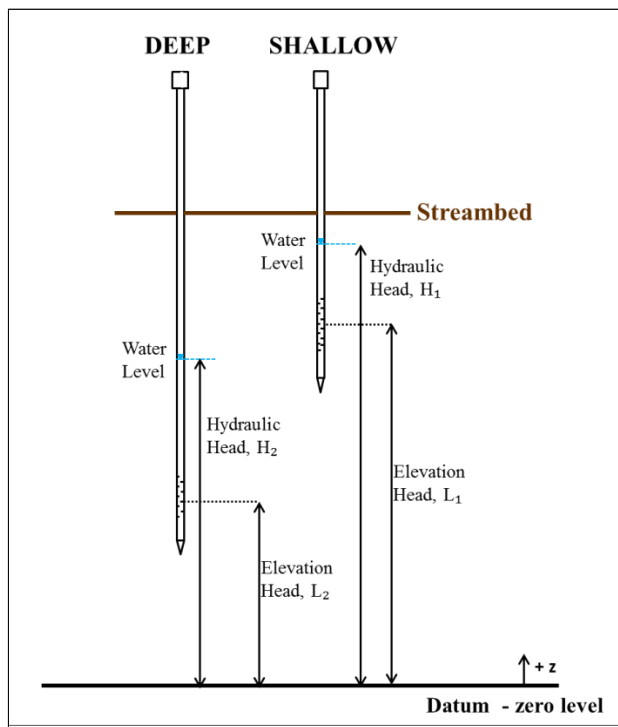


Figure 16: Hydraulic and elevation heads in the nested piezometers.

For piezometers installed in S9-P location which are not nested, VHG values were calculated using the water level differences between groundwater and pond water level. Head differences between surface water and groundwater levels provide information about the direction of water movement between these two sources.

Vertical hydraulic gradient values of this site were calculated using the equation below (Dahm & Valett, 1996):

$$\text{VHG} = \frac{h_s - h_p}{L} \quad (16)$$

where,  $h_s$  is the distance from top of the piezometer to the stream surface (m),  $h_p$  is the distance from top of the piezometer to the water level inside the piezometer (m), and  $L$  is the depth of the middle of the screen section in the riverbed (m).

The piezometer method gives point measurements of hydraulic head. This method is more appropriate for small scale applications and allows a detailed investigation of the heterogeneity of flow conditions in the subsurface. However, groundwater movement is affected from temporal variations as well. Therefore, all hydraulic head measurements at a study site should be taken approximately at the same time so that the data only reflect the situation of that specific time. In this study, all water level measurements were performed within a day.

### **4.3. Stream Discharge Measurements**

Mass balance approaches can be used to understand any gain or loss of surface water. Measurements of streamflow discharge in successive cross sections allow the determination of the groundwater - surface water exchange by computing the differences in discharge between the cross sections.

Vertically averaged stream velocities were measured regularly bi-weekly between the dates 9<sup>th</sup> of September 2014 to 14<sup>th</sup> of September 2015 (totally 15 times) by FP111 Globe Water Flow Probe having 0.1-6.1 m/s range and 0.1 m/s accuracy. During the measurements, stream was divided into subsections depending on the width of it. The width of these subsections range between 5 cm to 40 cm for different monitoring locations within this study. After determining the width of each



subsection, the Flow Probe was moved vertically from surface to the bottom, up and down, slowly and smoothly at mid-points of each subsection until the average velocity was fixed. Then, the flow of each subsection was estimated as the product of the average velocity and cross sectional area. Once the flow of each subsection was obtained, the total streamflow at one cross section was calculated by adding all of the subsection flows.

First measurements were taken from the monitoring locations, S12-D, S13-D and S17-D. As study continues, S16-D was designated as another discharge measurement location because of stream morphology. Lastly, S3-P, S6-P and SW26 were added for better observation of gains and losses and to understand the groundwater contribution to Kirmir Stream. Sites S3-P and S17-D are located at the most upstream and downstream parts of the study area respectively. S12-D and S13-D are side by side as two separate river reaches and after a short distance they join and flow towards S16-D and S17-D. SW26 is located approximately 7 km downstream of S17-D and before this site so many tributaries join Kirmir Stream. SW26 is out of the boundaries of the study area. As a result, discharge measurements were taken regularly from locations S3-P, S6-P, S12-D, S13-D, S16-D, S17-D and infrequently from SW26. Change in discharge (L/sec) in each section with respect to time was observed, so that gains and losses to Kirmir Stream were understood. During comparison and analysis of flow values S12-D and S13-D were taken as a single stream reach, that is, their summation was taken into consideration. Evaluation of the results can be seen in detail in Section 5.3.



Figure 17: Measurement of discharge by FP111 Globe Water Flow Probe in monitoring location S17-D.

#### **4.4. Water Flux Calculations**

Vertical fluid flow was calculated using the temperature time series method developed by Hatch et al. (2006) and Keery et al. (2007). This method is based on the measurement of temperature values in streambed at different depths for a period of time, that is, time series thermal data is used to determine streambed seepage rates. By quantifying changes in phase and amplitude of temperature variations between pairs of subsurface sensors, one dimensional vertical fluid flow – seepage flux is obtained (Hatch et al., 2006) (see section 2.2.2.1 for more details). Also, Hatch et al. (2006) emphasized that this method can be applied under a wide range of flow conditions regardless of streambed scour and sedimentation.

##### **4.4.1. Streambed Temperature Measurements**

Thermochron iButtons (model DS1922L-F5) were used as temperature sensors and data loggers. This model has a temperature range of  $-40^{\circ}\text{C}$  to  $+85^{\circ}\text{C}$ , an accuracy of  $\pm 0.5^{\circ}\text{C}$ , and a resolution of  $0.0625^{\circ}\text{C}$ . The iButtons have been used successfully in various previous studies for understanding groundwater-surface water interaction processes (Daniluk, Lautz, Gordon, & Endreny, 2013; Fanelli & Lautz, 2008; Gordon, Lautz, Briggs, & McKenzie, 2012; Hester, Doyle, & Poole, 2009; A. N. Johnson et al., 2005). Temperature loggers were placed into streambed at different depths. For this purpose, iron rods, PVC or wooden sticks can be used. Temperature loggers are mounted to one of these materials and then installed into the streambed to obtain diurnal temperature variations for a period of time. In different studies, different pipe materials have been used and investigated whether different materials do have an impact on temperature in the subsurface. According to Alexander et al. (2005), different tube materials such as steel and PVC do not have an effect on temperature measurements. Also, both wooden and iron probes were used and it was shown that the temperature profiles of two materials are nearly the same (Kerry, Binley, Crook, & Smith, 2007). At least two temperature loggers should be placed on a pipe to obtain the phase and amplitude changes of the temperature variations in

different depths, because from these differences vertical fluid flux values are calculated. The distance between the ibuttons is optional. It can be 5 cm, 10 cm or 15 cm etc and measurement time intervals range between 10 to 90 minutes. Also, the top ibutton in the pipe can come exactly the same level with the streambed surface or it can be placed a few or more cm below or above it. Depending on the purpose of the study (such as for numerical modeling), deeper sections of the streambed can be investigated and sensors can be placed below one meter.

First of all, ibutton installation locations were determined as S3-P, S4-P and S16-D in order to observe Kirmir Stream at the beginning, middle and at the end of the study area. In the light of information given above, temperature loggers were mounted on wooden sticks, having 30 cm length, 4 cm width and 2.8 cm thickness. Each stick included two ibuttons and lastly they were installed into streambed at determined locations. The procedure is as following and also can be examined in Figure 18:

1. i-buttons were placed into hollows opened in each stick.
2. Stainless steel washer was placed on to each i-button.
3. Then, i-buttons were wrapped by packing tape to prevent any movement and tape was perforated to allow the water entrance.
4. Lastly, they were installed into streambed as top ibutton remained 5 cm below streambed.

iButtons were left in the study area for three different period of times. In first measurement period, the distance between the top and the bottom ibutton was 15 cm, that is, the bottom ibutton was 20 cm below the streambed. In the second and the third installations, the distance between the top and the bottom ibuttons was reduced

to 10 cm, that is, the bottom i-buttons were 15 cm below the streambed. For each measurement period, streambed temperatures were recorded in every 15 minutes.

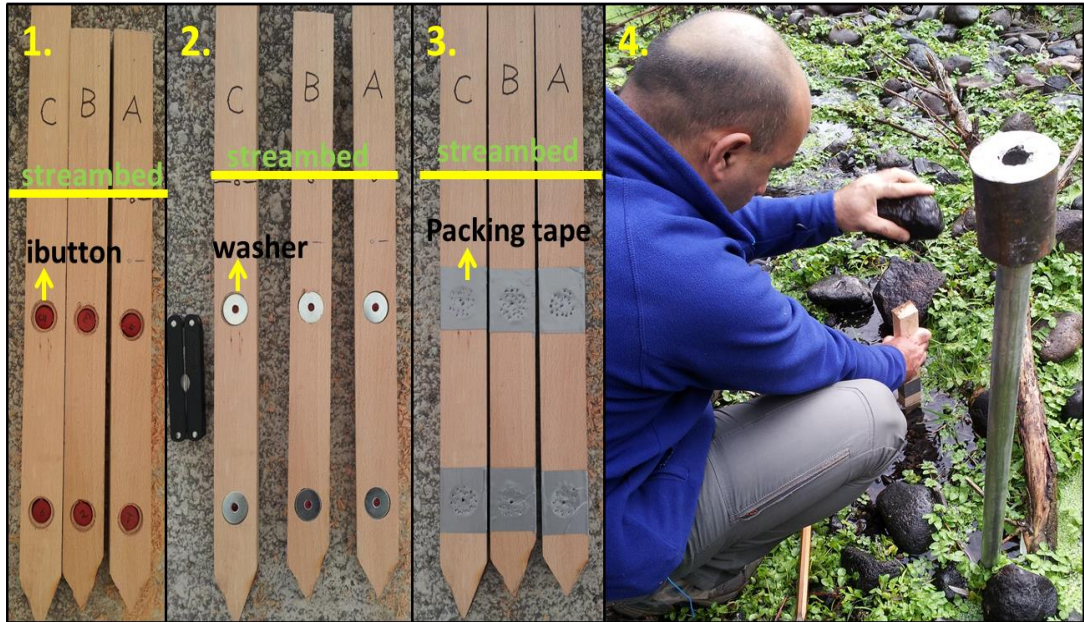


Figure 18: Preparation and installation of i-buttons.

Table 2: Streambed temperature measurement periods

Measurement Period	Time interval	Installation Site
1	12.03.2015 - 26.03.2015	S3-P and S4-P
	12.03.2015 - 27.04.2015	S16-D
2	10.07.2015 - 03.08.2015	S3-P, S4-P and S16-D
3	03.09.2015 - 14.09.2015	S3-P, S4-P and S16-D

Time interval of first measurement period is different for S16-D. Reservoir water was released from Doğanözü Dam on 26<sup>th</sup> of March. iButtons in S16-D could not be reached because of turbulent flow and they were left in the field for a longer period

of time. Temperature values corresponding to time intervals when reservoir water was released were ignored and whole data was divided into four parts (for more details see section 5.4.1). Evaluation of temperature data and the calculation of vertical fluxes given in Chapter 5 were performed in terms of these separate parts. Only four parts were taken into account.

#### **4.4.2. Calculation of Water Flux**

Water flux values were calculated using Hatch et al. (2006) method with the VFLUX program created in MATLAB environment by the authors. This program calculates vertical water fluxes by processing temperature time series collected from a single streambed vertical profile. Time series data should involve a column of recording times (in days) and a column of temperature values ( $^{\circ}\text{C}$ ) of each sensor (Table 3). Recording times should be evenly spaced and monotonically increasing. This program uses these time and temperature columns, the distance between temperature loggers, total porosity (volume of the pore spaces divided by the total volume – typical value is 0.28) and thermal properties of the sediment as inputs. Thermal properties of the sediment are dispersivity in meters (0.001 as typical value), thermal conductivity in  $\text{cal}/(\text{s}\cdot\text{cm}\cdot\text{C})$  (0.0045 as typical value), volumetric heat capacity of the sediment in  $\text{cal}/(\text{cm}^3\cdot\text{C})$  (0.5 as typical value) and lastly volumetric heat capacity of the water in  $\text{cal}/(\text{cm}^3\cdot\text{C})$  (1.0 as typical value). The parameters given above were determined for this study according to Lapham (1989). The following steps are applied by the VFLUX program (Gordon et al., 2012):

1. It is important that all the sensors have the same start time, end time and sampling rate. If this is not the case, VFLUX cuts the data to the shortest time range which is common to all sensors, so that a common time vector is created. For this study, input series for every depth (or sensor) has the same sampling rate so formatting of the time series was not applied.

2. The data is resampled to the recommended sample number which is 12 – 24 samples per day if the original sampling rate is greater. In this study, 12 samples per day were preferred and the data is filtered by low – pass filtering for noise reduction.
3. The diurnal signal which is the tracer signal is isolated from a single fundamental frequency using Dynamic Harmonic Regression (DHR) (Young, Pedregal, & Tych, 1999).
4. The amplitude and phase are calculated during DHR analysis mentioned above.
5. If more than one sensor pairs are available, desired sensor pairs are chosen to calculate vertical flux. In this study, there is only one sensor pair for each installation location; therefore no selection is required.
6. The final step is to calculate the vertical flux values using the equations developed by Hatch et al. (2007). Negative flux values indicate upward movement of water while the positive ones indicate downward movement.

Table 3: A sample input temperature time series data collected from a single streambed vertical profile.

Recording Time (days)	Temperature of streambed in different depths (°C)	
	Sensor @ 5 cm	Sensor @ 20 cm
42079.958333	7.449	7.917
42079.968750	7.387	7.917
42079.979167	7.324	7.917
42079.989583	7.324	7.854
42080.000000	7.261	7.854
42080.010417	7.261	7.854
42080.020833	7.199	7.854
42080.031250	7.199	7.854
...	...	...

#### 4.5. Measurement of Water Quality Field Parameters

Water quality field parameters were measured in all monitoring locations (from S1-P to S17-D) for stream water by YSI 556 multi – parameter water quality meter (Figure 19). It simultaneously measures numerous water quality parameters including temperature, conductivity, salinity, dissolved oxygen, pH, and ORP. Except conductivity and pH all parameters were measured using this device. For conductivity and pH measurements YSI EcoSense EC300 (having resolution of 0.1  $\mu$ S/cm to 0.1 mS/cm and accuracy of  $\pm$  (1% of reading to 2.5% of reading)) and YSI EcoSense pH100 (having resolution of 0.01 unit and accuracy of  $\pm$ 0.1%  $\pm$ 2 digit) were used respectively. Measurements were performed biweekly between dates October 2014 and November 2015. During measurements of stream water, the section of the stream which is clear and close to piezometers was chosen.





Figure 19: Measurement of water quality field parameters for stream water in the field.

In addition to stream water, water samples were taken from deep piezometers for each piezometer location (S1-P, S2-P, S3-P, S4-P, S6-P, S7-P, S9-P, S10-P) and water quality field parameters of these water samples were measured. For this purpose, water was drawn by pumping with the help of a hand pump (Figure 20) constructed at the Hydrogeology Lab. It simply includes a pipe (in 3 m length), pipe handle and two turncock controlling the entering of water and air inside the pipe. These turncocks and pipe handle are controlled manually by an operator. Pipe was placed into deep piezometers up to screen middle and the whole water inside the piezometer was pumped. By this way, this water was drained and the piezometer was purged. After that, filling of water to the piezometers was waited and this new water

was pumped again to take as a sample. As final step, field parameters were measured from these pumped water samples using same devices mentioned above. Measurement of water samples from piezometers were performed only in July, August and September 2015 (two times in September). Therefore, water quality field parameters for both stream water and water samples taken from piezometers have only these common dates. All processes including measurement of parameters from both stream water and piezometer were finished within a day for comparison. All collected data were evaluated in terms of interaction processes in section 5.5.1. During evaluation, S15 site was denoted as S15-12 and S15-13 separately representing the branches of S15 coming from S12-D and S13-D respectively, because S15 is the combination of these two branches. Also, S17-D was investigated as S17-D-I and S17-D-II. These refer two different water characteristics detected in S17-D.



Figure 20: Purging of deep piezometer in S4-P site for measurement of water quality field parameters.

#### **4.5.1. Major Anions**

From sites S2-P, S4-P, S6-P, S10-P, S12-D, S13-D, S16-D and S17-D water samples were taken from both surface water (a few meter upstream and downstream of the given locations) and from deep piezometers, where available, to analyze major anion concentrations (Figure 21). These locations were chosen because they reflect the upstream, middle and downstream of the study area. Water samples were taken by plastic bottles having a volume of 0.5 L. During sampling of stream water, the bottle was submerged to the half depth of stream at that point to prevent the entrance of streambed sediments and the particles on the stream surface. Water samples from piezometers (deep piezometers of S2-P, S4-P, S6-P and S10-P) were taken by purging again as explained in previous section 4.5. These water samples were analyzed in Hydrochemistry Laboratory of Hacettepe University by the ion chromatography method. Ion chromatography measures concentrations of ionic species by separating them according to their interaction with a resin. Sample solutions pass through a pressurized chromatographic column where ions are absorbed by column constituents. An ion extraction liquid runs through the column, the absorbed ions begin separating from the column. The retention time of different species determines the ionic concentrations in the sample.

After determination of major anion chemistry in determined locations, chloride concentrations were used for solute mass balance calculations to understand the contribution of groundwater to the Kirmir stream. In addition to chloride ion concentrations, discharge measurements were taken in determined locations for mass balance calculation (see Section 2.2.1.1.)



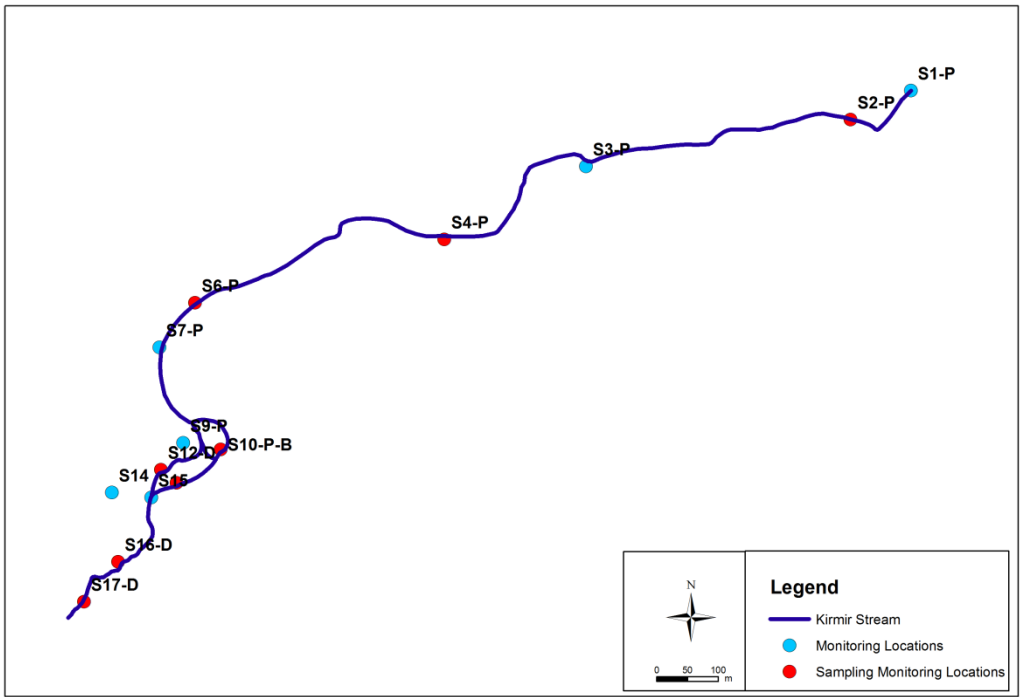


Figure 21: Chloride sampling monitoring locations through the study area.



Figure 22: Some of water samples taken for major anion analysis.

## CHAPTER 5

### RESULTS AND DISCUSSIONS

#### 5.1. Water Skin Temperatures Using Thermal Camera

With the help of remote sensing measurements collected with handheld thermal infrared (TIR) camera, groundwater seepage zones that are detectable on the surface water skin and along the streambank were investigated in this study. In summer months cold anomalies in the surface water indicate locations where groundwater flows through streambed into the stream. In winter months the situation is reverse, that is, warmer stream temperature than expected (e.g. air temperature) may indicate the contribution of groundwater to the Kirmir Stream. This method will work only if the temperature anomaly could be detected at the skin of the surface water. In thermal images used in this study, dark colors represent cold spots and lighter colors (e.g. orange, yellow) represent hot spots. Thermal images were taken on 9<sup>th</sup> and 24<sup>th</sup> of September 2014, 15<sup>th</sup> of January 2015 and 26<sup>th</sup> of February 2016.

Figure 23 shows the TIR and visible images taken at S9-P site, which is a pool full of reeds. Marked area in the visible image corresponds to the whole thermal image on the right. Maximum water temperature within the Area 1 in thermal image is 15.4 °C, although the air temperature was measured as 2.87 °C. In thermal image the arrows show the flow direction which is clear in the video. Orange colors indicate relatively colder areas and yellow colors indicate warmer areas. Stones are significantly cold and reflect the air temperature. The interface between two water characteristics can be seen clearly. White line in the thermal image represents the temperature profile and relative increase can be seen in temperature values through the profile.

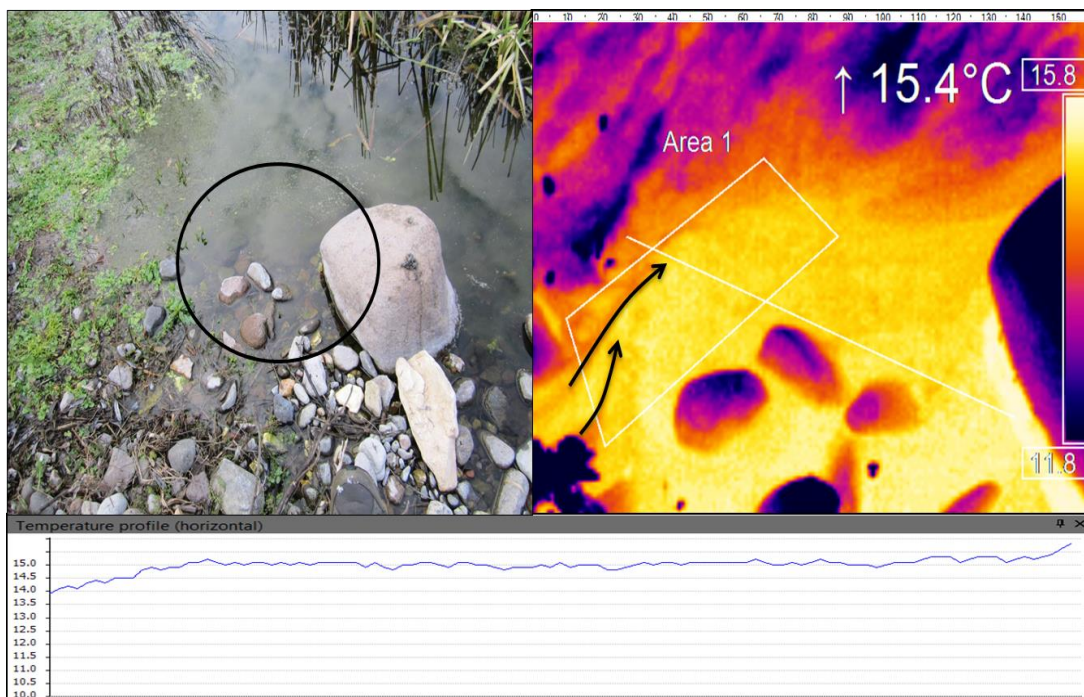


Figure 23: Mixing of two different waters in S9-P

Figure 24 shows the TIR and visible images taken at S10-P monitoring location on 15<sup>th</sup> of January. Air temperature was measured as 2.55 °C. However, surface water

temperature was changing between 15.2°C and 20.2°C. Relatively warmer and buoyant groundwater discharging to the stream is the reason of this warm surface skin temperature. As can be understood from Figure 24, TIR image was rotated about 90° to the right to capture the same view as visible image. During field trips, it was observed that groundwater seeps through the streambed sediments just beneath the two stones and they are encircled in the visible image by black color. Same area was marked in TIR by black rectangle and maximum temperature of this area was detected as 20.2°C. Black vertical line in TIR image is the indicator of the temperature profile. Through the temperature profile, temperature values almost do not change. It is always around 19°C except the point where the cable of Solinst Water Level Meter is cut. Surface water temperature of this location is always around 19°C - 20°C due to groundwater contribution. Also, temperature of stream was measured by Solinst Model 107 TLC meter as 19.3 °C on the same date and this is very close to the temperature value obtained by thermal camera.

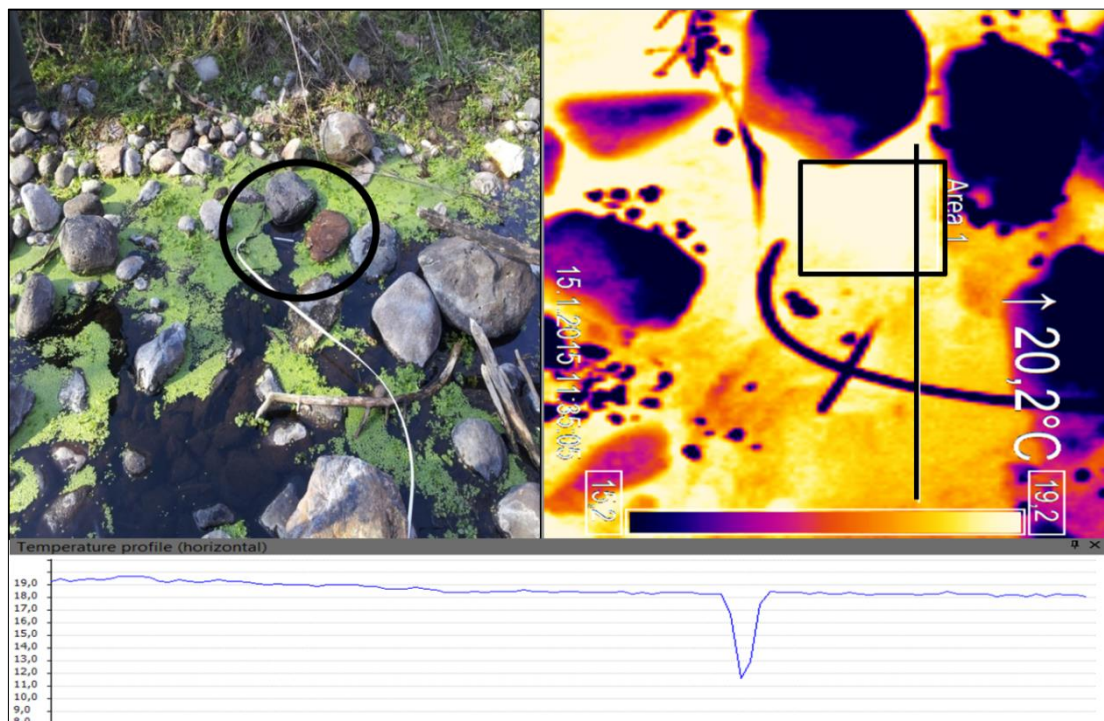


Figure 24: TIR and visible images taken from S10-P-B.

Figure 25 shows the TIR image taken at S10-P-B on 26<sup>th</sup> of February 2016. The interface between warm and cold water can be seen clearly. Area 1 and Area 2 are representative of the warm and cold water respectively. The maximum temperature values of Area 1 and Area 2 are 21.7 °C and 9.7 °C respectively. Area 1 represents the upwelling warm groundwater whereas the colder Area 2 represents the surface water. Horizontal and vertical white lines in the image correspond to blue and green lines in the temperature profile. Effect of groundwater can be seen in each of these profiles. The sharp interface between groundwater and surface water can be clearly seen in this thermal image. The temperature of cold water was measured as 8.1 °C by Solinst Model 107 TLC meter and 10.63°C by YSI 556 multi – parameter water quality meter. Therefore, thermal camera, Solinst Model 107 TLC meter and YSI 556 multi – parameter water quality meter gave similar values with each other.

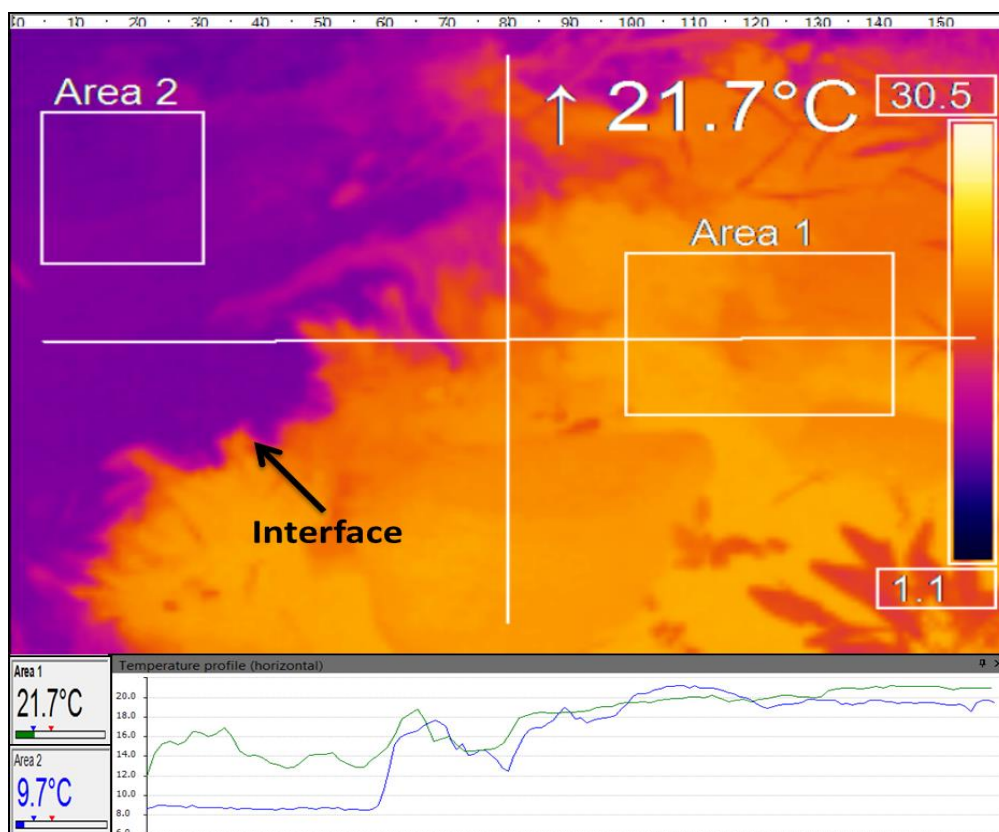


Figure 25: The interface of cold and warm water in S10-P-B



Figure 26 shows the TIR and visible images taken at S15 on 15<sup>th</sup> of January 2015. Note that S12-D and S13-D branches converge at S15. SW1 and SW2 on the image denote branches on which S12-D and S13-D are located respectively. On this date, air temperature was 7.2°C. On the other hand, stream water temperature was measured at Area 1 and Area 2 as 15.4°C and 11.6° C respectively by the TIR camera (Figure 26). Especially in Area 2 representing the SW1 is significantly warmer than the expected. The white line in the TIR image is the temperature profile and it ranges between 7°C and 15°C. 7°C reflects the temperature of grass on the temperature profile and higher temperatures belong to surface skin temperature. Temperature values of Area 1 and Area 2 are 14.9°C and 12.0°C respectively by Solinst meter.

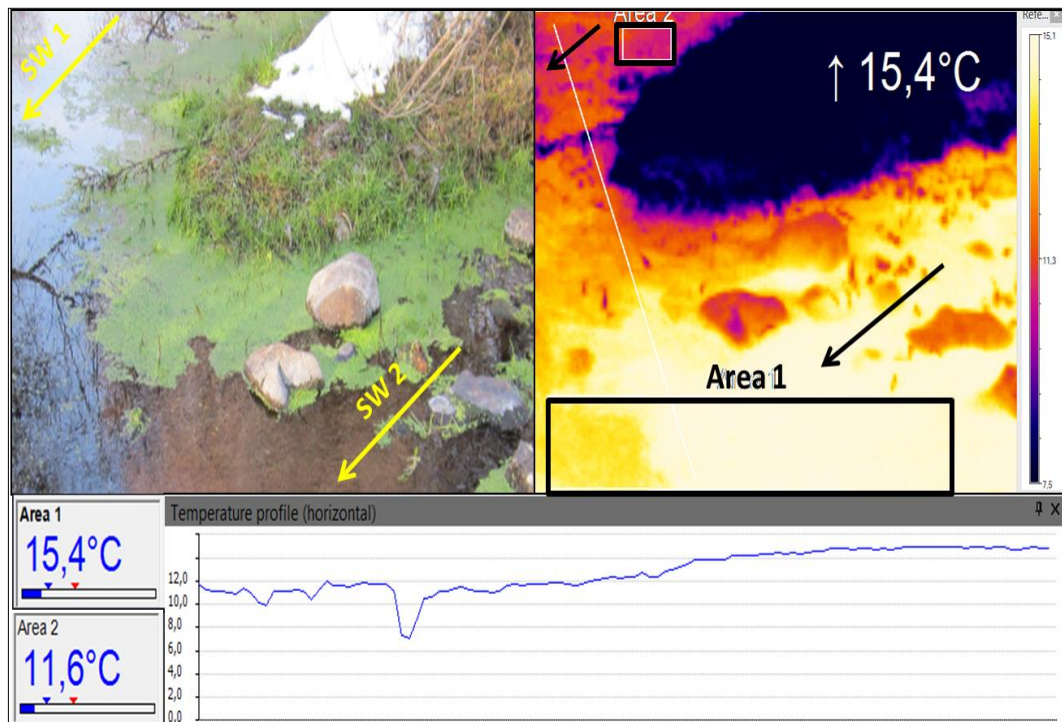


Figure 26: TIR and visible images taken from S15.

Figure 27 shows the TIR and visible images taken at S17-D on 9<sup>th</sup> of September 2014. This site is the last monitoring location of the study area. Two different body of water join to each other in this location. One has the surface water characteristics whereas the other is the spring discharge location. Air temperature was measured as 21.73°C on the same date. As can be understood from the TIR image, spring discharge location has lower temperature and its takes 15.2 °C as the lowest temperature value. However, Area 2 reflects the warmer surface water properties.

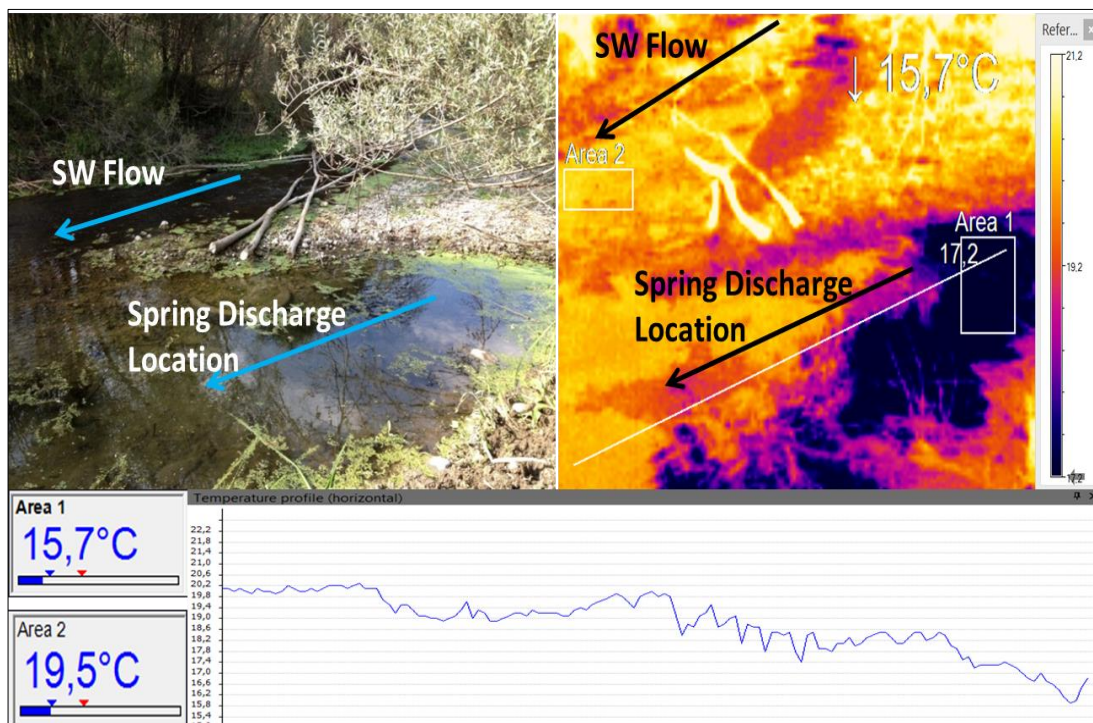


Figure 27 : TIR and visible images taken from S17-D.

## **5.2. Hydraulic Head and Vertical Hydraulic Gradient Values**

As mentioned in Chapter 4.1.1. water level measurements were performed in each monitoring location where piezometers were installed (stream stage and water levels inside piezometers were measured). Then, hydraulic head and vertical hydraulic gradient values were calculated for these sites. Negative values of vertical hydraulic gradient values (VHG) indicate upward movement of water, that is, groundwater discharges into Kirmir Stream. On the other hand, vertical hydraulic gradient values are positive under downwelling conditions in which Kirmir Stream feeds adjacent shallow groundwater system.

In summary, the obtained results have shown that the study area can be considered broadly as three separate regions (Figure 28). In the first region, hydraulic head values of piezometers which were installed at deeper sections in hyporheic zone are lower than the hydraulic head values of piezometers which were installed at shallower sections. VHG values of this region are positive indicating downwelling movement of water. Therefore, stream continuously contributes to groundwater in this part of the study area throughout the observed period. However, in the second region, gaining and losing reaches of Kirmir Stream are interchangeable depending on the time period. In other words, the direction of flow changes with time in these sites. Monitoring sites S1-P, S2-P and S3-P are included in the first region and they are consistently characterized as losing reaches of the Kirmir Stream. The other monitoring sites located downstream which are S4-P, S6-P, S7-P and S9-P show both gaining and losing characters, hence they are grouped in the second region of the study area. Except these two regions, only the monitoring site S10-P-B consistently showed a gaining character during the whole observation period.

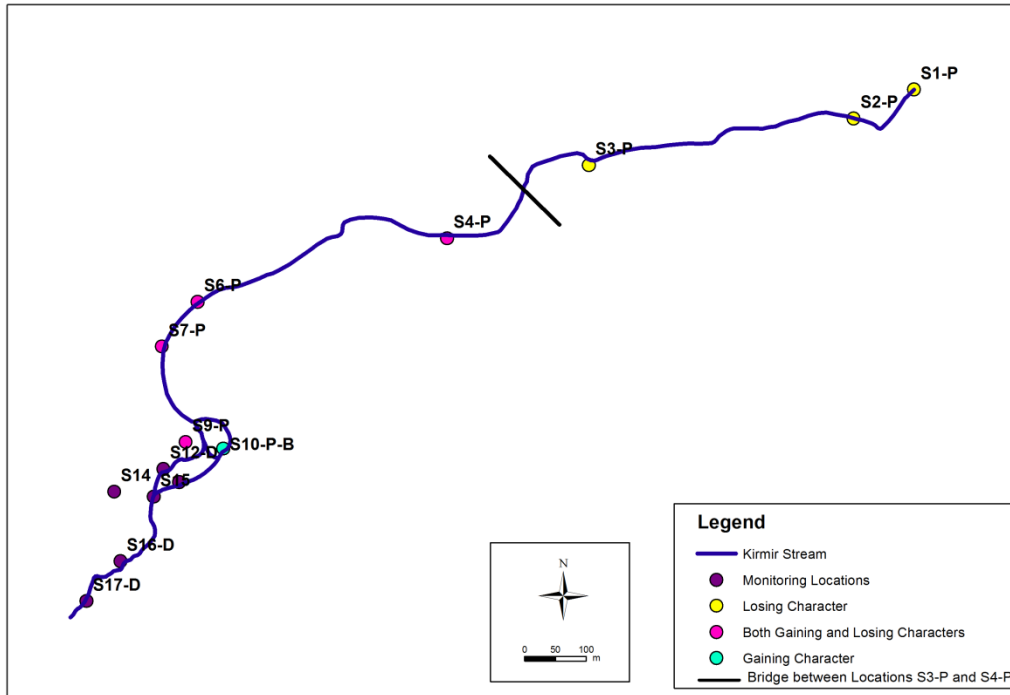


Figure 28: Sites having losing, both gaining - losing and gaining characters.

Stream reach showing losing character

S1-P, S2-P and S3-P are located between the Doğanözü Dam and the bridge and present the most upstream part of the study area (Figure 28). In Figure 29, change in water level inside nested piezometers (shallow and deep) and change in surface water level in time is shown. Streambed elevation was also added to these graphs as a reference. As mentioned in section 4.2 “Nested Piezometers”, these three locations were included later in the study compared to other locations. Within the observation period, between 21.11.2014 and 19.11.2015, surface water level is higher than the water level inside shallower piezometer, which are both higher than the water level inside the deeper piezometer. Total head and vertical hydraulic gradient values (VHG) of these sites directly indicate the downwelling direction (positive VHG) of water movement (Table 4). Total head values of shallower piezometers are higher than the total head values of deeper piezometers. Therefore, water moves from stream to groundwater.

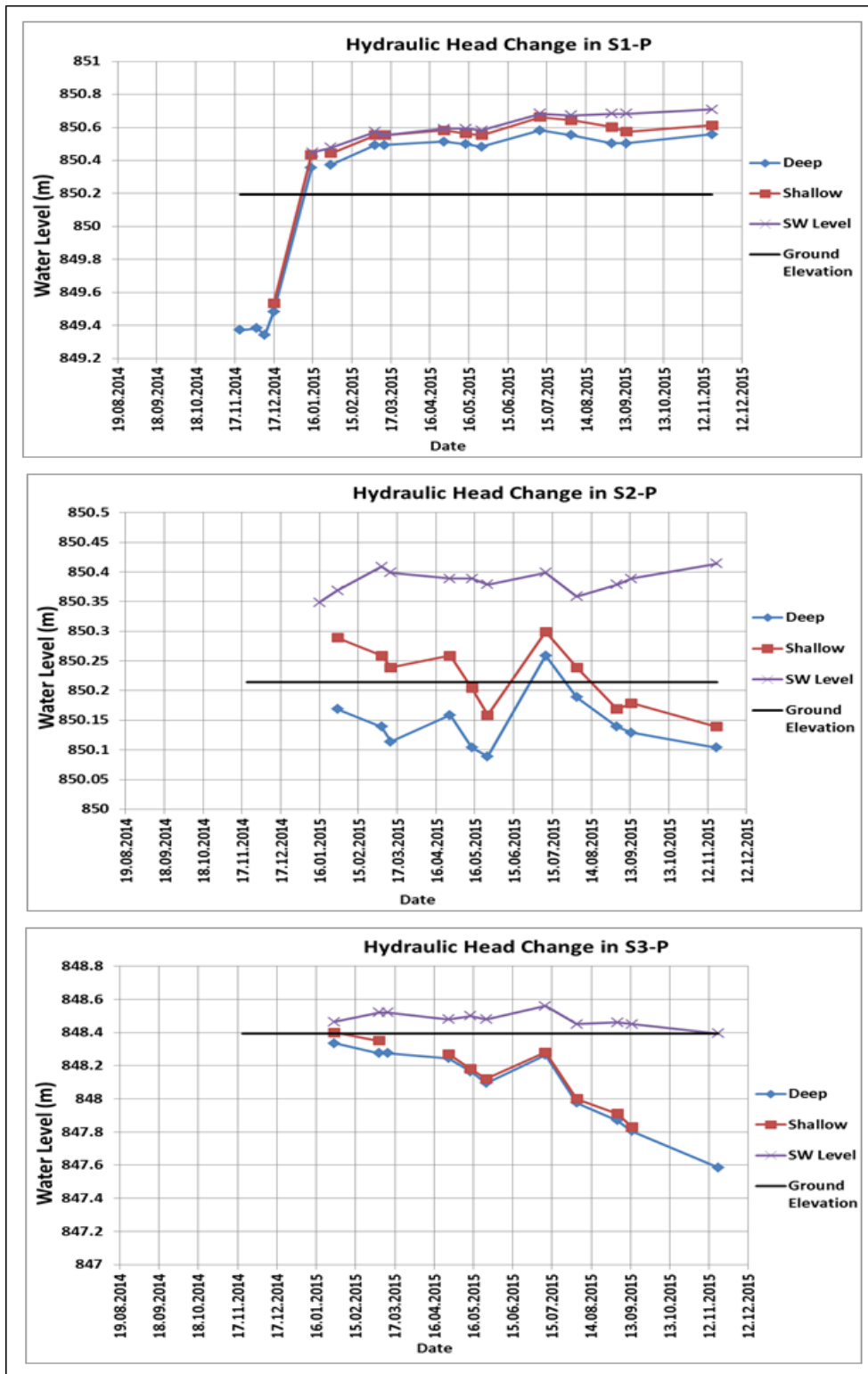


Figure 29: Water level change in time at the losing reach of the study area (S1-P, S2-P and S3-P).

Table 4: Total head values, VHG values and flow directions in S1-P, S2-P and S3-P.

Site	Date	Total Head of Deep (m)	Total Head of Shallow (m)	Vertical Hydraulic Gradient	Flow Direction
S1-P	21.11.2014	849.373	nm	nm	nm
	04.12.2014	849.383	nm	nm	nm
	10.12.2014	849.343	nm	nm	nm
	17.12.2014	849.483	849.533	0.064	Downward
	15.01.2015	850.355	850.435	0.103	Downward
	16.01.2015	nm	nm	nm	nm
	30.01.2015	850.373	850.443	0.090	Downward
	05.03.2015	850.493	850.553	0.077	Downward
	12.03.2015	850.493	850.553	0.077	Downward
	27.04.2015	850.513	850.583	0.090	Downward
	14.05.2015	850.498	850.563	0.083	Downward
	26.05.2015	850.483	850.553	0.090	Downward
	10.07.2015	850.583	850.663	0.103	Downward
	03.08.2015	850.553	850.643	0.115	Downward
	03.09.2015	850.503	850.603	0.128	Downward
	14.09.2015	850.503	850.573	0.090	Downward
19.11.2015	850.558	850.613	0.071	Downward	
S2-P	21.11.2014	nm	nm	nm	nm
	04.12.2014	nm	nm	nm	nm
	10.12.2014	nm	nm	nm	nm
	17.12.2014	nm	nm	nm	nm
	15.01.2015	nm	nm	nm	nm
	16.01.2015	nm	nm	nm	nm
	30.01.2015	850.169	850.289	0.143	Downward
	05.03.2015	850.109	850.259	0.172	Downward
	12.03.2015	850.084	850.239	0.178	Downward
	27.04.2015	850.129	850.259	0.149	Downward
	14.05.2015	850.074	850.204	0.149	Downward
	26.05.2015	850.059	850.159	0.115	Downward
	10.07.2015	850.229	850.299	0.080	Downward
	03.08.2015	850.159	850.239	0.092	Downward
	03.09.2015	850.109	850.169	0.069	Downward
	14.09.2015	850.099	850.179	0.092	Downward
19.11.2015	850.074	850.139	0.075	Downward	
S3-P	21.11.2014	nm	nm	nm	nm
	04.12.2014	nm	nm	nm	nm
	10.12.2014	nm	nm	nm	nm
	17.12.2014	nm	nm	nm	nm
	15.01.2015	nm	nm	nm	nm
	16.01.2015	nm	nm	nm	nm
	30.01.2015	848.335	848.400	0.078	Downward
	05.03.2015	848.275	848.350	0.090	Downward
	12.03.2015	848.275	848.395	0.144	Downward
	27.04.2015	848.245	848.270	0.030	Downward
	14.05.2015	848.165	848.180	0.018	Downward
	26.05.2015	848.095	848.120	0.030	Downward
	10.07.2015	848.265	848.280	0.018	Downward
	03.08.2015	847.975	848.000	0.030	Downward
	03.09.2015	847.870	847.910	0.048	Downward
	14.09.2015	847.805	847.830	0.030	Downward
19.11.2015	847.585	dry	dry	dry	

\* nm denotes no measurement

Stream reach showing both gaining and losing characters

At the downstream of S1-P, S2-P and S3-P, groundwater starts to feed Kirmir Stream. As mentioned, these reaches include S4-P, S6-P, S7-P and S9-P locations. Water level changes observed in these sites can be seen in Figure 30. Only the piezometers in S9-P are not nested. They are located at opposing sides of a small pond in the study area. Hence, water level changes inside these piezometers were examined separately and compared with surface water level only. As can be seen from these graphs, water levels during which deep vs shallow piezometer/surface water is higher than the other change over time. Total head and vertical hydraulic gradient values of S4-P, S6-P, S7-P and S9-P are shown in Table 5 and Table 6 respectively.

- In monitoring location S4-P, up to date 30<sup>th</sup> of January 2015, water level in shallower piezometer is higher than the water level in the deeper piezometer and VHG values are positive. As a result, during time period between 16.10.2014 and 30.01.2015, this site is a losing reach of the study area. However, only on 27<sup>th</sup> of October 2014 flow direction of water is upward. Starting from 30.01.2015 to last monitoring date which is 19.11.2015, deeper piezometer has higher water level and higher total head values with respect to shallower one. Moreover, VHG values are negative referring the upward riverbed flow direction. During this time period, this site behaves as a gaining reach.
- In S6-P location, mostly deeper piezometer has higher head values than the shallower piezometer and more often negative VHG values were calculated. As a result, the flow regime of this site is usually under the control of groundwater contribution (gaining stream). However, on October 2014, 16<sup>th</sup> of January 2015 and 12<sup>th</sup> of March 2015 Kirmir Stream feeds groundwater (losing stream).

- In S7-P, there is a continuous downwelling movement of water up to date 30<sup>th</sup> of January 2015 (higher total head in shallower piezometer and positive VHG values). Starting from this date, negative VHG results points to variation in direction of flow and groundwater starts to contribute to Kirmir Stream. However, on August and September of 2015, again vertical flow direction changes and become in downward direction.
- In S9-P location, mostly stream water flows through the adjacent hyporheic zone into the aquifer. Rarely, groundwater feeds the Kirmir Stream. In 15<sup>th</sup> of January 2015, VHG values are positive indicating downward direction; however, according to the thermal image given in section 5.1, stream water temperature is warm. Piezometer gives point measurements. Due to this both information can be different.



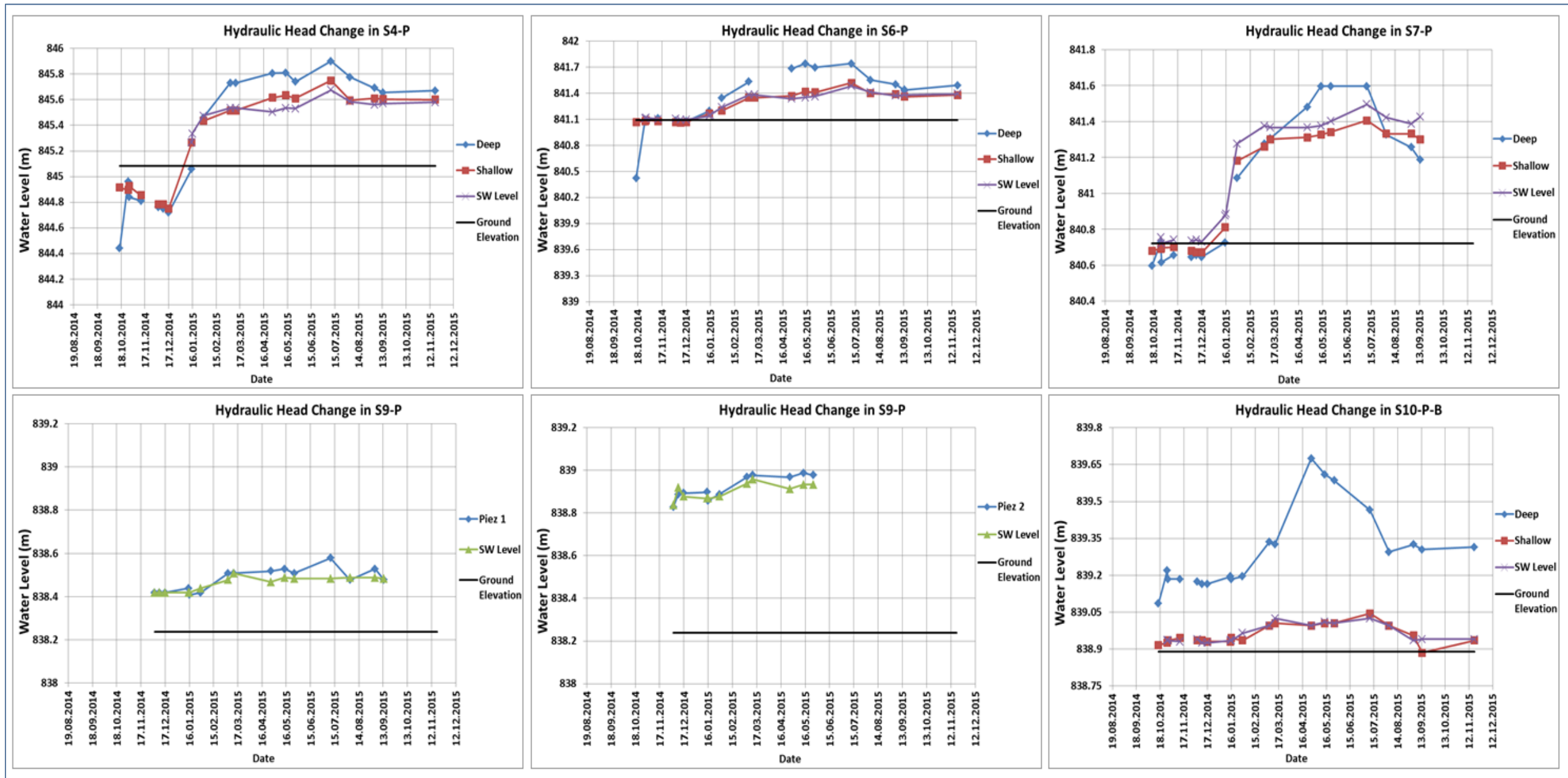


Figure 30: Water level change in S4-P, S6-P, S7-P, S9-P and S10-P-B.



Table 5: Total head values, VHG values and flow directions in S4-P, S6-P and S7-P.

Site	Date	Total Head of Deep (m)	Total Head of Shallow (m)	Vertical Hydraulic Gradient	Flow Direction
S4-P	16.10.2014	844.440	844.915	0.446	Downward
	27.10.2014	844.960	844.895	-0.061	Upward
	28.10.2014	844.840	844.925	0.080	Downward
	12.11.2014	844.810	844.855	0.042	Downward
	21.11.2014	nm	nm	nm	nm
	04.12.2014	844.760	844.785	0.023	Downward
	10.12.2014	844.750	844.785	0.033	Downward
	17.12.2014	844.720	844.750	0.028	Downward
	15.01.2015	845.060	845.265	0.192	Downward
	16.01.2015	nm	nm	nm	nm
	30.01.2015	845.460	845.435	-0.023	Upward
	05.03.2015	845.730	845.515	-0.202	Upward
	12.03.2015	845.730	845.515	-0.202	Upward
	27.04.2015	845.805	845.615	-0.178	Upward
	14.05.2015	845.810	845.635	-0.164	Upward
	26.05.2015	845.740	845.610	-0.122	Upward
	10.07.2015	845.900	845.750	-0.141	Upward
	03.08.2015	845.775	845.595	-0.169	Upward
	03.09.2015	845.690	845.610	-0.075	Upward
	14.09.2015	845.655	845.605	-0.047	Upward
19.11.2015	845.670	845.600	-0.066	Upward	
S6-P	16.10.2014	840.423	841.070	0.649	Downward
	27.10.2014	841.093	841.080	-0.013	Upward
	28.10.2014	841.073	841.090	0.017	Downward
	12.11.2014	841.113	841.080	-0.033	Upward
	21.11.2014	nm	nm	nm	nm
	04.12.2014	841.083	841.070	-0.013	Upward
	10.12.2014	841.063	841.060	-0.003	Upward
	17.12.2014	841.078	841.070	-0.008	Upward
	15.01.2015	841.198	841.165	-0.033	Upward
	16.01.2015	nm	nm	nm	nm
	30.01.2015	841.343	841.200	-0.143	Upward
	05.03.2015	841.533	841.350	-0.184	Upward
	12.03.2015	841.090	841.350	0.261	Downward
	27.04.2015	841.683	841.370	-0.314	Upward
	14.05.2015	841.743	841.420	-0.324	Upward
	26.05.2015	841.698	841.410	-0.289	Upward
	10.07.2015	841.743	841.520	-0.224	Upward
	03.08.2015	841.553	841.400	-0.153	Upward
	03.09.2015	841.503	841.390	-0.113	Upward
	14.09.2015	841.438	841.360	-0.078	Upward
19.11.2015	841.493	841.380	-0.113	Upward	
S7-P	16.10.2014	840.596	840.681	0.083	Downward
	27.10.2014	840.726	840.691	-0.034	Upward
	28.10.2014	840.616	840.696	0.078	Downward
	12.11.2014	840.656	840.701	0.044	Downward
	21.11.2014	nm	nm	nm	nm
	04.12.2014	840.646	840.681	0.034	Downward
	10.12.2014	840.656	840.671	0.015	Downward
	17.12.2014	840.646	840.671	0.024	Downward
	15.01.2015	840.726	840.811	0.083	Downward
	16.01.2015	nm	nm	nm	nm
	30.01.2015	841.086	841.181	0.093	Downward
	05.03.2015	841.276	841.261	-0.015	Upward
	12.03.2015	841.306	841.301	-0.005	Upward
	27.04.2015	841.481	841.311	-0.166	Upward
	14.05.2015	841.596	841.326	-0.263	Upward
	26.05.2015	841.596	841.341	-0.249	Upward
	10.07.2015	841.596	841.406	-0.185	Upward
	03.08.2015	841.326	841.331	0.005	Downward
	03.09.2015	841.256	841.331	0.073	Downward
	14.09.2015	841.186	841.301	0.112	Downward
19.11.2015	nm	nm	nm	nm	

\* nm denotes no measurement

Table 6: Total head, surface water level, VHG values and flow directions in S9-P.

Site	Piezometer	Date	Total Head (m)	Surface Water Level (m)	VHG	Flow Direction
S9-P	Piezometer 1	04.12.2014	838.418	838.418	0.000	-
		10.12.2014	838.418	838.418	0.000	-
		17.12.2014	838.418	838.418	0.000	-
		15.01.2015	838.438	838.418	0.011	Downward
		16.01.2015	nm	nm	nm	nm
		30.01.2015	838.418	838.438	-0.011	Upward
		05.03.2015	838.508	838.478	0.017	Downward
		12.03.2015	838.508	838.508	0.000	-
		27.04.2015	838.518	838.468	0.028	Downward
		14.05.2015	838.528	838.488	0.023	Downward
		26.05.2015	838.508	838.483	0.014	Downward
		10.07.2015	838.578	838.483	0.054	Downward
		03.08.2015	838.478	838.488	-0.006	Upward
		03.09.2015	838.528	838.488	0.023	Downward
		14.9.2015	838.478	838.483	-0.003	Upward
	19.11.2015	nm	nm	nm	nm	
	Piezometer 2	04.12.2014	838.828	838.838	-0.007	Upward
		10.12.2014	838.888	838.918	-0.021	Upward
		17.12.2014	838.893	838.878	0.010	Downward
		15.01.2015	838.898	838.868	0.021	Downward
		16.01.2015	nm	nm	nm	nm
		30.01.2015	838.888	838.878	0.007	Downward
		05.03.2015	838.968	838.938	0.021	Downward
		12.03.2015	838.978	838.958	0.014	Downward
		27.04.2015	838.968	838.913	0.038	Downward
		14.05.2015	838.988	838.933	0.038	Downward
		26.05.2015	838.978	838.933	0.031	Downward
		10.07.2015	nm	nm	nm	nm
03.08.2015		nm	nm	nm	nm	
14.9.2015	nm	nm	nm	nm		
19.11.2015	nm	nm	nm	nm		

\* nm denotes no measurement

Stream reach showing gaining character

The monitoring location S10-P-B is the most downstream part of the study area where a piezometer is installed. This site consistently has negative VHG values due to higher head values of deeper piezometer in comparison with the shallower piezometer head values. Consequently, there is always upwelling movement of water. Groundwater continuously feeds Kirmir Stream at this location. Water level

change inside the nested piezometers of S10-P-B is shown in Figure 30. Moreover, the total head and VHG results are given in Table 7.

Table 7: Total head, VHG values and flow directions in S10-P-B.

Site	Date	Total Head of Deep (m)	Total Head of Shallow (m)	Vertical Hydraulic Gradient	Flow Direction
S10-P-B	16.10.2014	839.085	838.917	-0.185	Upward
	27.10.2014	839.220	838.925	-0.324	Upward
	28.10.2014	839.185	838.935	-0.275	Upward
	12.11.2014	839.185	838.945	-0.264	Upward
	21.11.2014	nm	nm	nm	nm
	04.12.2014	839.175	838.935	-0.264	Upward
	10.12.2014	839.165	838.935	-0.253	Upward
	17.12.2014	839.165	838.930	-0.258	Upward
	15.01.2015	839.195	838.930	-0.291	Upward
	16.01.2015	nm	nm	nm	nm
	30.01.2015	839.195	838.935	-0.286	Upward
	05.03.2015	839.335	838.995	-0.374	Upward
	12.03.2015	839.325	839.005	-0.352	Upward
	27.04.2015	839.675	838.995	-0.747	Upward
	14.05.2015	839.610	839.005	-0.665	Upward
	26.05.2015	839.585	839.005	-0.637	Upward
	10.07.2015	839.465	839.045	-0.462	Upward
	03.08.2015	839.295	838.995	-0.330	Upward
	03.09.2015	839.325	838.955	-0.407	Upward
	14.09.2015	839.305	838.885	-0.462	Upward
19.11.2015	839.315	838.935	-0.418	Upward	

\* nm denotes no measurement

From the results, we can understand that there is downward movement of water in upstream part of the study area, that is, Kirmir Stream feeds the groundwater. As we move towards downstream, in the mid-section of the study area groundwater – Kirmir stream feeds the other in different periods. Finally, in most downstream piezometer monitoring location there is continuous groundwater discharge to the stream. The minimum, mean and maximum values of absolute VHG values for each site are listed in Table 8.

Table 8: Mean, minimum and maximum VHG values for each monitoring location.

<b>Site</b>	<b>  Min  </b>	<b>  Mean  </b>	<b>  Maximum  </b>
<b>S1-P</b>	0.064	0.091	0.128
<b>S2-P</b>	0.034	0.088	0.144
<b>S3-P</b>	0.018	0.051	0.144
<b>S4-P</b>	0.023	0.121	0.446
<b>S6-P</b>	0.003	0.156	0.649
<b>S7-P</b>	0.005	0.087	0.263
<b>S9-P-I</b>	0	0.014	0.054
<b>S9-P-II</b>	0.007	0.021	0.038
<b>S10-P-B</b>	0.185	0.382	0.747

The site S10-P-B has the greatest absolute VHG values among all locations (Table 8). Usually, this location has the highest values with respect to other locations for all measurement dates. The absolute minimum value was calculated as 0.00 in S9-P monitoring location among all sites indicating no interaction. When we examine this site, it is clear that S9-P has relatively lower vertical hydraulic gradient values than the rest of the study area. Especially, its negative values indicating upward movement (Table 6) are significantly low when compared to negative values of the other sites. The losing reach including S1-P, S2-P, S3-P and the locations S4-P, S6-P, S7-P have similar values. Their values are neither low as the values of S9-P nor high as the values of S10-P-B. However, S6-P has the maximum VHG value after S10-P-B with the value of 0.649.

In Figure 31 and Figure 32, the variation of vertical hydraulic gradient values in time for each piezometer location can be seen.

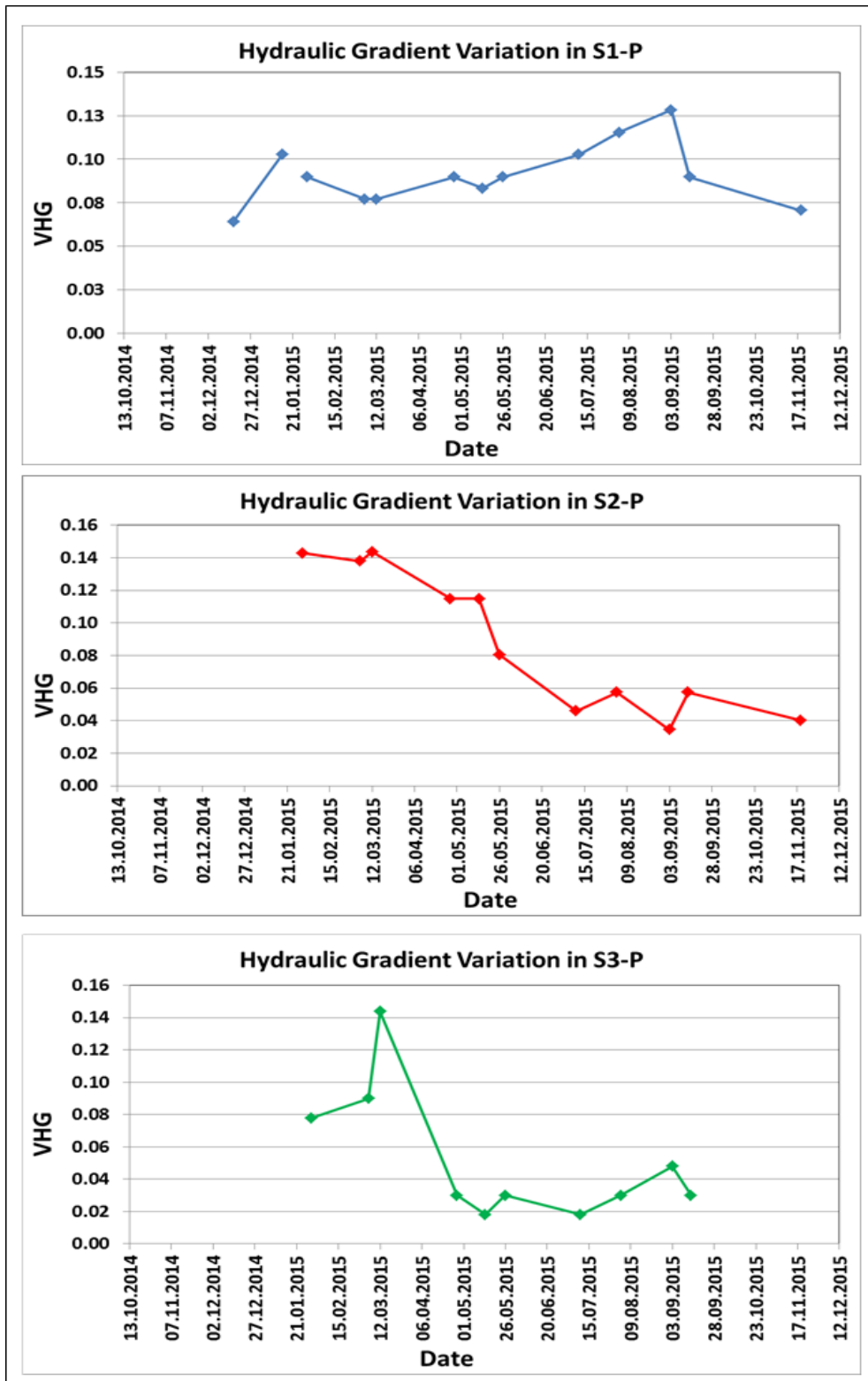


Figure 31: Vertical hydraulic gradient change in S1-P, S2-P and S3-P in time.





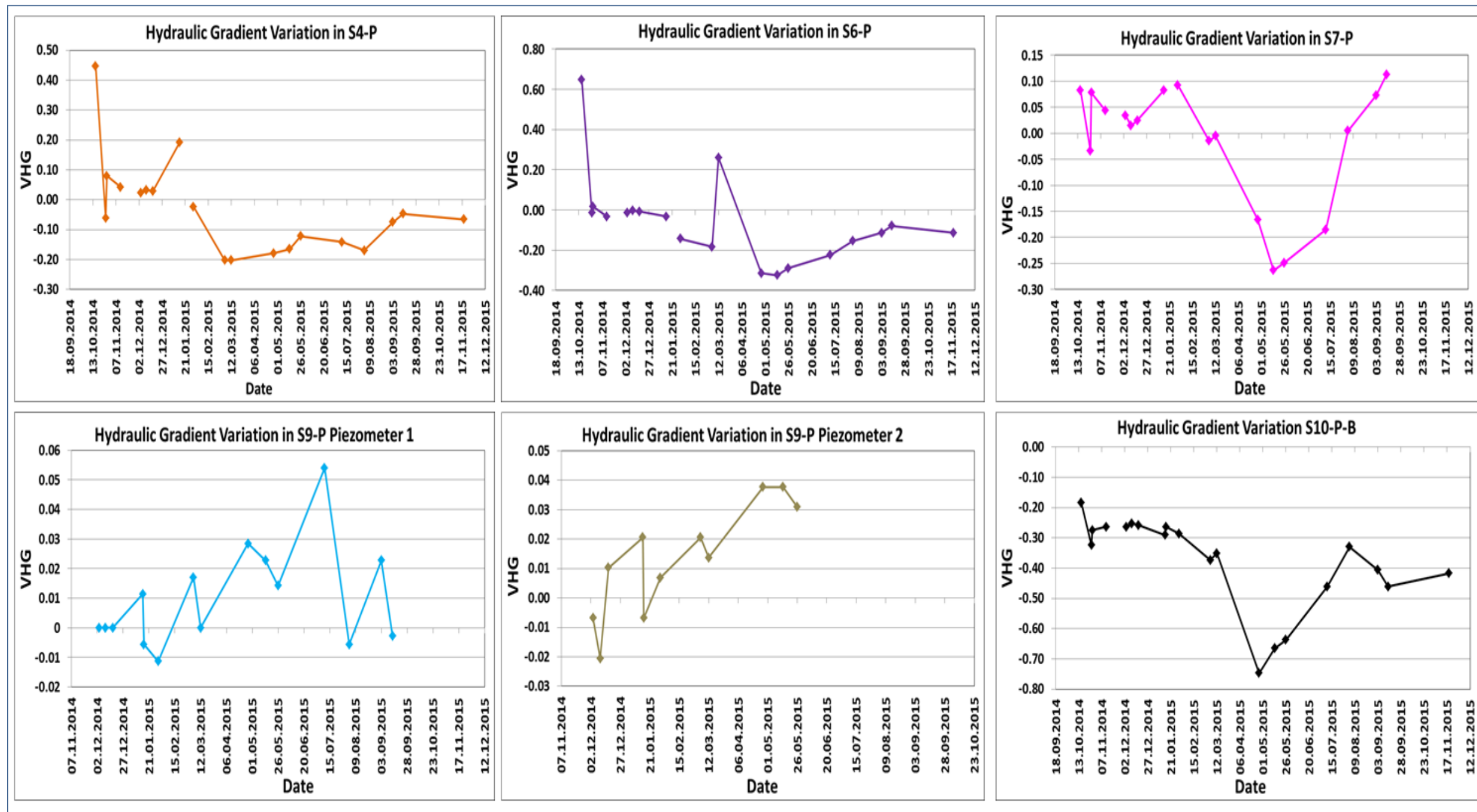


Figure 32: Vertical hydraulic gradient change in S4-P, S6-P, S7-P, S9-P and S10-P-B in time.



In Figure 31, the variation in the VHG values of S1-P, S2-P and S3-P are given.

- In S1-P the minimum VHG value occurs in December 2014. Its value increases sharply in January 2015. Up to date July 2015, this location shows similar VHG values. Starting from July, VHG values show an increase and reach the maximum value at the beginning of September 2015. After that, a significant decrease is observed. For this location, it can be said that the summer season has higher VHG values with respect to winter season.
- However, for sites S2-P and S3-P the situation is reverse. These sites show higher VHG values in winter season than in summer season. S2-P takes its maximum value in January and March 2015. After that, it has an undulating decrease. There is significant difference between winter and summer values (up to 0.10). At this location, the lowest value is observed in September 2015. Furthermore, July, August and November 2015 values are significantly lower (close to September value) with respect to the winter values.
- As mentioned S3-P has higher VHG values in winter season. In January and at the beginning of March 2015, this location shows relatively lower VHG values with respect to the end of March. After March, a sudden decrease is observed. This location takes its minimum values in May and July months. In April, August and September, very low values were calculated as well. The difference between the winter vertical hydraulic gradient values and the summer values reach up to 0.12. In November 2015, this location was dry.

In Figure 32, temporal change in the VHG values for locations S4-P, S6-P, S7-P, S9-P and S10-P-B are shown.

- S4-P has the maximum VHG value in October 2014. Then, this location shows a sudden decrease in magnitude. VHG value becomes negative and later positive at the end of October 2014. Until January 2015, positive values continue. Towards the end of January, VHG value turns to negative and this continues through summer, fall and winter 2015, until the last measurement in December. Positive VHG values change in a wider range than the negative values. All winter VHG values including January and March 2015 (except the VHG value calculated at the middle of January) are greater than the summer season values for 2015 measurement period.
- S6-P site has the highest VHG value in October 2014. Almost all VHG values are negative. Vertical hydraulic gradient values in both winter and summer seasons are close to each other in magnitude. They vary in the same range, approximately between 0.1 to 0.3. Both seasons have similar values.
- S7-P site has significantly higher VHG values in summer season than the winter season. In winter, most of the values are positive and 0.10 is the greatest value for this period. In summer, almost all values are negative and they are greater than the values of winter season. In magnitude, the highest VHG value occurs in March 2015.
- Piezometer 1 installed in S9-P location has a very undulating VHG trend. Summer values are significantly higher than the winter values in 2015. The greatest VHG value in magnitude occurs in July 2015. However, this location generally has lower VHG values when compared to other locations. Piezometer 2 in S9-P mostly shows positive values. In winter season, lower VHG values are evident. Towards summer, values show an increase in magnitude. However, in peak summer months (July, August, September),

measurements could not be taken from this piezometer because of field conditions.

- As mentioned before, all VHG values are negative in S10-P-B site. Vertical hydraulic gradient values in summer season are noticeably higher in magnitude with respect to the values in winter season. VHG values suddenly increase in magnitude (becomes more negative) between March and April 2015. After April, VHG values decrease again. The maximum VHG magnitude (negative) was obtained in April 2015. Trends of S10-P-B and S7-P are very similar with each other.

The results of the analysis indicate that the fundamental reason of this situation is the changes in the streambed elevation. Topography has fundamental importance in controlling interactions between regional and local groundwater flow and water exchange between groundwater and surface water (Harvey & Bencala, 1993). According to Toth (1963), slope discontinuities and land surface create numerous localized groundwater flow paths that are likely isolated from the regional groundwater flow. Groundwater typically discharges to surface water bodies where the slope of the water table changes suddenly (e.g. Winter et al., 1998). For instance, steeper and undulating landscapes have the most local flow patterns. In the study area, there is an elevation difference between upstream and downstream parts (Figure 33). This situation probably controls the groundwater discharge and recharge zones locally in different parts.

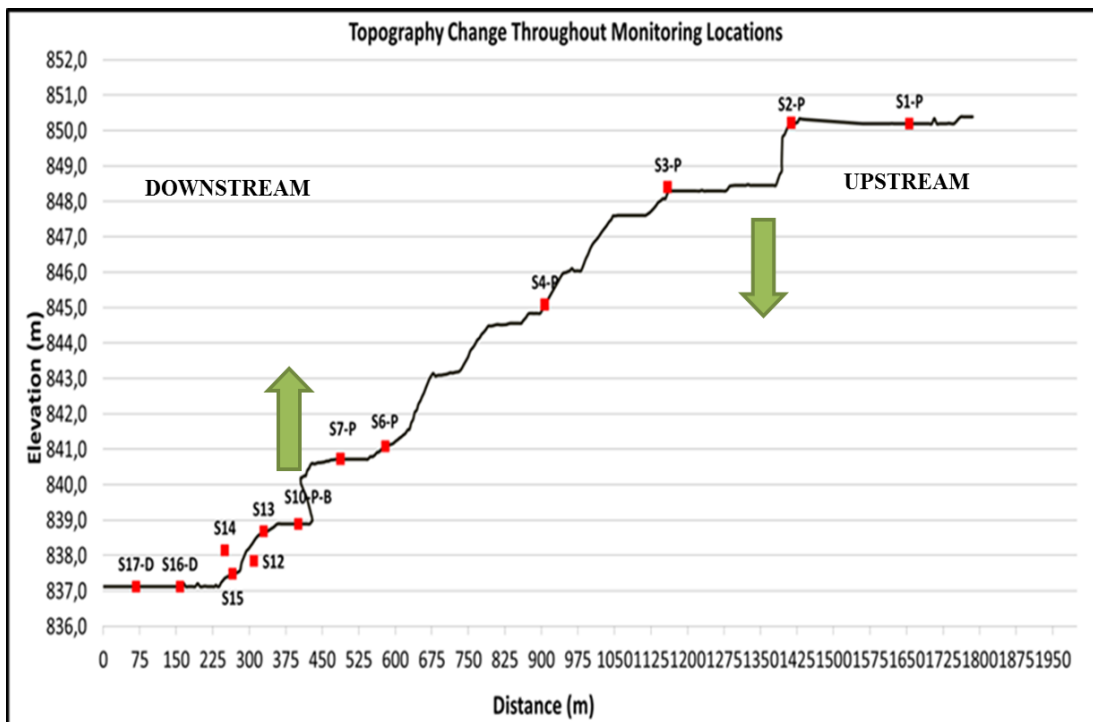


Figure 33: The variation in streambed elevation throughout the monitoring locations in the study area.

### 5.3. Temporal Changes in Discharge Measurements

Discharge values measured at the monitoring locations can be seen in Table 9 and Figure 34. S3-P is the most upstream location where discharge measurements have been collected. Location S3-P has higher discharge values compared to the location S6-P, possibly indicating that some of the downwelling water at S3-P upwells after S6-P. It is also clear that discharge values significantly increase towards downstream as moving downstream from S6-P towards S17-D. This increase is likely due to the contribution of groundwater to Kirmir Stream. To investigate the changes in discharge along the study reach further, discharge values for each consecutive discharge measurement sites were subtracted from each other and listed in Table 10.

Also, VHG values (flow directions obtained from piezometer data) and discharge results can be compared. As mentioned before, flow direction in S1-P, S2-P and S3-P is always in downward direction, and groundwater feeds Kirmir Stream starting from S4-P location in terms of the piezometer information. Based on this, it is expected that downstream monitoring locations have higher discharge values with respect to upstream ones. On the contrary, sites S3-P and S6-P show exactly the opposite relationship. Discharge in S3-P is greater than discharge in S6-P for all dates (Table 10) despite the flow directions in both sites. This can be a result of any significant water loss occurring in the region between S3-P and S4-P (this area was not investigated by piezometers or temperature loggers and the length of this area is about 295 m) or amount of water loss occurred in S3-P is greater than the amount of water gain occurred in the later section investigated (see Table 10). After S4-P location, vertical hydraulic gradient and discharge results are consistent with each other. Towards downstream of the study area discharge values increase and VHG results show continuous upwelling movement of groundwater. Therefore, discharge measurements and piezometer measurements support each other in determining the character of stream and groundwater exchange in the study area.

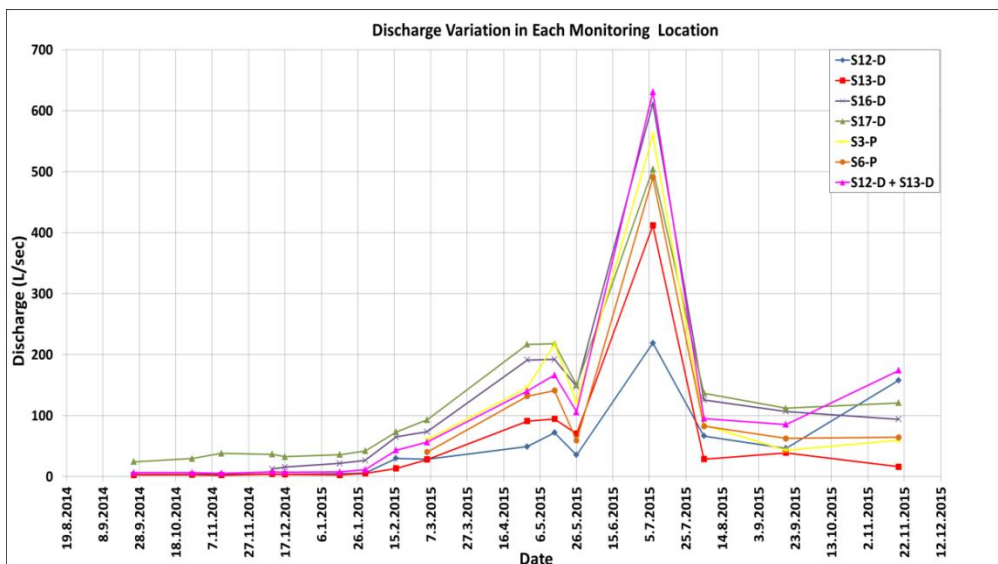


Figure 34 : Discharge variation in time for each measurement location.

Table 9 : Discharge values in each measurement location.

Discharge Values (L/sec)						
Date	S3-P	S6-P	S12-D + S13-D	S16-D	S17-D	SW26
25.9.2014	nm	nm	6.5	nm	24.4	nm
27.10.2014	nm	nm	6.4	nm	29.6	nm
12.11.2014	nm	nm	5.6	nm	38.3	nm
10.12.2014	nm	nm	8.0	12.4	36.7	nm
17.12.2014	nm	nm	7.2	15.7	32.6	nm
16.1.2015	nm	nm	7.5	21.5	36.1	nm
30.1.2015	nm	nm	11.3	26.6	42.1	nm
16.2.2015	nm	nm	43.4	65.1	73.4	nm
5.3.2015	60.4	40.3	56.6	73.6	93.3	589.2
29.4.2015	146.1	132.0	140.3	191.2	216.8	586.7
14.5.2015	217.3	141.2	166.6	192.2	218.0	459.0
26.5.2015	121.5	59.2	105.9	147.6	150.2	363.7
7.7.2015	559.2	490.6	630.9	611.8	504.4	1043.9
4.8.2015	84.7	82.8	95.4	125.5	136.9	nm
18.9.2015	43.2	62.6	85.5	107.0	112.0	216.7
19.11.2015	59.4	64.4	174.2	94.0	121.0	nm

\* nm denotes no measurement

Table 10 : Difference between discharge values of consecutive measurement locations (negative (positive) values indicate decreasing (increasing) discharge downstream).

Discharge Differences (L/sec)							
Date	S6P- S3P	(S12D+S13D) - S6P	S16D - (S12D+S13D)	S17D - S16D	SW26 - S17D	S17D - S6P	S17D - S3P
25.9.2014	-	-	-	-	-	-	-
27.10.2014	-	-	-	-	-	-	-
12.11.2014	-	-	-	-	-	-	-
10.12.2014	-	-	4.4	24.3	-	-	-
17.12.2014	-	-	8.5	16.9	-	-	-
16.1.2015	-	-	14.0	14.6	-	-	-
30.1.2015	-	-	15.2	15.5	-	-	-
16.2.2015	-	-	21.7	8.3	-	-	-
5.3.2015	-20.1	16.4	17.0	19.7	495.9	53.0	32.9
29.4.2015	-14.1	8.2	51.0	25.6	369.9	84.8	70.7
14.5.2015	-76.1	25.5	25.5	25.8	241.1	76.8	0.6
26.5.2015	-62.3	46.6	41.7	2.7	213.5	91.0	28.7
7.7.2015	-68.6	140.3	-19.1	-107.4	539.5	13.8	-54.8
4.8.2015	-1.9	12.6	30.1	11.4	-	54.1	52.3
18.9.2015	19.3	23.0	21.5	4.9	104.8	49.4	68.7
19.11.2015	5.0	109.8	-80.2	27.0	-	56.6	61.6

\* nm denotes no measurement



As can be understood from the values given in Table 9 and Table 10, there is a significant discharge difference between the most downstream and the most upstream discharge measurement locations namely S17-D and S3-P respectively. In March 2015, this difference is equal to 32.0 L/sec. In the mid of May 2015, discharge values of two locations are almost the same; however, towards the end of the May it increases and reaches almost 28.7 L/sec again. Surprisingly, reverse relationship between them was observed on 7<sup>th</sup> of July 2015. Discharge amount measured in S17-D on this date is lower than the discharge amounts of S3-P, S12-D, S13-D and S16-D. As mentioned in previous section (Section 4.4.1), reservoir water was released from Doğanözü Dam on 26<sup>th</sup> of March and on 30<sup>th</sup> of June. It is likely that increase surface water stage during water release turns the stream into a dominantly losing character along the study area. After this date, discharge amount in S17-D becomes higher and the difference from the S3-P is around 50.0 L/sec and 68.7 L/sec.

If the differences in discharge values between each successive locations are examined separately, they range from low values to significantly high values (Table 10). For S6-P and the summation of S12-D & S13-D, the differences range between 8.2 L/sec to 140.3 L/sec. The lowest and the highest contributions belong the dates 29<sup>th</sup> of April 2015 and 7<sup>th</sup> of July 2015 respectively. S12-D, S13-D and S16-D have more common measurement dates. The difference between discharge values (S16-D – (S12-D + S13-D)) change between 4.4 L/sec and 41.7 L/sec The lowest difference occurred in December 2014. On dates 7<sup>th</sup> of July 2015 and 19<sup>th</sup> of November 2015, S16-D has lower discharge values. When S17-D and S16-D are examined, the amount of excess water in S17-D ranges from 2.7 L/sec (in 26<sup>th</sup> of May) to 27.0 L/sec (in 19<sup>th</sup> of November). As in others, influence of reservoir water release can be seen on 7<sup>th</sup> of July 2015. On this date, S16-D has higher discharge amount than S17-D. The greatest discharge differences occur between S6-P and the summation of S12-D and S13-D. This may be due to the effect of S10-P-B. Significant amount of groundwater contribution in this location may cause large discharge differences between previous locations and the next locations.

Therefore, between each successive location, groundwater discharges to Kirmir stream in a wide range of values. From S3-P to S17-D, at least 28.7 L/sec groundwater contribution can be observed and this value can reach up to 50 L/sec and 68.7 L/sec on August and September 2015 respectively (Table 10). In addition, the difference between S6-P and S17-D is important because S6-P is the first discharge location where groundwater contribution occurs. Between S6-P and S17-D, groundwater contribution was calculated as at least 13.8 L/sec (in 7<sup>th</sup> of July) (the effect of reservoir water release) and 91.0 L/sec (in 26<sup>th</sup> of May) at most (Table 10). The amount of groundwater discharge to Kirmir stream from S6-P and S17-D ranges between these two values and significant contributions belong to the end of April 2015 and end of May 2015. As mentioned, SW26 is not located within the boundaries of the study area. If discharge values measured in the study area and in SW26 are compared, significant differences can be observed. Because tributaries join to Kirmir stream before SW26, this site has significantly higher discharge values. To distinguish the tributary effect and groundwater effect, the area between S17-D and SW26 should be investigated in detail. However, the purpose of this study was only to observe groundwater contribution. Because of this, the study was limited to a relatively small area where no entrance of tributaries are observed. Discharge measurements in SW26 were performed just to have an idea. According to Table 9, higher discharge amounts were measured in summer season than in winter season.

## **5.4. Groundwater Discharge**

### **5.4.1. Temperature Data - VFLUX**

Streambed temperatures were measured by temperature loggers (ibuttons) at two different depths in monitoring sites S3-P, S4-P and S16-D (see section 4.4.1 for more details). Temperature values in streambed show variation in terms of measurement period and location. As a general rule, diurnal temperature fluctuations are less in deeper sections of the streambed since they are less affected from surface water temperature variations (both for losing and gaining streams). Groundwater

temperature is relatively constant throughout the year, but surface water temperature changes daily and seasonally based on air temperature. Winter et al (1998) indicated that gaining reaches of streams are characterized by relatively stable sediment temperatures and damped diurnal variations in surface water temperatures while losing reaches are characterized by highly variable sediment and surface water temperatures. Changes in surface water temperatures likewise affect the subsurface sediment temperatures in losing streams.

Maximum, minimum streambed temperatures and their differences in each site for each measurement period are given in Table 11. Also, graphs of streambed temperature variations in S3-P, S4-P and S16-D for all measurement periods are given in Figure 35 (12.03.2015 – 26.03.2015 for S3-P & S4-P, 12.03.2015 – 27.04.2015 for S16-D), Figure 36 (10.07.2015 – 03.08.2015) and Figure 37 (03.09.2015 – 14.09.2015). In all graphs, time axis refers to days.

Table 11: Minimum, maximum streambed temperature values and their differences in monitoring sites S3-P, S4-P and S16-D for each measurement period.

Site	Measurement Period	Depth	Max (°C )	Min (°C )	Difference (°C )
S3-P	12.03.2015 - 26.03.2015	Shallow	9.831	5.255	4.576
		Deep	7.979	7.100	0.879
	10.07.2015 - 03.08.2016	Shallow	27.650	19.708	7.942
		Deep	25.877	21.250	4.627
S4-P	12.03.2015 - 26.03.2015	Shallow	13.702	11.886	1.816
		Deep	14.560	12.993	1.567
	10.07.2015 - 03.08.2015	Shallow	15.678	14.863	0.815
		Deep	15.531	14.529	1.002
	03.09.2015 - 14.09.2015	Shallow	17.181	16.805	0.376
		Deep	17.033	16.72	0.313
S16-D	12.03.2015 - 27.04.2015	Shallow	16.805	8.277	8.528
		Deep	17.682	11.226	6.456
	10.07.2015 - 03.08.2015	Shallow	18.458	18.082	0.376
		Deep	18.381	18.068	0.313
	03.09.2015 - 14.09.2015	Shallow	18.458	18.333	0.125
		Deep	18.381	18.318	0.063

When the whole data are compared, it is seen that the highest temperature value (27.650 °C at 5 cm depth) was recorded in July - early August measurement period and the lowest temperature value (5.255 °C at 5 cm depth) was recorded in March in S3-P monitoring location among all three sites (Table 11). As explained in section 5.2, this location is situated in the losing reach of the study area according to VHG values. This means that streambed temperatures are under the control of stream water not the groundwater (because of downwelling movement of surface water). Sharp changes in surface water temperatures due to air temperature directly affect the streambed temperatures. Having the highest and lowest temperature values in S3-P can be explained in this way. In March 2015, temperature fluctuation is significantly observable at 5 cm depth but the same is not valid for 20 cm depth (Figure 35a). This is a result of temperature damping with depth, in addition to more groundwater effect in deeper sections. In S3-P location, significant diurnal variations in streambed temperatures were recorded for measurement period 10<sup>th</sup> of July and 3<sup>rd</sup> of August 2015 at 5 cm and 15 cm depths (Figure 36a) (due to the stream water influence, diurnal temperatures vary in a wide range; however, less fluctuation occurs at 15 cm depth). In September, measurement could not be performed in this site because of sensor failure. In addition, if measurement periods are examined separately, there exists a significant difference (up to 8°C) between maximum and minimum temperature values as can be seen in Table 11.

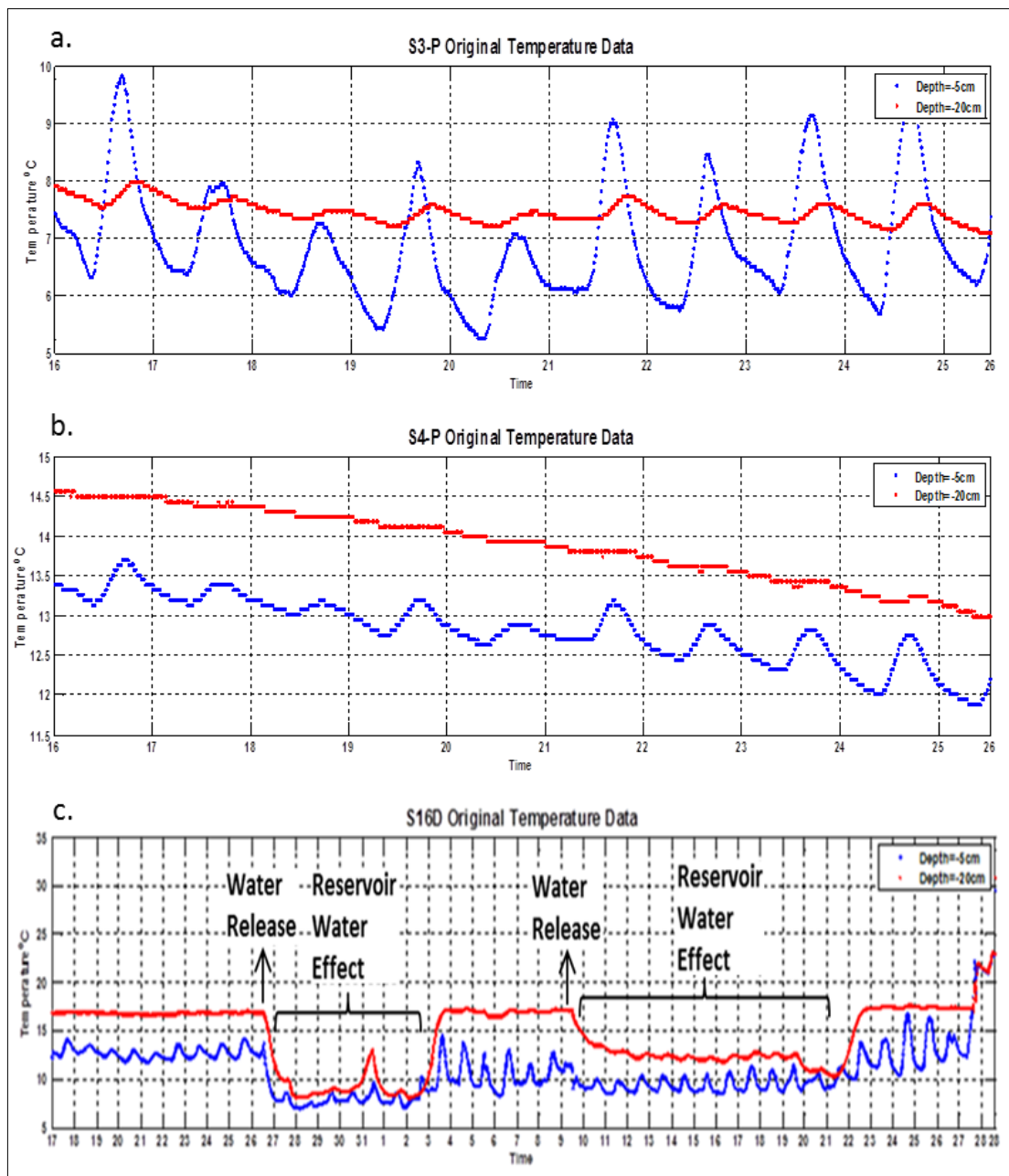


Figure 35: a) Streambed temperature variations in S3-P at depths of 5 cm and 20 cm during 12.03.2015 – 26.03.2015 measurement period. b) Streambed temperature variations in S4-P at depths of 5 cm and 20 cm during 12.03.2015 – 26.03.2015 measurement period. c) Streambed temperature variations in S16-D at depths of 5 cm and 20 cm during 12.03.2015 – 27.04.2015 measurement period.

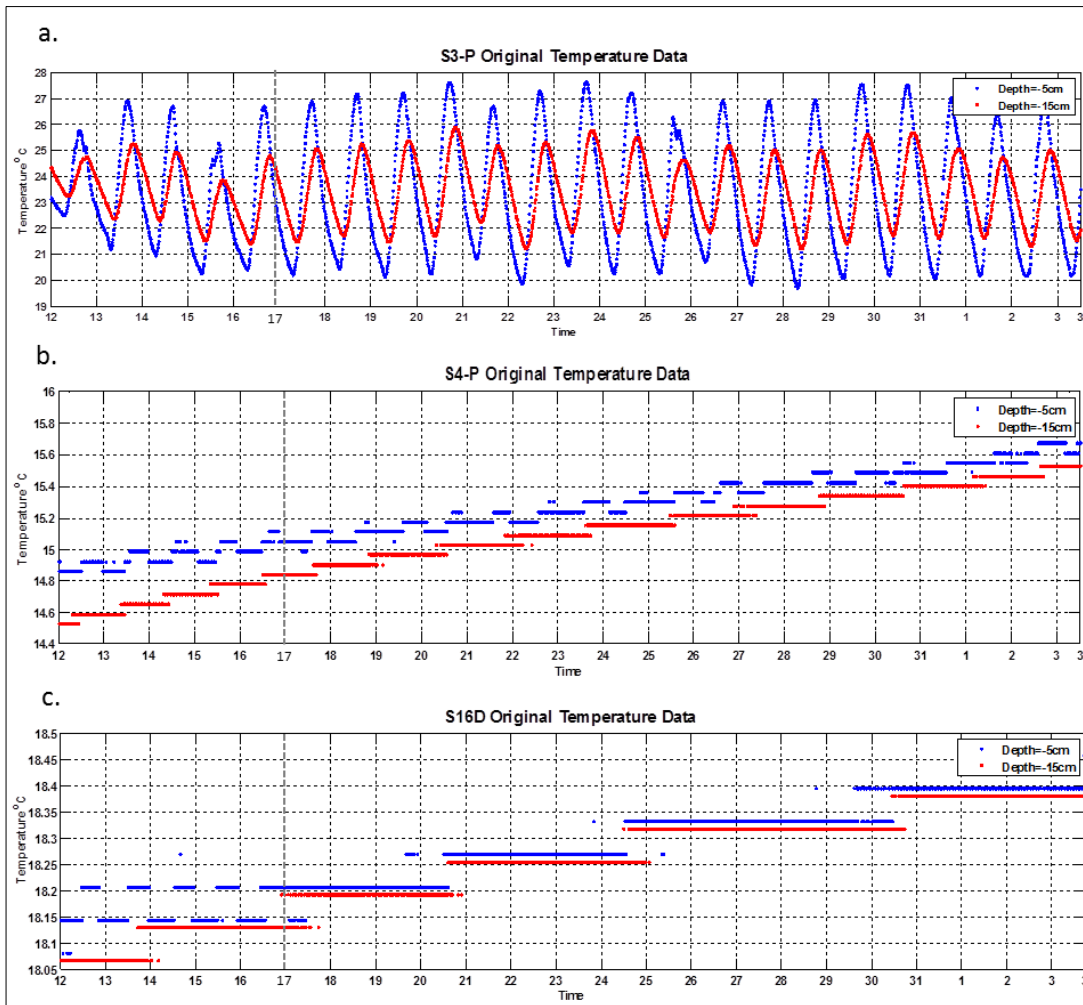


Figure 36: Streambed temperature variations in each location at depths of 5 cm and 15 cm during 10.07.2015 - 03.08.2015 measurement period.

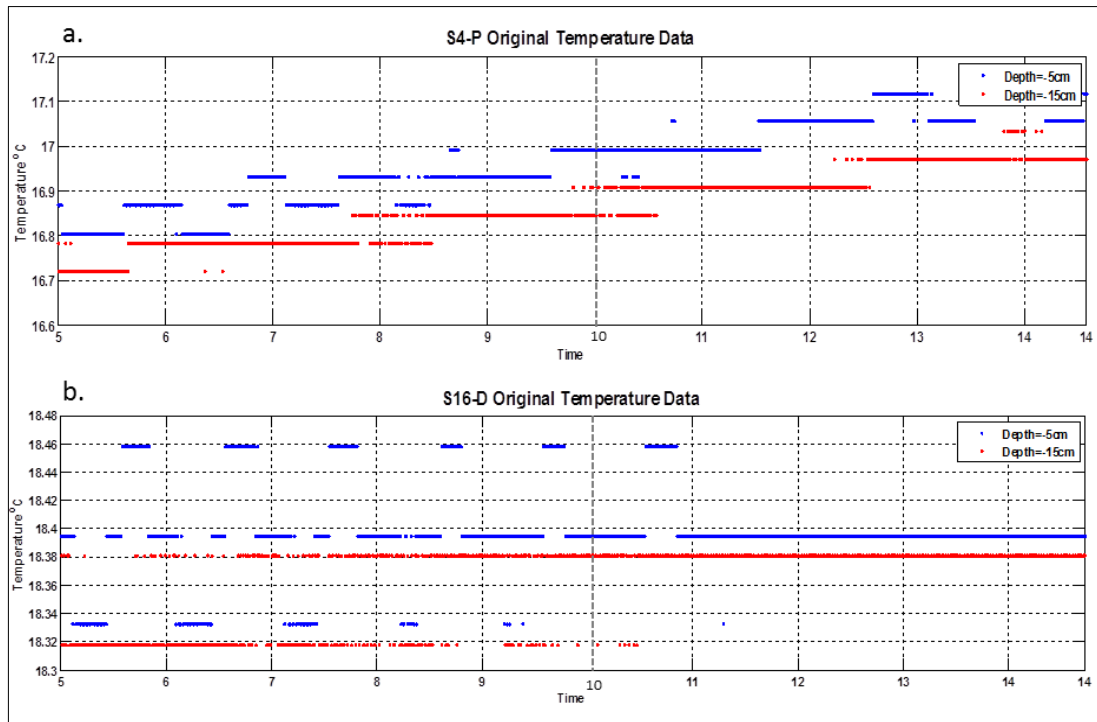


Figure 37: Streambed temperature variations in S4-P and S16-D at depths of 5 cm and 15 cm during 03.09.2015 – 14.09.2015 measurement period.

In location S4-P, minimum and maximum temperature values which are 11.886°C (at 5 cm depth) and 17.181°C (at 5 cm depth) belong to March and September months respectively (Table 11). When temperature time series of March 2015 is examined (Figure 35b) it can be realized that fluctuation is obvious in shallower streambed temperature values while it is not observed in deeper ones because of relatively more groundwater effect. However, as can be seen in Table 11, difference between maximum and minimum temperature values at two different depths are approximately the same. This indicates the upwelling groundwater effect in shallower sections. For observation periods 10<sup>th</sup> of July – 3<sup>rd</sup> of August and 3<sup>rd</sup> – 14<sup>th</sup> of September, streambed temperature variations at 5 cm and 15 cm depths can be seen in Figure 36b. For this measurement period, maximum and minimum streambed temperatures are close to each other, their difference does not exceed 1.0°C (Table

11). Also, temperature values at two different depths show no significant fluctuation, they vary intermittently in time (Figure 36b). It is clear that relatively stable sediment temperatures were measured at both depths with a stable increasing trend. In measurement period 03.09.2015 – 14.09.2015, streambed temperature variations are similar with July – August 2015. Again, no significant fluctuations are observed due to groundwater contribution (Figure 37a).

In S16-D, the minimum temperature was recorded in March and the maximum temperature was recorded in both July and September (Table 11). In July, August and September, streambed temperatures are relatively stable and observed around 18°C, maximum and minimum temperatures are significantly close to each other (difference is less than 0.5°C). Similar to S4-P location, rather than diurnal fluctuations intermittent change is observed in July – August 2015 and September 2015 measurement periods as can be seen in Figure 36c and Figure 37b. Again this is because of upwelling groundwater. However, there is a significant difference (8.5 °C) between maximum and minimum temperature values of March-April time period in S16-D (Table 11). Periodic temperature changes are observed in this location (Figure 35c). On 26<sup>th</sup> of March, reservoir water was released from Doğanözü Dam by V. Regional Directorate of State Hydraulic Works because of excessive rainfall and this process was repeated. Temperature loggers which had been installed in this site could not be reached due to excess released flow and left in the field for a longer time period with respect to S3-P and S4-P. The relatively lower streambed temperature values ranging between 8°C and 13°C were recorded after the release of reservoir water and the lowest value belongs to depth of 5 cm (this shows the direct effect of surface water temperature). Higher temperature values were recorded after some time with the decrease in the effect of reservoir water. The graph of streambed temperature variation at two different depths can be seen in Figure 35c. According to the graph, water was released from Doğanözü Dam two times during measurement period and these times corresponds to 26<sup>th</sup> of November and 9<sup>th</sup> of April. With the water release, significant decrease in streambed temperatures was recorded and these periods are also shown on the Figure 35c.



#### 5.4.2. Vertical Fluid Flux Values - VFLUX

Vertical fluid flux values were calculated using VFLUX program for time periods and locations mentioned in sections 4.4.1 and 5.4.1. Positive and negative flux values indicate movement of water in downward and upward directions respectively. Range in vertical flux values for each time interval in each site can be examined in Table 12. Also, graphs of flux variations in each location for each measurement period are given in Figure 38 (12.03.2015 – 26.03.2015 for S3-P and S4-P), Figure 39 (10.07.2015 – 03.08.2015), Figure 40 (03.09.2015 – 14.09.2015), Figure 41 (a single graph of S16-D for 12.03.2015 – 27.04.2015), Figure 42 (graphs of segments 1 and 2 in S16-D for 12.03.2015 – 27.04.2015), Figure 43 (graphs of segments 3 and 4 in S16-D for 12.03.2015 – 27.04.2015). In all graphs, time axis refers to days.

Table 12 : Minimum and maximum flux values for each time interval in each site.

Site	Measurement Period	Min (m/s)	Max (m/s)
S3-P	12.03.2015 - 26.03.2015	-5.129E-06	-3.996E-06
	10.07.2015 - 03.08.2015	1.489E-07	1.707E-06
S4-P	12.03.2015 - 26.03.2015	-5.497E-06	-2.333E-06
	10.07.2015 - 03.08.2015	-9.643E-06	-3.125E-06
	03.09.2015 - 14.09.2015	-6.981E-06	9.112E-06
S16-D	12.03.2015 - 27.04.2015	-9.542E-06	8.906E-07
	10.07.2015 - 03.08.2015	-1.362E-05	3.084E-05
	03.09.2015 - 14.09.2015	-1.298E-05	-1.246E-06

As mentioned before, S3-P is located in the losing reach of Kirmir Stream according to VHG values. However, when we look at the minimum and maximum flux values in 12.03.2015 – 26.03.2015 measurement period, we can realize that both are negative indicating the upward water movement (Figure 38a).

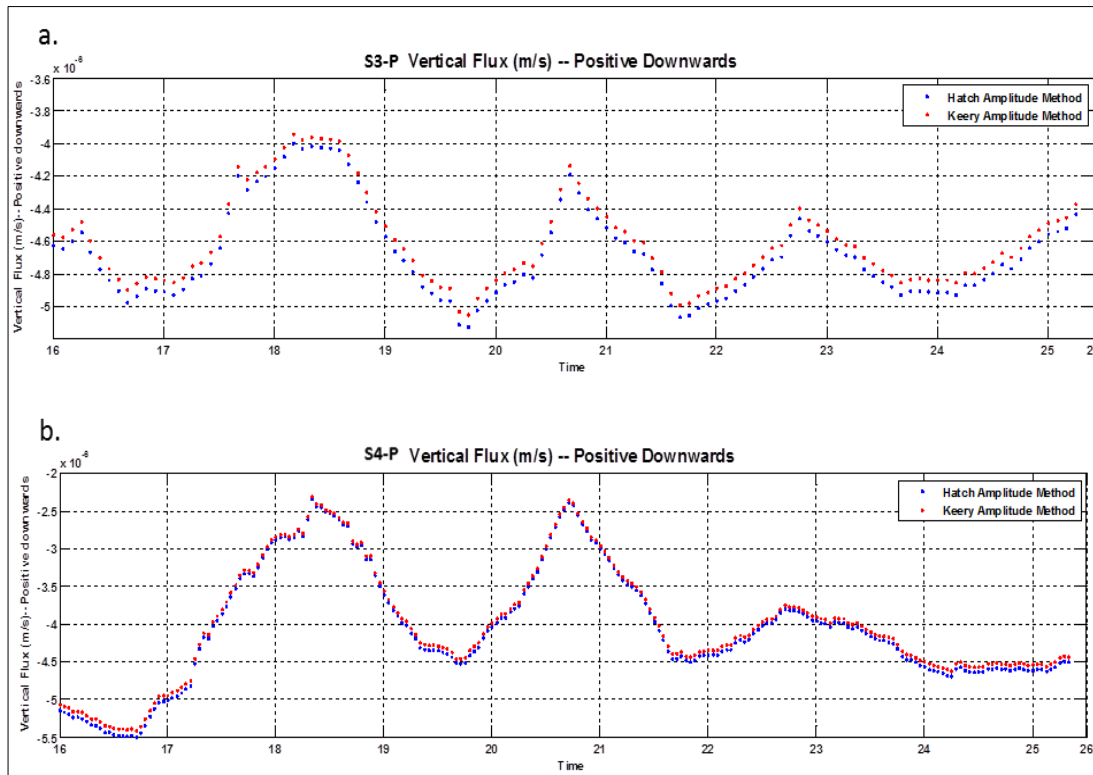


Figure 38 : Vertical flux variations in S3-P and S4-P calculated using temperature variations at depths of 5 cm and 20 cm during 12.03.2015 – 26.03.2015 measurement period.

Vertical flux values change between  $-5.129 \times 10^{-6}$  m/s and  $-3.996 \times 10^{-6}$  m/s (Table 12). This is possible due to the fact that temperature loggers in this site were installed approximately 20 - 25 m away from the nested piezometers to avoid frequent ponding conditions at the piezometer site. On the other hand, all flux values are positive in 10<sup>th</sup> of July - 3<sup>rd</sup> of August (Figure 39a). Flux values change between  $1.498 \times 10^{-7}$  and  $1.707 \times 10^{-6}$  (Table 12). This shows that the Kirmir Stream feeds the adjacent aquifer system during its time period, which is consistent with the VHG information.

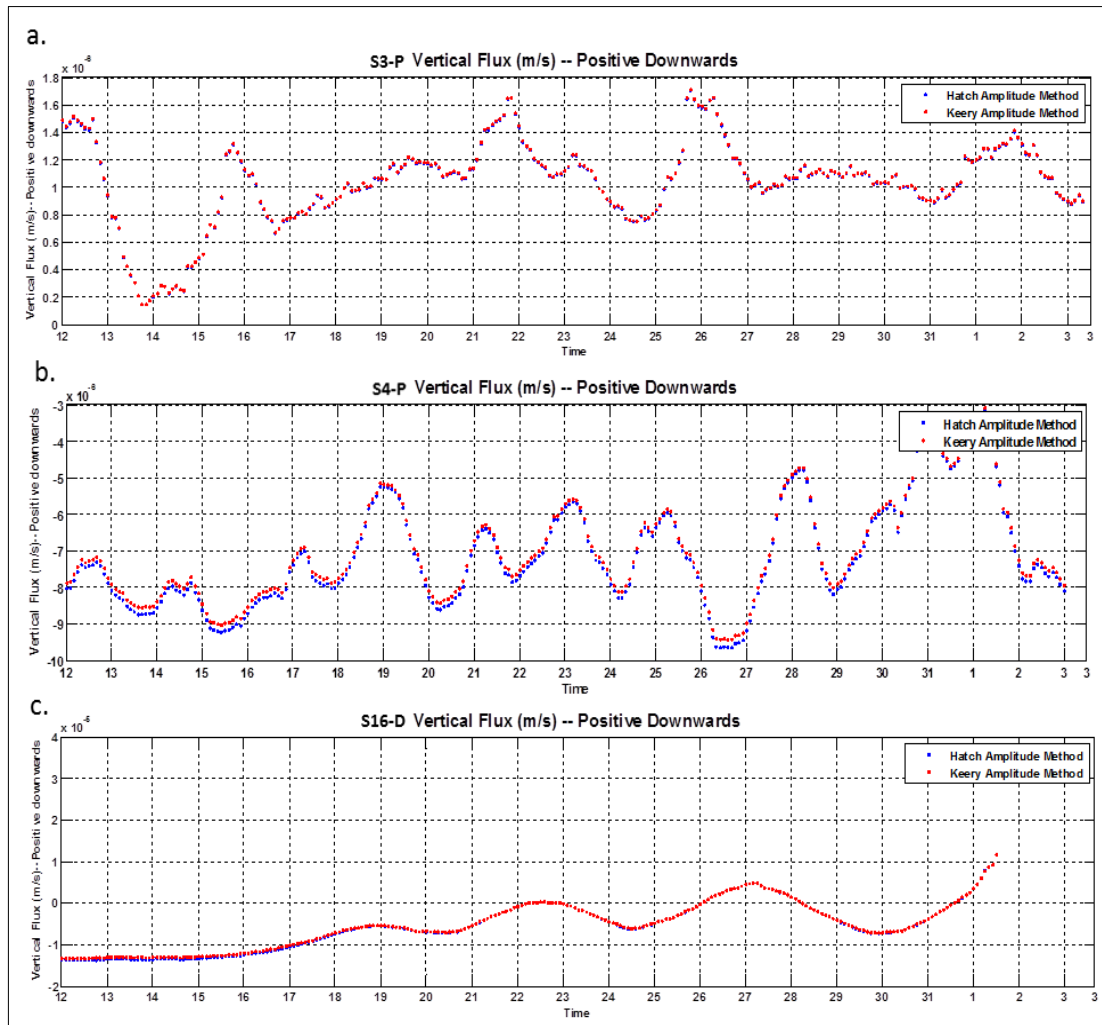


Figure 39: Vertical flux variations in each location at depths of 5 cm and 15 cm during 10.07.2015 - 03.08.2015 measurement period.

VHG values indicate that S4-P became a gaining reach beginning from January 2015. This information is also supported by temperature based negative flux values. In March, vertical flux values range from  $-5.497 \times 10^{-6}$  m/s to  $-2.333 \times 10^{-6}$  m/s (Table 12 and Figure 38b). In measurement period 10<sup>th</sup> of July - 3<sup>rd</sup> of August, all flux values are negative again and change between  $-9.643 \times 10^{-6}$  m/s and  $-3.125 \times 10^{-6}$  m/s (Figure 39b). In this period, groundwater contribution is relatively more to Kirmir Stream with respect to March as can be understood from the vertical flux values.

Therefore, existence of relatively more stable streambed temperatures in July-August period may be explained by more groundwater contribution. On the contrary, Kirmir Stream both gains and loses its water in this location on September according to vertical fluxes (Figure 40a). Maximum and minimum flux values are  $9.112 \times 10^{-6}$  and  $-6.981 \times 10^{-6}$  respectively (Table 12). However, stream loses its water for a short time period, only between 9<sup>th</sup> and 12<sup>th</sup> of September. Therefore, in a broader view this location can be identified as a gaining reach of the Kirmir Stream.

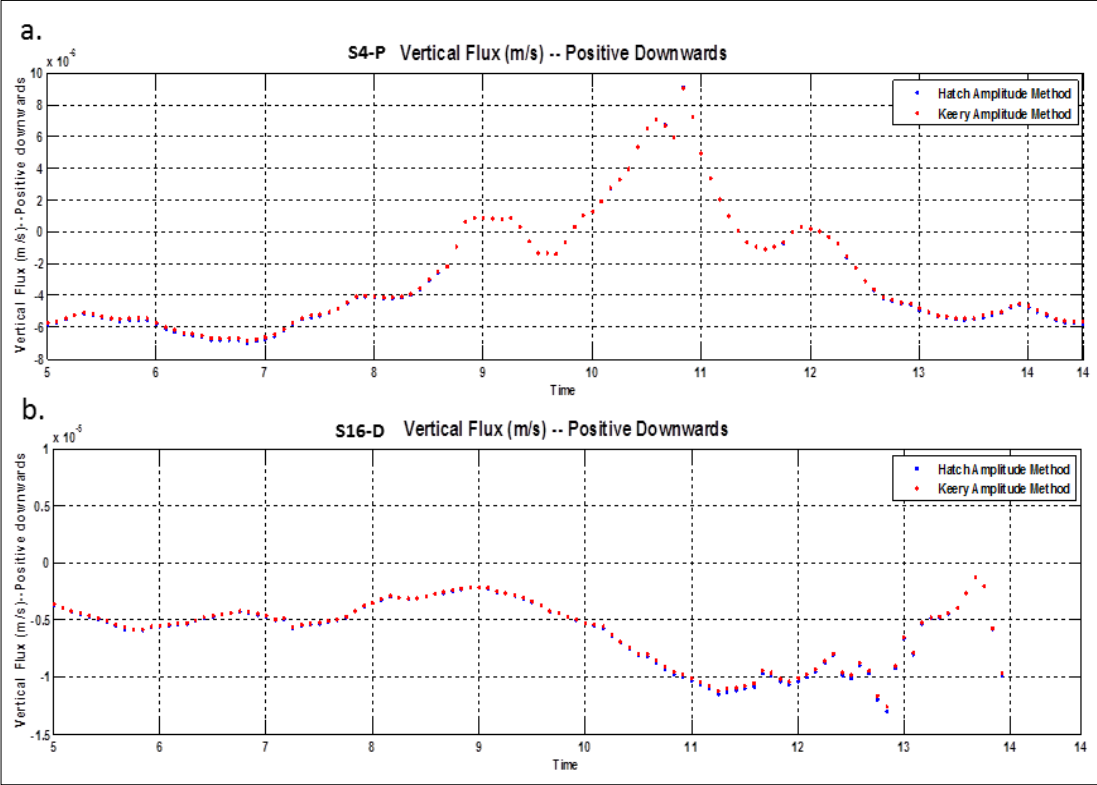


Figure 40 : Vertical flux variations in S4-P and S16-D at depths of 5 cm and 15 cm during 03.09.2015 – 14.09.2015 measurement period.

Vertical flux values at monitoring location S16-D are mostly negative values indicating upwelling direction of water movement at this location. Time intervals representing immediately after the release and hold of reservoir water were ignored while calculating vertical flux values in March-April measurement period to avoid bias in VFLUX calculations. Ignoring them caused the changes in flux values in terms of both magnitude and direction. In Figure 41, all flux values are negative because whole data were taken into account. However, when these time intervals are ignored, positive flux values are calculated. Therefore, time intervals when reservoir water was released were ignored in this study with a focus on four segments (division into four segments can be seen in Figure 41). Vertical fluxes were calculated separately for these segments. Maximum and minimum flux values were analyzed both separately (Table 13) and together (Table 12). The graphs (temperature and flux) of each segment are given in Figure 42 and Figure 43. Flux values are negative in all segments except segment 3. In this segment, there are only six positive flux values and they occur on 11<sup>th</sup> and 19<sup>th</sup> of April. For March, it can be said that, groundwater feeds Kirmir Stream. This analysis indicates that reservoir operation has an impact on the degree of groundwater stream interaction along the study area. In July-August measurement period, flux values range between  $-1.362 \times 10^{-5}$  m/s and  $3.084 \times 10^{-5}$  m/s. As can be seen in Figure 39, positive flux values are significantly less with respect to negative ones and they occur between 26<sup>th</sup> and 28<sup>th</sup> of July and on 31<sup>th</sup> of July. In September (Figure 40), all flux values were calculated as negative. As a result, generally this location can be identified as a gaining reach of the study area which is consistent with the discharge measurements (see section 5.3).

Table 13: Maximum and minimum flux values in S16-D for each segment.

Division	Time interval	Max Flux (m/s)	Min Flux (m/s)
Segment 1	6 March 22:59 - 26 March 13:4	-3.409E-06	-5.483E-06
Segment 2	3 April 20:29 - 9 April 07:14	-7.172E-06	-9.349E-06
Segment 3	11 April 0:14 - 20 April 0:14	8.906E-07	-3.497E-06
Segment 4	22 April 14:29 - 27 April 0:59	-6.011E-06	-9.542E-06

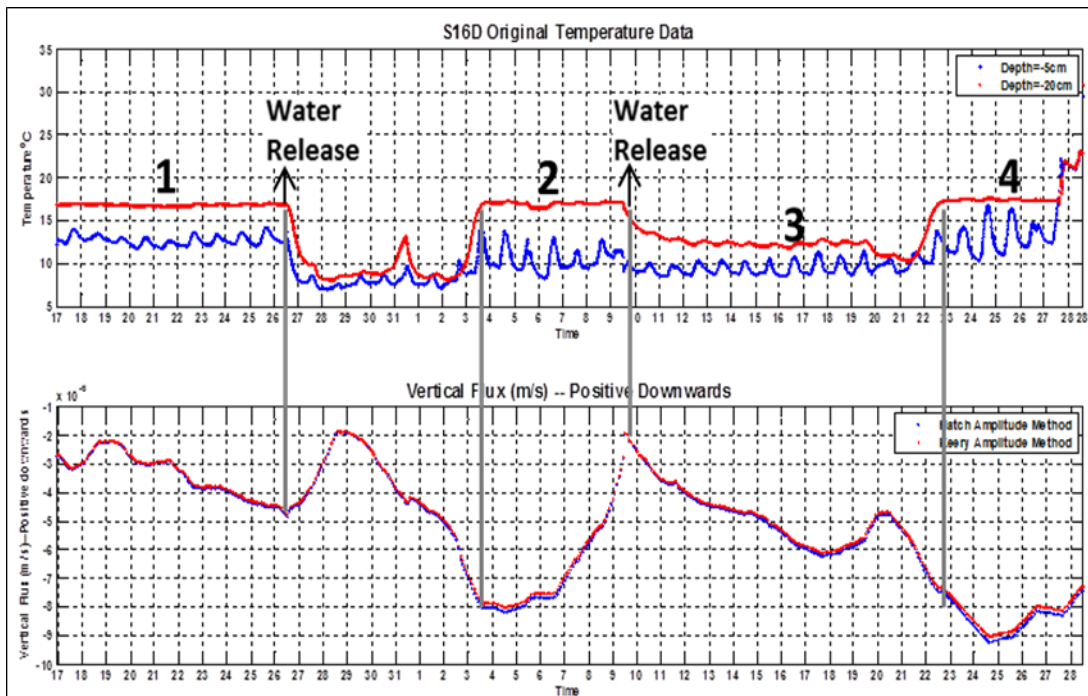


Figure 41 : Segments of whole temperature and flux data in S16-D for measurement period March – April.

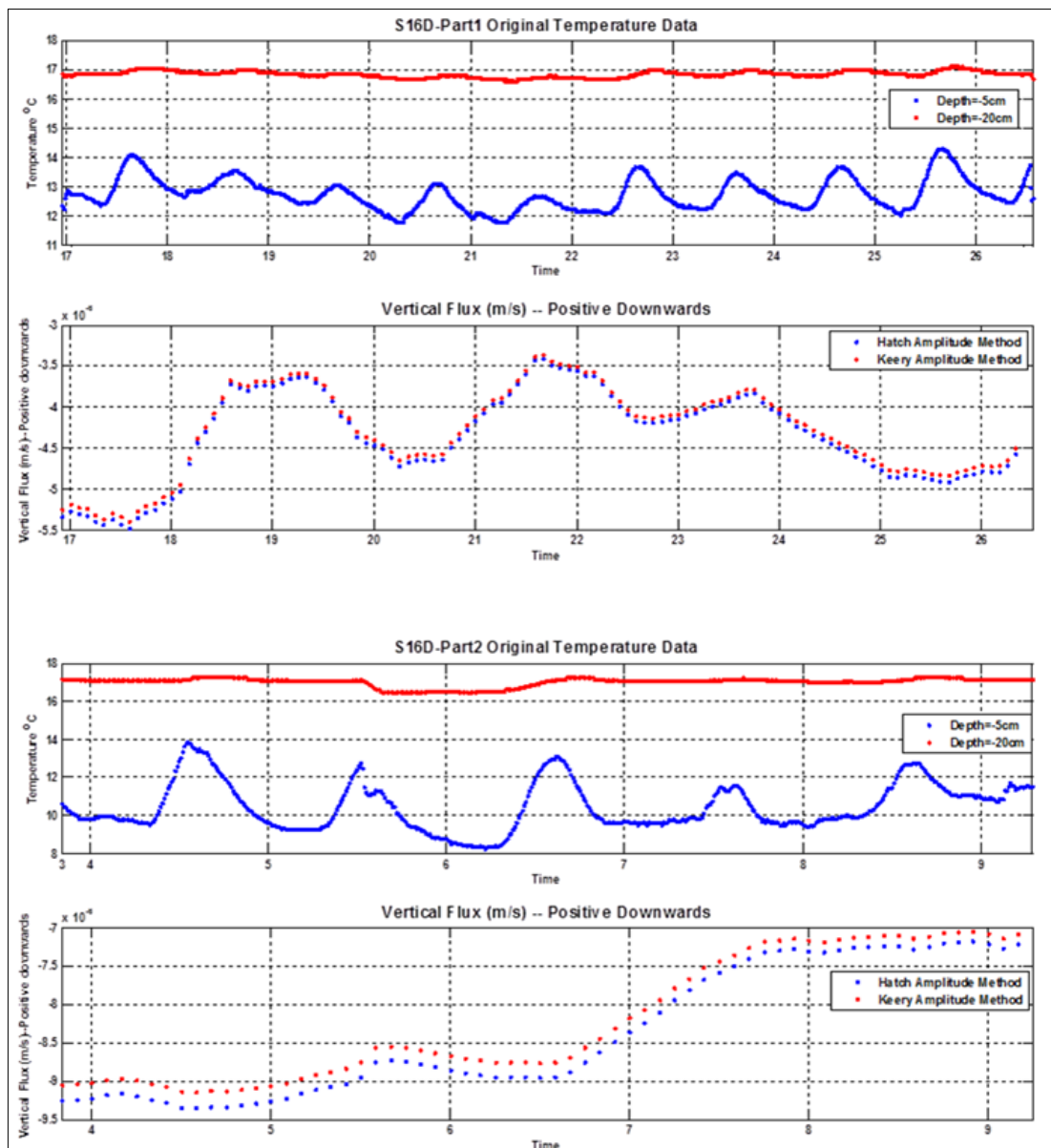


Figure 42: Temperature variation in streambed and flux values for segments 1 and 2 in S16-D during March - April 2015 measurement period.

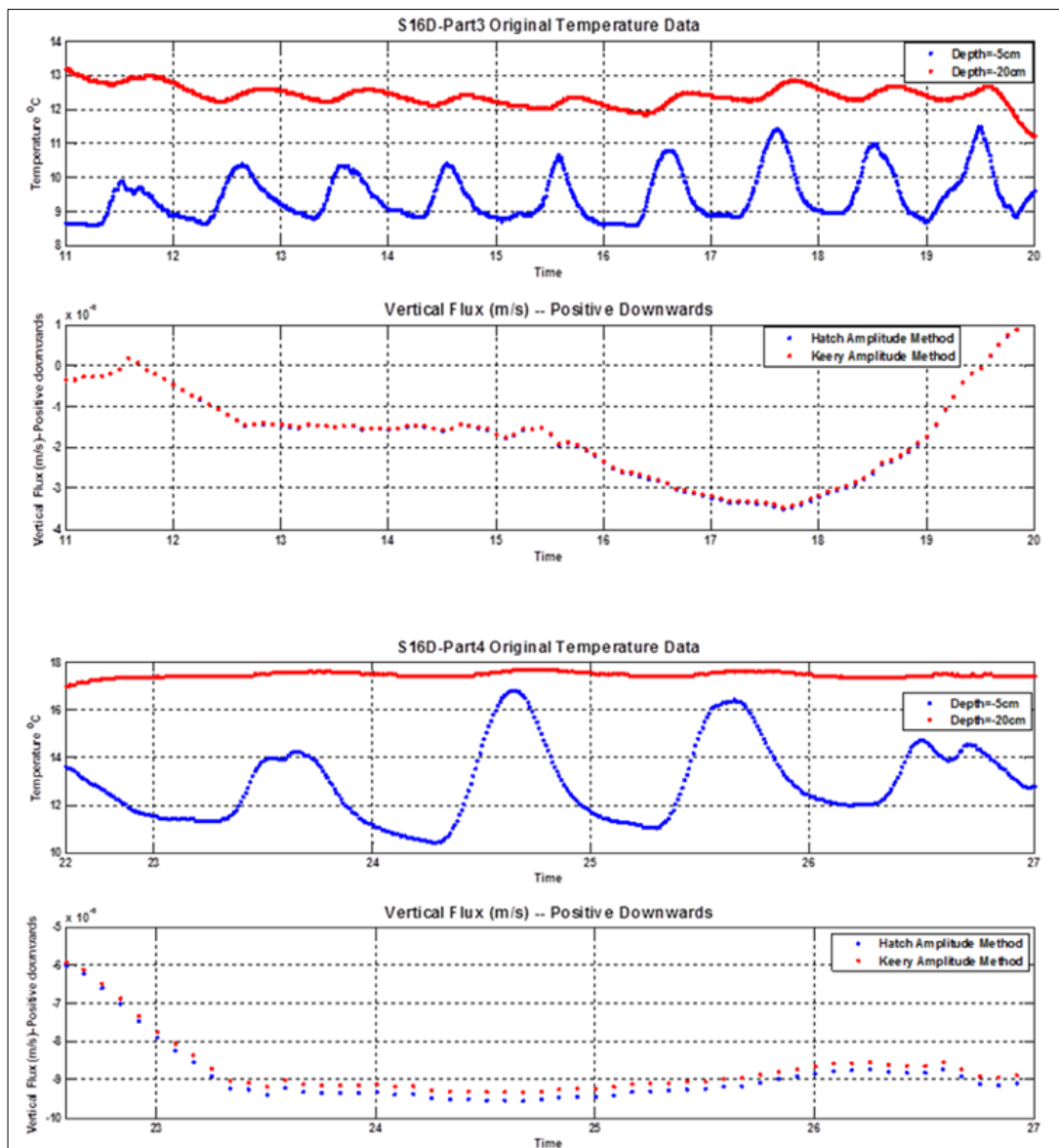


Figure 43: Temperature variation in streambed and flux values for segments 3 and 4 in S16-D during March - April 2015 measurement period.



#### 5.4.2.1. Calculation of Vertical Hydraulic Conductivity of the Streambed

In this study, VHG values obtained from piezometer data and flux values obtained from VFLUX program were used to calculate the streambed vertical hydraulic conductivity values for sites S3-P and S4-P using Darcy's equation (see section 2.2.1). These values can be seen in Table 14 and Table 16 for S3-P and S4-P respectively. Also their geometric means can be examined in Table 15 for each date. Because no piezometer was installed in S16-D, calculations could not be performed for this location. In S3-P, flux values do not exist for 3<sup>rd</sup> and 14<sup>th</sup> of September, and hence vertical hydraulic conductivity calculation could not be performed for these two dates. It is clear that, for all overlapping dates S3-P has higher  $K_v$  values than S4-P. As explained before S3-P is located in a losing reach of the study area but S4-P shows both losing and gaining character.

In S3-P monitoring location, vertical hydraulic conductivity values (m/sec) range between  $2.22 \times 10^{-5} - 7.47 \times 10^{-5}$ ,  $1.28 \times 10^{-4} - 2.20 \times 10^{-4}$  and  $3.21 \times 10^{-5} - 3.47 \times 10^{-5}$  for dates 12.03.2015, 10.07.2015 and 03.08.2015 respectively. Although there exist no significant differences,  $K_v$  values in July 2015 are greater. Geometric means for March, July and August 2015 are  $4.67 \times 10^{-5}$  m/sec,  $1.63 \times 10^{-4}$  m/sec and  $3.30 \times 10^{-5}$  m/sec respectively.

In S4-P site,  $K_v$  values could be calculated also for September 2015. They vary between values  $2.11 \times 10^{-5} - 3.08 \times 10^{-5}$ ,  $5.70 \times 10^{-5} - 7.21 \times 10^{-5}$ ,  $2.64 \times 10^{-5} - 2.82 \times 10^{-5}$ ,  $7.62 \times 10^{-5} - 1.06 \times 10^{-4}$  for dates 12.03.2015, 10.07.2015, 03.08.2015 and 03.09.2015 respectively. For the date 14.09.2015 there are only two values  $1.64 \times 10^{-4}$  and  $2.57 \times 10^{-4}$ . Geometric mean values (Table 15) are  $2.54 \times 10^{-5}$  m/sec,  $6.47 \times 10^{-5}$  m/sec,  $2.85 \times 10^{-5}$  m/sec,  $9.15 \times 10^{-5}$  m/sec,  $2.05 \times 10^{-4}$  m/sec for 12.03.2015, 10.07.2015, 03.08.2015, 03.09.2015 and 14.09.2015 dates respectively. It can be seen that the estimated  $K_v$  values are similar for different periods; while the highest values belong to 3<sup>rd</sup> and 14<sup>th</sup> of September 2015. When these two dates are compared, it is realized that, mid-September has higher values.

Table 14: Vertical Hydraulic Conductivity values in location S3-P.

S3-P								
12.3.2015			10.7.2015			3.8.2015		
q	VHG	Kv	q	VHG	Kv	q	VHG	Kv
6.20E-06	0.1437	4.31E-05	3.96E-06	0.0180	2.20E-04	9.72E-07	0.0299	3.25E-05
1.07E-05	0.1437	7.47E-05	3.25E-06	0.0180	1.81E-04	9.70E-07	0.0299	3.24E-05
9.26E-06	0.1437	6.44E-05	3.04E-06	0.0180	1.69E-04	9.61E-07	0.0299	3.21E-05
9.24E-06	0.1437	6.43E-05	2.75E-06	0.0180	1.53E-04	1.00E-06	0.0299	3.35E-05
8.73E-06	0.1437	6.08E-05	2.53E-06	0.0180	1.41E-04	1.04E-06	0.0299	3.47E-05
3.19E-06	0.1437	2.22E-05	2.31E-06	0.0180	1.28E-04	nm	nm	nm
3.84E-06	0.1437	2.68E-05	nm	nm	nm	nm	nm	nm

Table 15: Geometric means of vertical hydraulic gradient values in S3-P and S4-P for each flux measurement dates.

Site / Date	12.3.2015	10.7.2015	3.8.2015	3.9.2015	14.9.2015
<b>S3-P</b>	4.666E-05	1.628E-04	3.303E-05	nm	nm
<b>S4-P</b>	2.539E-05	6.472E-05	2.853E-05	9.150E-05	2.049E-04

\* nm denotes no measurement

Table 16: Vertical hydraulic conductivity values in location S4-P.

S4-P														
12.3.2015			10.7.2015			3.8.2015			3.9.2015			14.9.2015		
q	VHG	Kv	q	VHG	Kv	q	VHG	Kv	q	VHG	Kv	q	VHG	Kv
6.22E-06	0.2019	3.08E-05	1.01E-05	0.1408	7.21E-05	4.46E-06	0.1690	2.64E-05	7.97E-06	0.0751	1.06E-04	1.20E-05	0.0469	2.57E-04
6.13E-06	0.2019	3.04E-05	9.67E-06	0.1408	6.86E-05	4.62E-06	0.1690	2.73E-05	7.46E-06	0.0751	9.93E-05	7.69E-06	0.0469	1.64E-04
5.73E-06	0.2019	2.84E-05	9.20E-06	0.1408	6.53E-05	4.77E-06	0.1690	2.82E-05	6.99E-06	0.0751	9.30E-05	nm	nm	nm
5.41E-06	0.2019	2.68E-05	8.68E-06	0.1408	6.17E-05	5.51E-06	0.1690	3.26E-05	6.45E-06	0.0751	8.58E-05	nm	nm	nm
5.03E-06	0.2019	2.49E-05	8.03E-06	0.1408	5.70E-05	nm	nm	nm	5.72E-06	0.0751	7.62E-05	nm	nm	nm
4.87E-06	0.2019	2.41E-05	nm	nm	nm	nm	nm	nm	nm	nm	nm	nm	nm	nm
4.83E-06	0.2019	2.39E-05	nm	nm	nm	nm	nm	nm	nm	nm	nm	nm	nm	nm
4.72E-06	0.2019	2.34E-05	nm	nm	nm	nm	nm	nm	nm	nm	nm	nm	nm	nm
4.46E-06	0.2019	2.21E-05	nm	nm	nm	nm	nm	nm	nm	nm	nm	nm	nm	nm
4.25E-06	0.2019	2.11E-05	nm	nm	nm	nm	nm	nm	nm	nm	nm	nm	nm	nm

### 5.4.3. Solute Mass Balance

The locations where water samples and discharge measurements were taken are given (Figure 44). In some locations both groundwater and surface water chloride concentrations were measured. In Table 17, chloride concentrations and discharge values in sampling locations are listed. In the light of this information, solute mass balance was applied to understand groundwater - surface water interaction in the region.

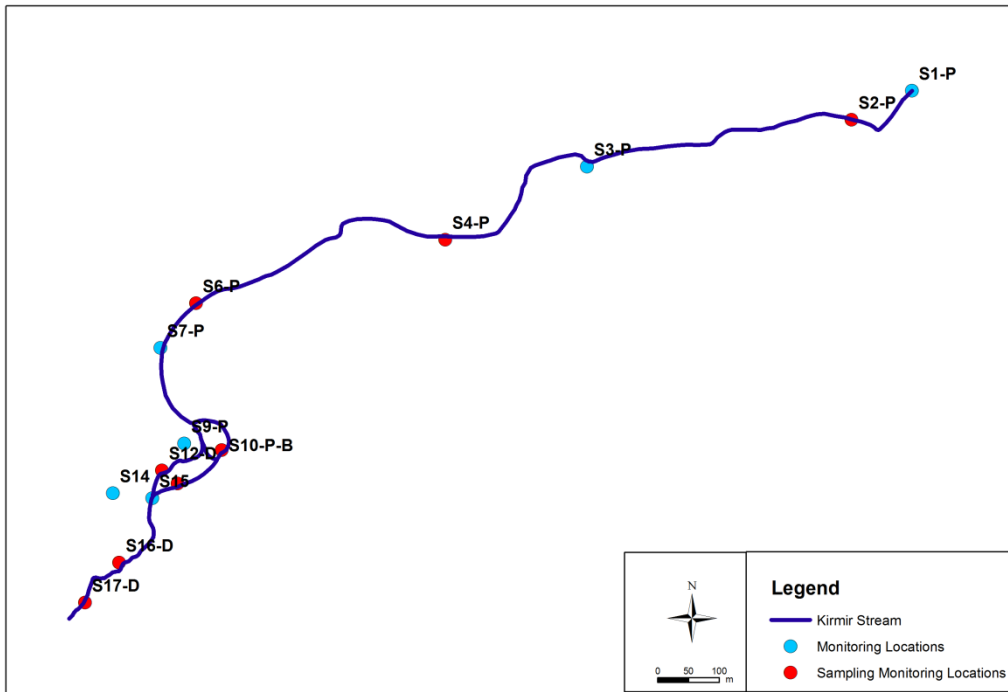


Figure 44: Chloride sampling monitoring locations through the study area.

Releasing of reservoir water from Doğanözü Dam due to excessive precipitation caused the formation of new stream reaches in the study area. One connects the site S7-P to the stream section between S10-P-B and S13-D and the other reach connects S7-P to S9-P. Therefore, surface water coming from S7-P have been separated into

three parts, but only small amount of it contributes the S10-P-B as can be understood from the discharge amount. During sampling and mass balance application, these circumstances were taken into consideration. Between several locations solute mass balance was applied. In this section, the results were briefly examined and discussed.

Table 17 : Chloride concentrations and discharge values in sampling locations.

Locations	Cl (mg/L)	Q(L/sec)
S2-P Upstream	28.499	nm
S2-P Piezometer	28.755	nm
S2-P Downstream	28.605	85.5
S4-P Upstream	28.565	48.7
S4-P Piezometer	27.821	nm
S4-P Downstream	29.376	nm
S6-P Upstream	30.213	82.8
S6-P Piezometer	33.457	nm
S6-P Downstream	29.217	73.3
S10-P-B Upstream	6.889	6.5
S10-P-B Piezometer	7.421	nm
S10-P-B Downstream	7.057	nm
S12-D	28.664	66.7
S13-D	19.966	28.7
S16-D	24.269	125.5
S17-D	24.623	136.9

Between Sites S6-P, S10-P-B and S13-D

Solute mass balance including these locations was performed to find the discharge - amount of the new reach which connects the S7-P to the stream section between S10-P-B and S13-D. As the chloride concentration of this new reach, the averages of three values measured in S6-P were used (dowstream concentration could also be used, but both values are very similar to each other), because it is located very close

to this site. However, it has unknown amount of discharge. For mass balance, downstream chloride concentration and upstream discharge amount of S10-P-B were taken into concentration, because there is no flow in downstream part of this location, that is, flowing surface water becomes stagnant. Mass balance equation is:

$$Q_{10} \times C_{10} + Q_{\text{new}} \times C_{\text{new}} = Q_{13} \times C_{13}$$

where;

$Q_{10}$  is 6.5 L/sec,  $C_{10}$  is 7.057 mg/L,  $Q_{13}$  is 28.7 L/sec,  $C_{13}$  is 19.966 mg/L,  $C_{\text{new}}$  is 30.963 mg/L and  $Q_{\text{new}}$  is unknown.

By substituting these values, the discharge amount of the new reach was found as 17.0 L/sec. The difference between discharge amounts of S13-D and S10-P-B is 22.2 L/sec and the estimated discharge almost is very close to this value.

#### Between S12-D, S13-D and S16-D

As mentioned before, S12-D and S13-D join and form S15 and later flow towards S16-D and S17-D. There are no side tributaries joining the Kirmir stream within the boundaries of the study area. When discharge amounts, measured in S12-D, S13-D and S16-D on sampling date are examined (Table 17), discharge amount in S16-D is significantly greater than the total discharge amount of S12-D and S13-D. The difference corresponds to 30.10 L/sec. Because of this, mass balance was performed between these locations to find the source of this addition. Mass balance is as follows:

$$Q_{12} \times C_{12} + Q_{13} \times C_{13} + [Q_{16} - (Q_{12} + Q_{13})] \times C_{\text{excess water}} = Q_{16} \times C_{16}$$

where;

$Q_{12}$  is 6.7 L/sec,  $C_{12}$  is 28.664 mg/L,  $Q_{13}$  is 28.7 L/sec,  $C_{13}$  is 19.966 mg/L,  $Q_{16}$  is 125.5 L/sec and  $C_{16}$  is 24.269 mg/L.

By substituting the values,  $C_{\text{unknown source}}$  was calculated as 19.0 mg/L. This concentration corresponds to the concentration of S13-D. Therefore, this amount of Kirmir Stream may go subsurface at S13-D which then emerges in S16-D.

*Between S16-D and S17-D*

S16-D and S17-D are the last two sites of the study area and there is a discharge difference between them. Mass balance was performed for these locations to find the source of discharging water to Kirmir Stream. Mass balance is as follows:

$$Q_{16} \times C_{16} + [(Q_{17} - Q_{16}) \times C_{\text{excess water}}] = Q_{17} \times C_{17}$$

where;

$Q_{16}$  is 125.5 L/sec,  $C_{16}$  is 24.269 mg/L,  $Q_{17}$  is 136.9,  $C_{17}$  is 24.623 mg/L.

As a result, the concentration of excess water was calculated as 28.526 mg/L. This is equal to the concentration of both stream water and water sample taken from piezometer S2-P as can be seen in Table 17. This can mean that downwelling stream water in S2-P may come to surface between S16-D and S17-D.

*Between S4-P and S6-P*

The difference between discharge amounts of S6-P and S4-P corresponds to 34.1 L/sec. Mass balance applied to find the chloride concentration of this excess water is as follows:

$$Q_4 \times C_4 + [(Q_6 - Q_4) \times C_{\text{excess water}}] = Q_6 \times C_6$$

where;

$Q_6$  is 82.8 L/sec,  $C_6$  is 30.213 mg/L,  $Q_4$  is 48.7 and  $C_4$  is 28.565 mg/L.

$C_{\text{excess}}$  was found as 32.5731 mg/L. As can be seen in Table 17, chloride concentration of water sample taken from deeper piezometer of S4-P is 27.821 mg/L. The chloride concentration of excess water is almost equal to the concentration of the water sample. This indicates that excess water can be the groundwater contribution. The vice versa was also performed for affirmation:

$Q_4 \times C_4 + (Q_{\text{gw}} \times C_{\text{gw}}) = Q_6 \times C_6$  where  $C_{\text{gw}}$  is 27.821 mg/L and  $Q_{\text{gw}}$  is unknown.

Then,  $Q_{\text{gw}}$  was found as 39.9 L/sec. This value is significantly close to the discharge amount differences between S4-P and S6-P. Therefore, the increase in discharge amount in site S6-P with respect to S4-P can be because of groundwater contribution.

#### Between S6-P, S10-P, S12-D and S13-D

The purpose of mass balance performed between these locations is to understand the effect and contribution of S10-P-B location to the downstream locations. We have upstream discharge amount in S10-P-B, but downstream discharge amount could not be measured because of field conditions in this site. First of all, the difference between the discharge amounts of upstream and downstream were used to find the amount of coming water from S10-P-B and it was found as 12.62 L/sec. After that, mass balance was performed and the chloride concentration of S10-P-B in downstream was used. From this mass balance a new  $Q$  was calculated. This  $Q$  and the discharge difference between upstream and downstream were compared to understand the effect of S10-P-B location to the downstream sites. Therefore, following steps were applied:

1.  $(Q_{12} + Q_{13}) - (Q_{10} + Q_6) = (28.742 + 66.7) - (Q_{10} + 82.8) = 12.619 \text{ L/sec}$

2.  $(Q_6 \times C_6) + (Q_{10} \times C_{10}) = Q_{12} \times C_{12} + Q_{13} \times C_{13}$  where;



$Q_{12}$  is 66.7 L/sec,  $C_{12}$  is 28.664 mg/L,  $Q_{13}$  is 28.7 L/sec,  $C_{13}$  is 19.966 mg/L,  $Q_6$  is 82.8 L/sec,  $C_6$  is 29.217 mg/L and  $C_{10}$  is 7.057 mg/L and  $Q_{10}$  was calculated.

Therefore,  $Q_{10}$  was found as 9.99 L/sec. This amount is significantly close to the result in step 1 and it can be said that S10-P-B location has a significant influence on the sites located at more downstream with respect to it.

## **5.5. Chemical Interactions of Groundwater - Stream Water and Indications of Water Quality**

### **5.5.1. Water Quality Field Parameters**

Water quality field parameters include, temperature, electrical conductivity (normalized to 25°C), total dissolved solids, pH, dissolved oxygen, and oxidation – reduction potential. Box plots of each parameter for all measurement dates (between October 2014 and November 2015) for each surface water monitoring location are given in Figure 45 to observe the variations in stream water values. These box plots summarize the distributions by showing maximum, minimum and median values. In addition, Figure 46 shows individual measurements that are grouped into summer and winter seasons to investigate the seasonal variations in the surface water field quality parameters from upstream to downstream of the study area. These graphs show how values of each parameter show variation throughout monitoring locations. In the graphs given in Figure 46, summer season (July, August and September 2015) and winter season (December 2014, January and March 2015) measurements for surface water and piezometer water samples are shown for comparison. In this figure, red and blue points represent stream water values belonging to summer and winter months, respectively. Green and purple points, on the other hand, represent the shallow and deeper piezometers for summer season only. Mean, maximum and minimum values of water quality field parameters for surface water in summer and winter seasons are listed in Table 18. The same information but for piezometers in summer season only is listed in Table 19.

### 5.5.1.1. Temperature Measurements

In summer months, temperature values range between 18.36°C and 28.20°C (Table 18). The lowest and the highest temperatures were measured in sites S14 (a spring) and S4-P respectively. Temperature values of S10-P-B change between 22.41°C and 24.59°C. In winter season, temperature values vary between 4.20°C and 19.25°C (Table 18). The lowest temperature was measured in S3-P and the highest value belongs to S10-P-B since it is a groundwater discharge location. S1-P, S2-P and S3-P has lower temperature values than the remaining of the study area. Starting from S4-P, surface water temperatures increase. As explained in section 5.2, groundwater starts to feed Kirmir Stream after the monitoring location S3-P. Therefore, increase in the surface water temperatures starting from S4-P is possibly due to the contribution of warmer groundwater and it is seen in S10-P-B more clearly. After S10-P-B, surface water temperature values decrease but still they are higher than the first three monitoring locations which are definitely under the control of surface water. Temperature values of water samples taken from piezometers (Table 19) are as high as the surface water temperature values for summer season. The highest value is observed in S3-P shallow piezometer as 27.91°C and the lowest value was measured as 17.56°C in S6-P deeper piezometer.

In Figure 45, temperature range and variability at each monitoring location is shown. In S1-P, S2-P and S3-P temperature values show a wider range with respect to other locations because of stream water effect (influenced by air temperature). It can be realized that temperature values of stream water in S10-P-B site do not change significantly due to groundwater effect. Same observation could also be extended to S14 spring location. When the seasonal temperature variation is examined (Figure 46), the differences between the summer and winter temperature values are evident. In summer season, it can be seen that the locations close to the dam spillway, namely S1-P, S2-P, and S3-P have similar trends. Temperature values of stream and water samples taken from piezometers are close to each other for sites S1-P, S2-P and S3-P. Also, for these locations seasonal temperature difference is significant. In site S3-P, piezometer values rise slightly.

Table 18: Mean, maximum and minimum values of water quality field parameters measured from surface water in summer and winter seasons.

Parameters Units	T (°C)		EC(25°C) (µS/cm)		TDS (g/lit)		Salinity		DO (mg/lit)		pH		ORP mV	
	Summer	Winter	Summer	Winter	Summer	Winter	Summer	Winter	Summer	Winter	Summer	Winter	Summer	Winter
<b>S1-P</b>														
Mean	22.46	5.80	365.5	604.0	0.290	0.393	0.22	0.29	10.01	13.53	8.89	7.50	140.3	128.5
Maximum	23.48	6.95	376.6	605.0	0.318	0.393	0.24	0.29	11.37	17.32	9.30	7.61	184.2	179.0
Minimum	21.07	4.64	354.5	603.0	0.265	0.392	0.20	0.29	7.41	9.73	8.30	7.39	75.4	78.0
<b>S2-P</b>														
Mean	21.16	5.99	360.3	598.3	0.254	0.393	0.19	0.27	8.56	13.37	8.47	8.18	31.1	195.5
Maximum	23.17	6.25	365.2	617.0	0.258	0.410	0.19	0.30	11.62	15.92	9.09	8.30	50.3	214.0
Minimum	20.07	5.54	355.4	585.0	0.251	0.380	0.18	0.23	7.08	11.57	7.95	7.96	-16.1	177.0
<b>S3-P</b>														
Mean	23.80	5.45	369.3	596.3	0.255	0.388	0.19	0.29	8.56	14.85	8.94	8.41	4.8	191.5
Maximum	26.49	7.37	375.1	601.0	0.259	0.391	0.19	0.29	9.09	17.90	9.35	8.90	26.8	210.0
Minimum	21.84	4.20	362.8	588.0	0.244	0.382	0.18	0.29	7.92	12.34	8.72	8.02	-49.6	173.0
<b>S4-P</b>														
Mean	26.20	11.26	375.7	604.7	0.262	0.394	0.19	0.30	6.78	4.36	8.81	7.77	-5.3	193.5
Maximum	28.20	12.20	386.1	629.0	0.267	0.409	0.20	0.31	7.22	6.58	8.94	7.84	7.4	202.0
Minimum	24.74	10.07	358.0	585.0	0.249	0.382	0.18	0.29	6.24	3.21	8.52	7.68	-31.7	185.0
<b>S6-P</b>														
Mean	24.64	11.19	401.3	611.7	0.276	0.398	0.21	0.30	7.08	9.76	9.03	7.86	-14.3	194.7
Maximum	25.19	14.53	414.0	655.0	0.282	0.426	0.21	0.32	7.73	12.83	9.09	8.70	10.9	253.0
Minimum	23.74	7.60	380.7	582.0	0.257	0.379	0.19	0.28	5.39	7.10	8.89	6.82	-46.3	117.0
<b>S7-P</b>														
Mean	24.59	11.13	403.5	575.5	0.276	0.379	0.21	0.28	7.17	9.83	9.15	8.10	-15.1	180.0
Maximum	25.30	13.00	415.0	602.0	0.284	0.391	0.21	0.29	8.23	12.73	9.27	8.82	4.5	221.0
Minimum	23.74	8.94	385.2	531.0	0.257	0.373	0.19	0.28	6.29	4.67	9.06	7.50	-48.9	141.0
<b>S9-P</b>														
Mean	20.66	13.45	436.7	528.8	0.315	0.344	0.23	0.26	2.60	6.73	7.68	7.69	-20.1	185.7
Maximum	21.22	15.97	453.1	613.0	0.328	0.398	0.23	0.30	3.26	9.17	7.69	8.16	-3.0	245.0
Minimum	20.20	8.67	420.1	504.0	0.305	0.328	0.23	0.24	1.97	4.95	7.68	7.21	-46.6	106.0
<b>S10-P-B</b>														
Mean	23.04	17.34	405.5	461.8	0.282	0.300	0.21	0.23	4.74	6.68	8.08	7.43	-22.9	227.7
Maximum	24.59	19.25	416.2	528.0	0.292	0.343	0.22	0.26	5.59	9.68	8.79	7.64	12.9	273.0
Minimum	22.41	13.29	390.6	439.0	0.265	0.286	0.19	0.21	4.11	5.62	7.73	7.01	-45.8	179.0
<b>S12-D</b>														
Mean	23.72	12.09	405.9	525.3	0.282	0.341	0.21	0.26	6.01	7.97	9.11	7.70	-23.2	201.7
Maximum	24.26	14.35	409.4	591.0	0.282	0.382	0.21	0.29	6.56	10.84	9.29	8.25	-9.5	254.0
Minimum	23.17	9.19	402.3	506.0	0.281	0.329	0.21	0.25	5.45	6.43	8.92	7.09	-36.8	136.0
<b>S13-D</b>														
Mean	23.02	15.31	414.8	474.6	0.288	0.302	0.21	0.22	6.64	8.51	8.82	7.77	-9.2	227.5
Maximum	23.47	17.65	419.3	564.0	0.290	0.367	0.21	0.27	7.34	11.43	9.27	8.21	8.6	236.0
Minimum	22.56	11.15	410.2	438.0	0.286	0.282	0.21	0.21	5.94	6.72	8.36	7.31	-26.9	219.0
<b>S14</b>														
Mean	18.39	13.92	475.8	574.8	0.333	0.374	0.25	0.28	1.65	3.12	8.59	7.78	-23.4	207.0
Maximum	18.42	15.72	476.4	619.0	0.333	0.402	0.25	0.30	2.45	4.38	9.30	7.91	10.9	231.0
Minimum	18.36	12.60	475.2	562.0	0.333	0.365	0.25	0.27	0.84	1.68	7.88	7.53	-57.7	183.0
<b>S15-12</b>														
Mean	23.33	13.10	429.8	480.6	0.286	0.311	0.21	0.23	5.48	7.74	9.12	7.74	-24.2	231.0
Maximum	23.45	16.12	451.3	508.0	0.290	0.330	0.21	0.25	5.85	11.21	9.27	7.85	-12.3	247.0
Minimum	23.20	11.20	408.2	446.0	0.282	0.290	0.21	0.22	5.10	6.24	8.96	7.43	-36.0	215.0
<b>S15-13</b>														
Mean	22.56	15.13	418.9	451.4	0.291	0.290	0.22	0.22	5.50	8.15	9.26	7.74	-9.5	252.5
Maximum	22.71	16.55	419.2	460.0	0.292	0.297	0.22	0.22	5.80	11.21	9.27	7.97	5.4	255.0
Minimum	22.41	12.77	418.5	438.0	0.290	0.280	0.22	0.21	5.20	5.57	9.25	7.43	-24.3	250.0
<b>S16-D</b>														
Mean	22.04	12.33	418.2	496.2	0.292	0.322	0.22	0.24	5.67	11.04	8.42	8.04	-6.3	227.0
Maximum	22.06	14.02	419.1	579.0	0.293	0.376	0.22	0.28	5.99	14.86	8.54	8.31	14.8	251.0
Minimum	22.01	8.73	417.3	470.0	0.291	0.305	0.21	0.23	5.35	9.19	8.30	7.57	-27.4	203.0
<b>S17-D-I</b>														
Mean	22.00	12.37	424.4	465.4	0.296	0.303	0.22	0.23	5.89	7.85	8.40	7.86	0.1	252.0
Maximum	22.13	13.27	424.7	543.0	0.296	0.353	0.22	0.26	6.28	9.71	8.60	8.16	19.4	276.0
Minimum	21.86	11.80	424.0	439.0	0.295	0.285	0.22	0.21	5.50	6.25	8.19	7.30	-19.1	228.0
<b>S17-D-II</b>														
Mean	22.13	12.50	426.2	503.0	0.296	0.327	0.22	0.25	5.13	10.55	8.26	7.99	-0.4	244.5
Maximum	22.30	14.67	428.0	576.0	0.296	0.375	0.22	0.28	5.46	14.33	8.60	8.21	23.5	261.0
Minimum	21.95	9.32	424.4	478.0	0.295	0.311	0.22	0.23	4.80	8.24	7.92	7.77	-24.2	228.0

Table 19: Mean, maximum and minimum values of water quality field parameters measured from nested piezometers in summer season.

Parameters	T	EC(25°C)	TDS	Salinity	DO	pH	ORP
Units	(°C)	(µS/cm)	(g/l)		(mg/l)		mV
Det Limit							
<b>S1-P Deep Piezometer</b>							
Mean	20.56	437.83	0.306	0.23	5.21	7.72	40.90
Maximum	21.84	490.31	0.341	0.25	14.70	7.95	83.10
Minimum	19.88	412.20	0.289	0.21	1.26	7.57	-65.80
<b>S1-P Shallow Piezometer</b>							
Mean	21.63	465.65	0.326	0.24	2.78	7.73	109.58
Maximum	22.04	503.19	0.348	0.26	3.14	8.13	150.30
Minimum	20.90	419.30	0.295	0.22	2.37	7.51	14.20
<b>S2-P Deep Piezometer</b>							
Mean	21.40	380.53	0.264	0.20	3.57	8.14	19.10
Maximum	22.15	384.60	0.266	0.20	4.71	8.36	36.30
Minimum	20.47	374.80	0.260	0.19	2.58	7.78	-22.50
<b>S2-P Shallow Piezometer</b>							
Mean	21.44	381.69	0.265	0.20	3.68	8.21	27.18
Maximum	22.36	387.40	0.267	0.23	4.40	8.39	44.20
Minimum	20.30	378.38	0.263	0.19	2.91	8.04	-12.00
<b>S3-P Deep Piezometer</b>							
Mean	24.17	378.08	0.267	0.20	2.93	8.34	1.98
Maximum	26.35	391.50	0.270	0.20	3.82	8.58	22.30
Minimum	22.71	350.73	0.260	0.19	1.87	8.06	-41.60
<b>S3-P Shallow Piezometer</b>							
Mean	25.98	384.79	0.265	0.20	4.13	8.52	-3.08
Maximum	27.91	392.50	0.269	0.20	5.06	8.66	12.00
Minimum	23.37	365.24	0.251	0.18	2.78	8.35	-42.60
<b>S4-P Deep Piezometer</b>							
Mean	20.30	477.66	0.333	0.25	3.86	7.99	4.45
Maximum	21.13	483.20	0.335	0.25	5.30	8.28	16.80
Minimum	19.22	473.50	0.332	0.25	3.23	7.63	-9.70
<b>S4-P Shallow Piezometer</b>							
Mean	19.22	488.36	0.344	0.26	1.94	7.80	3.28
Maximum	20.01	502.70	0.349	0.26	2.20	8.08	21.00
Minimum	18.61	469.45	0.334	0.25	1.73	7.54	-19.40
<b>S6-P Deep Piezometer</b>							
Mean	19.77	462.64	0.322	0.24	4.01	8.09	-19.75
Maximum	21.78	467.34	0.325	0.24	5.14	8.44	6.30
Minimum	17.56	453.40	0.318	0.24	2.88	7.64	-41.70
<b>S6-P Shallow Piezometer</b>							
Mean	20.38	447.93	0.310	0.23	2.39	8.03	-19.13
Maximum	20.99	458.30	0.319	0.24	3.79	8.29	-6.80
Minimum	19.90	420.30	0.292	0.22	1.61	7.90	-37.60
<b>S7-P Deep Piezometer</b>							
Mean	19.53	464.56	0.323	0.24	2.32	7.95	-13.65
Maximum	20.39	475.10	0.332	0.25	3.64	8.32	7.70
Minimum	18.14	457.20	0.318	0.24	1.21	7.50	-30.20
<b>S7-P Shallow Piezometer</b>							
Mean	20.05	451.51	0.314	0.23	1.45	7.96	-46.83
Maximum	21.23	477.30	0.332	0.25	1.75	8.03	-20.20
Minimum	18.52	432.06	0.295	0.22	1.10	7.89	-63.40
<b>S9-P Deep Piezometer</b>							
Mean	22.11	246.31	0.203	0.15	4.62	9.01	-49.40
Maximum	22.41	313.23	0.218	0.16	4.94	9.09	-15.40
Minimum	21.81	150.40	0.187	0.14	4.29	8.96	-83.40
<b>S10-P-B Deep Piezometer</b>							
Mean	21.65	421.08	0.292	0.22	6.50	7.83	-6.90
Maximum	21.98	443.63	0.305	0.23	7.30	8.00	19.10
Minimum	21.25	409.30	0.285	0.21	5.72	7.41	-26.30
<b>S10-P-B Shallow Piezometer</b>							
Mean	22.62	443.13	0.306	0.23	4.57	7.49	-6.45
Maximum	23.33	464.62	0.316	0.23	6.54	7.76	16.40
Minimum	21.94	422.90	0.296	0.22	3.10	7.17	-28.60

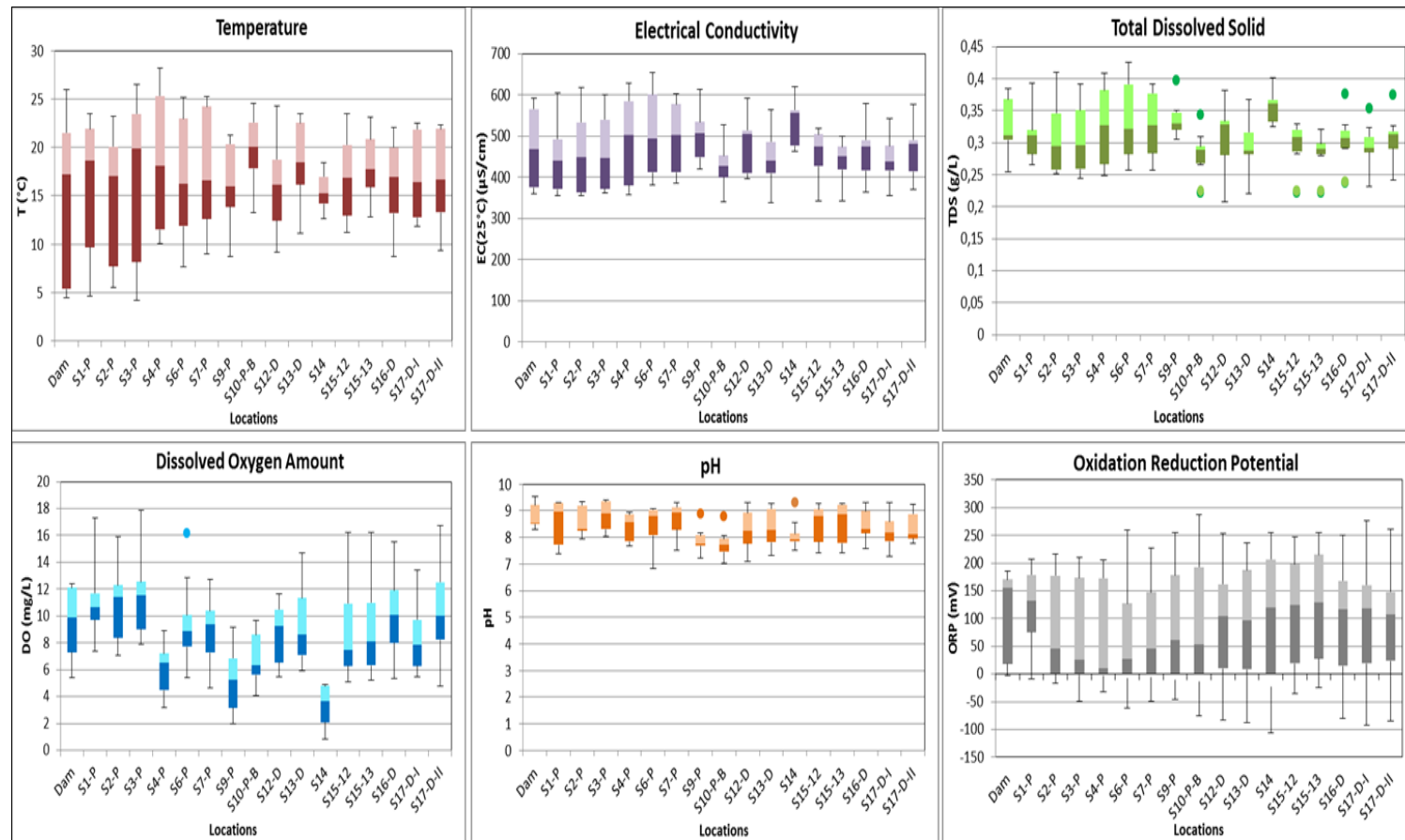


Figure 45 : Box plots of water quality field parameter for stream water.



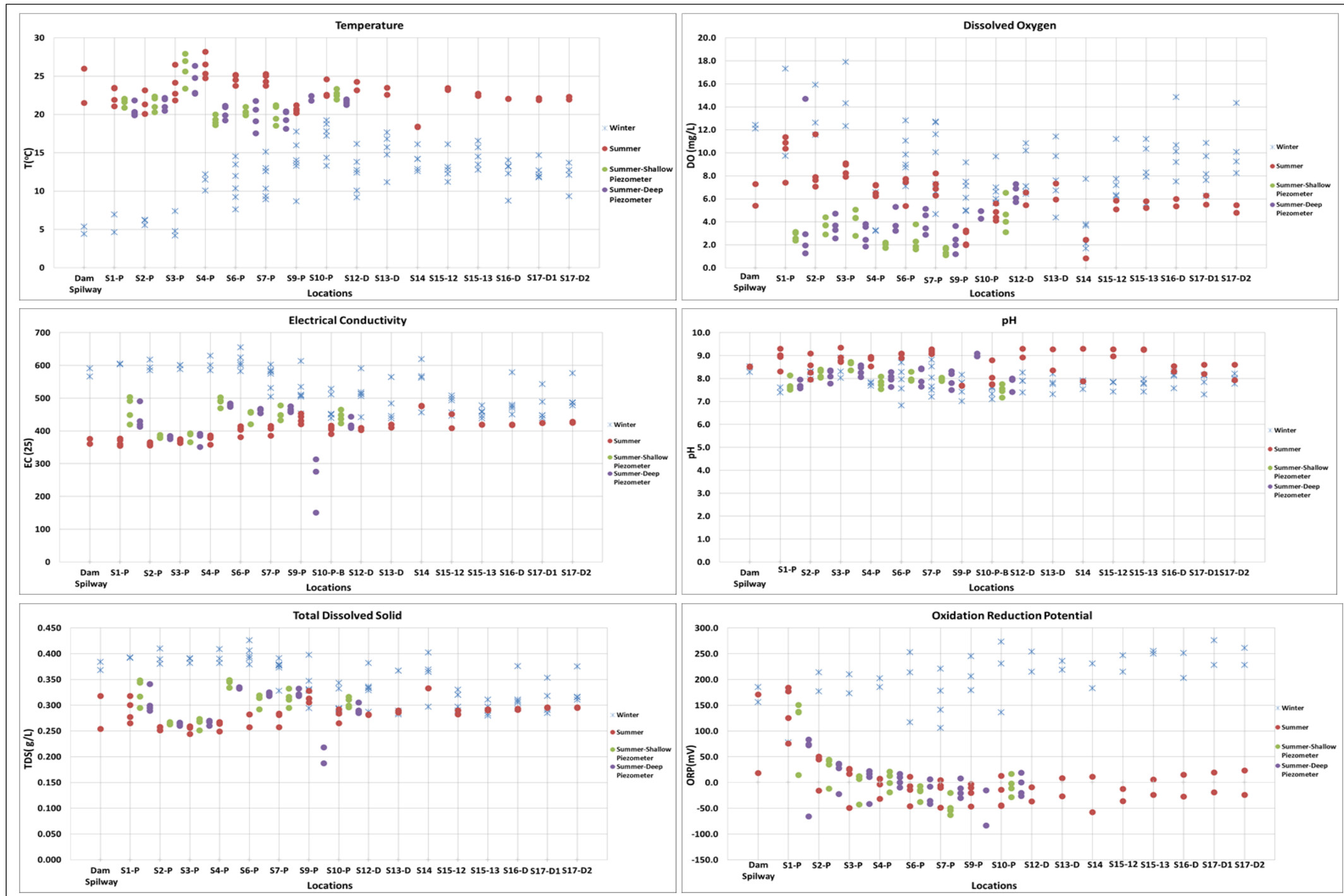


Figure 46: Change in water quality field parameters through monitoring locations for stream water and water samples taken from piezometers.





It is understood that, temperature values become different starting from S4-P. With this monitoring location, temperatures of stream and piezometer water samples become noticeably different, stream water has higher temperature values in summer, S9-P being an exception. Water samples taken from piezometers have higher temperatures at S9-P. Also, stream temperature values decrease towards downstream as a general trend. In sites S4-P, S6-P and S7-P lower temperatures were measured inside piezometers with respect to other locations in summer. In S10-P-B, temperatures of stream and piezometer water samples become close to each other again. The monitoring locations following S10-P-B have similar temperature values in summer (except the spring at S14). In winter season, two different trends (first increasing and then decreasing) are evident. Dam spillway, S1-P, S2-P and S3-P have the lowest and almost the same stream water temperature values. Again starting from S4-P, a sudden increase occurs in temperature values and this increase continues until S12-D. After the location S10-P-B, stream temperature values decrease but never become as low as the values in dam spillway, S1-P, S2-P, S3-P and S4-P. Temperature trends occurring in both winter and summer seasons support the interaction processes occurring in the study area which were explained in previous chapters. In chapter 5.2, the study area was divided into two regions. According to vertical hydraulic gradient results, the first region includes S1-P, S2-P and S3-P and the sites S4-P, S6-P, S7-P and S9-P were classified as the second region. Also, S10-P-B was defined as a groundwater discharge location additional to these regions. In both seasons, the first three locations S1-P, S2-P and S3-P have almost similar temperature behaviour which is distinguishable from the rest of the study area as in VHG values. In summer season, S4-P, S6-P and S9-P can be grouped and S10-P-B can be separated from all of the other monitoring locations. In winter season, continuous increase in the stream temperatures emphasizes the relatively warmer groundwater contribution. S10-P-B has the highest being a groundwater discharge location.

### 5.5.1.2. Electrical Conductivity (EC) Measurements

Electrical conductivity (EC) is an indicator of ionic content and proportional to the total dissolved ionic mass. EC (25°C) variation in each location can be seen in Figure 47. In winter months, all parameters have relatively higher values when compared to summer months.

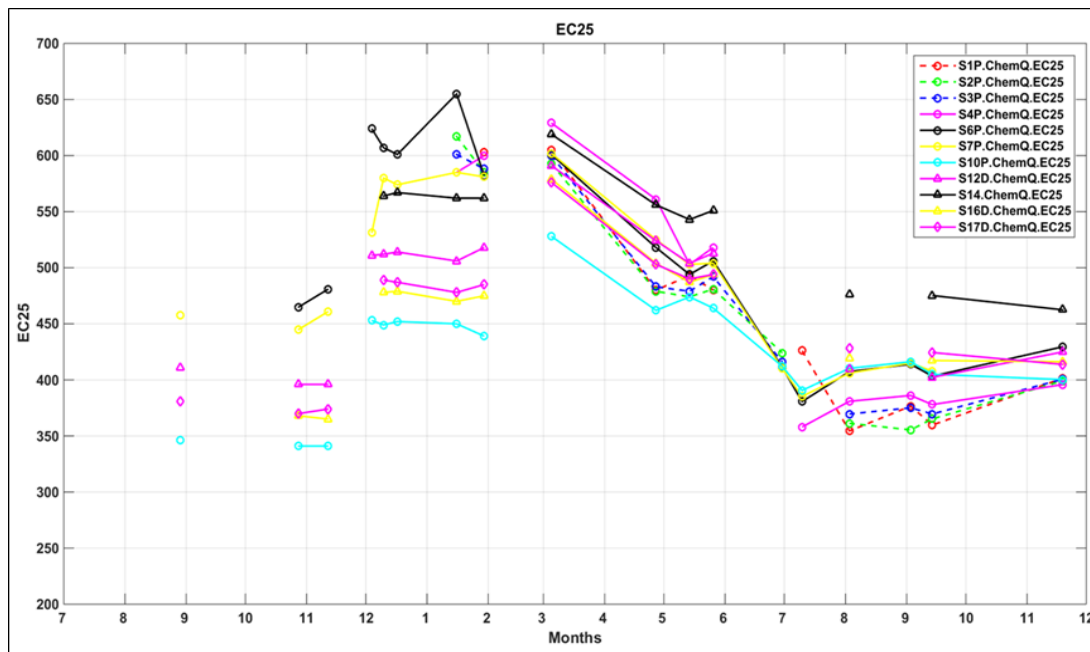


Figure 47: Normalized electrical conductivity change in each site during measurement period.

In summer, EC (25°C) values of stream water vary between 354.5  $\mu\text{S}/\text{cm}$  and 476.4  $\mu\text{S}/\text{cm}$  (Table 18). The highest and lowest values were measured in S14 and S1-P respectively. First four monitoring locations have the lowest EC (25°C) values (between 354.5  $\mu\text{S}/\text{cm}$  and 386.1  $\mu\text{S}/\text{cm}$ ). Starting from S6-P, values increase and reach around 400  $\mu\text{S}/\text{cm}$  (still the lowest value is 380.7  $\mu\text{S}/\text{cm}$  in this location). In the study area, except S1-P, S2-P, S3-P and S4-P, all values are above 400  $\mu\text{S}/\text{cm}$ .

However, only 390.6  $\mu\text{S}/\text{cm}$  was recorded as minimum  $\text{EC}(25^\circ\text{C})$  value in site S9-P. In winter, normalized EC values are relatively higher than the values recorded in summer season (Table 18). Site S6-P has the highest value with 655.0  $\mu\text{S}/\text{cm}$  and S15-13 (the monitoring location S15 is an intersection of S12-D and S13-D. S15-13 represents the follow-up of the monitoring location S13-D) has the lowest value with 538.0  $\mu\text{S}/\text{cm}$ . Site S1-P has significantly high EC ( $25^\circ\text{C}$ ) values (603.0 – 605.0  $\mu\text{S}/\text{cm}$ ). Although electrical conductivity values in upstream part of the study area (S1-P, S2-P, S3-P, S4-P) are low in summer season, they are significantly high in winter and range between 585.0  $\mu\text{S}/\text{cm}$  and 617.0. Starting from S7-P, the values decrease without a noticeable trend. Towards downstream, values around 400.0  $\mu\text{S}/\text{cm}$  and 500.0  $\mu\text{S}/\text{cm}$  were measured. Normalized EC values in water samples pumped from piezometers in summer season change in the range of 150.4  $\mu\text{S}/\text{cm}$  and 503.2  $\mu\text{S}/\text{cm}$  (Table 19). The lowest value is observed in S9-P and the highest value belongs to shallow piezometer of S1-P. Generally, values in downstream part are relatively higher than the values in upstream part. Although the highest value is observed in S1-P (vary between 400  $\mu\text{S}/\text{cm}$ -500  $\mu\text{S}/\text{cm}$ ), values of S2-P and S3-P are all below 400  $\mu\text{S}/\text{cm}$ . Starting from S4-P, locations take values above 400  $\mu\text{S}/\text{cm}$  (the second highest value belongs to this location).

Box plots of surface water monitoring locations for ( $25^\circ\text{C}$ ) are given in Figure 45. Again the site S10-P-B is noticeable with lower distribution of its values. According to  $\text{EC}(25^\circ\text{C})$  graph given in Figure 46, only S9-P piezometer has significantly low  $\text{EC}(25^\circ\text{C})$  values. Dam spillway and stream water in S1-P, S2-P, S3-P and S4-P almost have same electrical conductivity values in summer season. With the monitoring location S6-P,  $\text{EC}(25^\circ\text{C})$  values show a slight increase. This increasing trend continues down to S10-P-B. With this groundwater discharge location, electrical conductivity values of surface water decrease towards downstream. All monitoring locations after S10-P-B (except the site S14 which has the greatest conductivity value) have very similar  $\text{EC}(25^\circ\text{C})$  values. Normalized electrical conductivity values of piezometer water samples are higher compared to stream water. Especially, S1-P and S4-P demonstrate significantly high  $\text{EC}(25^\circ\text{C})$  values in

water samples. However, relatively lower values were observed in sites S2-P and S3-P. In sites S6-P, S7-P and S10-P-B piezometer water samples show similar EC(25°C) values. Significantly low conductivity values were measured from the piezometer installed in S9-P. Therefore, from upstream to downstream, electrical conductivity values for stream water have two trends, an increase followed by a decrease. The breaking points for these trends are S6-P and S10-P-B respectively. For piezometer water samples, S1-P, S4-P, S6-P, S7-P and S10-P-B have higher conductivity values than S2-P, S3-P and S9-P (Figure 46). As compared above, winter season has a different EC(25°C) trend compared to summer season. In winter, conductivity values decrease towards downstream. This decrease starts with S7-P. Before this location, EC(25°C) values do not show significant change and they are significantly different from the values measured in summer season. However, after S7-P, conductivity values show variations depending on the location. Furthermore, values for summer and winter seasons become closer to each other with this site. Especially, with the location S10-P-B the difference between the two seasons noticeably decreases and this can be possibly explained by groundwater contribution. Box plots of total dissolved solid amount for each monitoring location is given in Figure 45 and show similar trend with box plots of electrical conductivity values. Also, trends observed in the graph of “Total Dissolved Solid” in Figure 46 are exactly the same with the trends explained for EC(25°C) graph in the same figure since electrical conductivity is directly proportional to the dissolved solid amount.

#### **5.5.1.3. The pH and Redox Environment**

As can be seen from Table 18, Kirmir stream water has a basic character in all monitoring locations in both summer and winter seasons. The pH values of stream water range between 7.68 (in site S9-P) and 9.35 (in site S3-P) in summer. Generally, they vary between 8.00 and 9.00 for this season. Only in monitoring locations S2-P, S9-P, S10-P-B and S17-D-II, pH values decrease towards 7.00. The pH changes towards downstream but without a clear trend. In winter season, pH values are relatively lower than the values measured in summer season. The highest and lowest

stream water pH values are 8.90 (in S3-P) and 6.82 (in S6-P). The upstream part of the study area has relatively higher pH values (especially in locations S2-P, S3-P and S7-P) with respect to downstream. Also, according to the water quality measurements in piezometers during summer season, all water samples taken both from deeper and shallower sections have basic water characteristics (Table 19). The highest pH value is observed in location S9-P (Piezometer 1) as 9.09 and the lowest value which is 7.17 was measured in groundwater discharge location S10-P-B (in shallower piezometer). As in stream water, pH variation in piezometers does not follow a trend. Piezometer water samples have lower pH values than stream water for each monitoring location except the site S9-P. Sites S1-P, S2-P and S3-P are groundwater recharge locations (see section 5.2 for more details) and pH values of surface water and water samples taken from piezometers are close to each other for sites S2-P and S3-P. However, the same situation is not valid for the first monitoring location. Piezometer water samples have significantly lower pH values in S1-P. Similar trend is observable in S6-P and S7-P. The pH values of stream water and piezometer water samples in locations S4-P and S10-P-B show similar values within each other. The pH graph in Figure 46 supports these findings.

Dissolved oxygen amounts are higher in upstream part of the study area with respect to downstream part both in summer and winter seasons. The highest dissolved oxygen amounts occur in the first three monitoring locations (S1-P to S3-P) for both seasons. After these sites, DO amount decreases but this decrease does not follow a trend towards downstream, that is, monitoring site located at more downstream with respect to another can have higher DO value (but still lower than S3-P). In summer, DO amounts range between 11.62 mg/l and 0.84 mg/l (Table 18). The highest and lowest values occur in S2-P and S14 respectively. S2-P is located in the losing reach of the study area and it reflects the surface water characteristics. Therefore, it has significant amount of DO. DO values measured in S1-P are close to S2-P (in terms of maximum and minimum values). S3-P has relatively lower values than S1-P and S2-P. This location is located in the losing reach of the study area as S1-P and S2-P. However, as explained in section 5.4.2. , groundwater contribution was observed in

this site for some dates (even though for limited time); which can explain lower DO values observed in S3-P. S14 is a spring location and hence low DO values are expected. In winter season, DO amounts are higher than the summer season since cold water holds more DO than warm water. The highest value which is 17.90 mg/l is observed in S3-P and the lowest value which is 1.68 mg/l occur in S14 as in summer season (Table 18). In piezometer water samples, the highest value occur in S1-P deeper piezometer as 14.70 mg/l and the lowest value (1.10 mg/l) is observed in shallower piezometer of S7-P in summer season (Table 19). Occurrence of the highest value in deeper piezometer of S1-P is because of the downward movement of surface water which has higher DO amount than groundwater. As going deeper in subsurface DO amount decreases, because the contact with the atmosphere decreases also. Therefore, groundwater has lower DO amount than surface water. DO amounts obtained from water samples taken from each piezometer show changing characteristics. Some locations have higher DO amount in deeper piezometer while some have lower. Box plots of dissolved oxygen concentrations (Figure 45) show very changing trend through monitoring locations. S14, S4-P, S9-P and S10-P-B have relatively lower DO content than the other sites. As can be seen in “Dissolved Oxygen” graph in Figure 46, in both seasons dissolved oxygen amounts decrease towards downstream. Especially, S1-P, S2-P and S3-P have higher values with respect to the rest of the study area. Also, S4-P and S14 are recognizable with their low values for both seasons. In summary, the first three upstream monitoring locations are quite different from the other monitoring locations as in chapter 5.2. Starting from the monitoring location S4-P, dissolved oxygen amounts measured in winter and summer seasons become closer to each other. Generally, dissolved amounts in deeper piezometers are higher than the dissolved amounts in shallower piezometers (reverse is valid only for S3-P). Less DO amounts for both seasons towards downstream mean that groundwater is contributing the Kirmir Stream towards downstream sections of the study area? As emphasized in previous chapters, S1-P, S2-P and S3-P are located in a losing reach of the Kirmir Stream. Therefore, more dissolved oxygen amount is expected in these locations. A higher DO amount means higher oxidation – reduction potential and the higher the redox potential, the

more oxidizing the solution. In summer months the highest and the lowest ORP values are 184.2 mV and -57.7 mV and occur in S1-P and S14 respectively (Table 18), which is directly related to the DO amounts in these sites. S1-P has a high DO amount (just after S2-P and their values are very close to each other). In winter season, ORP values range between 78.0 mV and 276.0 mV and are observed in sites S1-P and S17-D-I respectively (Table 18). Although S14 has the lowest DO value among all locations, S7-P has the lowest ORP value. Oxidation – reduction potential of water samples taken from piezometers vary between -83.4 mV and 150.3 mV (Table 19). As in stream water values measured in summer season the highest value belongs to S1-P. However, the lowest value is in S9-P. Among all graphs, the biggest difference between summer and winter seasons occurs in oxidation - reduction potential (Figure 46). This is also clear in box plots given in Figure 45. For all sites, ORP values have wide ranges. In summer season, for both piezometers and stream water, oxidation reduction potential first decreases and then become nearly stable. Especially, S1-P has significantly high oxidation – reduction potential. On the other hand, ORP show a slight increase towards downstream in winter season. Although, upstream part of the study area has higher DO amounts in this season, it shows lower ORP. Moreover, ORP values of S1-P for each season are close to each other.

### **5.5.2. Major Anion Hydrochemistry**

As explained in detail in section 4.5.1 major anion hydrochemistry was analyzed in selected locations for both piezometers and stream water. Table 20 summarizes the concentrations (meq/l) of fluoride, chloride, nitrite, nitrate, phosphate and sulfate anions. In monitoring locations S2-P, S4-P, S6-P and S10-P-B anion concentrations were found for water sample taken from three points: deeper piezometers, stream water a few meter upstream and downstream of the piezometer. Total anion concentrations observed in S2-P, S4-P and S6-P are close to each other. However, a sudden decrease is observed in S10-P-B. In stream water monitoring locations S12-D, S13-D, S16-D and S17-D total anion concentrations increase again.

Table 20: Major anion concentrations of water samples taken from piezometers and surface water at selected monitoring locations (Us: upstream, Pz: piezometer, Dn: Downstream).

Major Anions in meq/L							
Locations	F <sup>-</sup>	Cl <sup>-</sup>	NO <sub>2</sub> <sup>-</sup>	NO <sub>3</sub> <sup>-</sup>	PO <sub>4</sub> <sup>3-</sup>	SO <sub>4</sub> <sup>2-</sup>	Total
S2-P Us	0.015	0.804	0.001	0.013	0.022	0.294	1.148
S2-P Pz	0.017	0.811	0.000	0.002	0.008	0.301	1.139
S2-P Dn	0.016	0.807	0.001	0.013	0.021	0.299	1.157
S4-P Us	0.025	0.806	0.000	0.009	0.021	0.296	1.158
S4-P Pz	0.028	0.785	0.005	0.024	0.022	0.334	1.198
S4-P Dn	0.017	0.829	0.000	0.009	0.021	0.305	1.182
S6-P Us	0.020	0.852	0.000	0.007	0.022	0.306	1.207
S6-P Pz	0.023	0.944	0.007	0.026	0.021	0.367	1.388
S6-P Dn	0.027	0.824	0.000	0.006	0.022	0.303	1.182
S10-P-B Us	0.019	0.194	0.000	0.039	0.007	0.391	0.649
S10-P-B Pz	0.019	0.209	0.003	0.032	0.000	0.410	0.673
S10-P-B Dn	0.019	0.199	0.000	0.036	0.006	0.415	0.675
S12-D	0.020	0.809	0.000	0.005	0.021	0.308	1.162
S13-D	0.019	0.563	0.000	0.016	0.016	0.341	0.955
S16-D	0.019	0.685	0.000	0.007	0.019	0.313	1.042
S17-D	0.020	0.695	0.000	0.008	0.018	0.316	1.056

Site S10-P-B has the lowest chloride (Cl<sup>-</sup>) and the highest nitrate (NO<sub>3</sub><sup>-</sup>) and sulfate (SO<sub>4</sub><sup>2-</sup>) concentrations (Table 20). S10-P-B location is a local groundwater discharge location in the study area. Generally, higher amount of NO<sub>3</sub><sup>-</sup>, PO<sub>4</sub><sup>3-</sup> (phosphate) and SO<sub>4</sub><sup>2-</sup> indicate mixing of agricultural fertilizers to surface water and the animal feeding. According to Krause et al. (2013) hyporheic zone can be a potential source of nitrate. Also the authors state that oxygen depleted hyporheic environment causes an increase of denitrification rates. This means that the more DO amount brings the more nitrification. S10-P-B location has relatively higher DO amount among other piezometer locations (Table 19). Therefore, this high amount of DO can cause high amount of NO<sub>3</sub><sup>-</sup> in this site. The higher Cl<sup>-</sup> in stream water could be coming from sewage waste potentially from the town of Kızılcahamam. In S10-P-B, chloride concentration in deep piezometer is lower with respect to other sites. This situation



also causes the low concentration of chloride in surface water at this location. Variations in major anion concentrations throughout the sampling locations are shown in Figure 48.

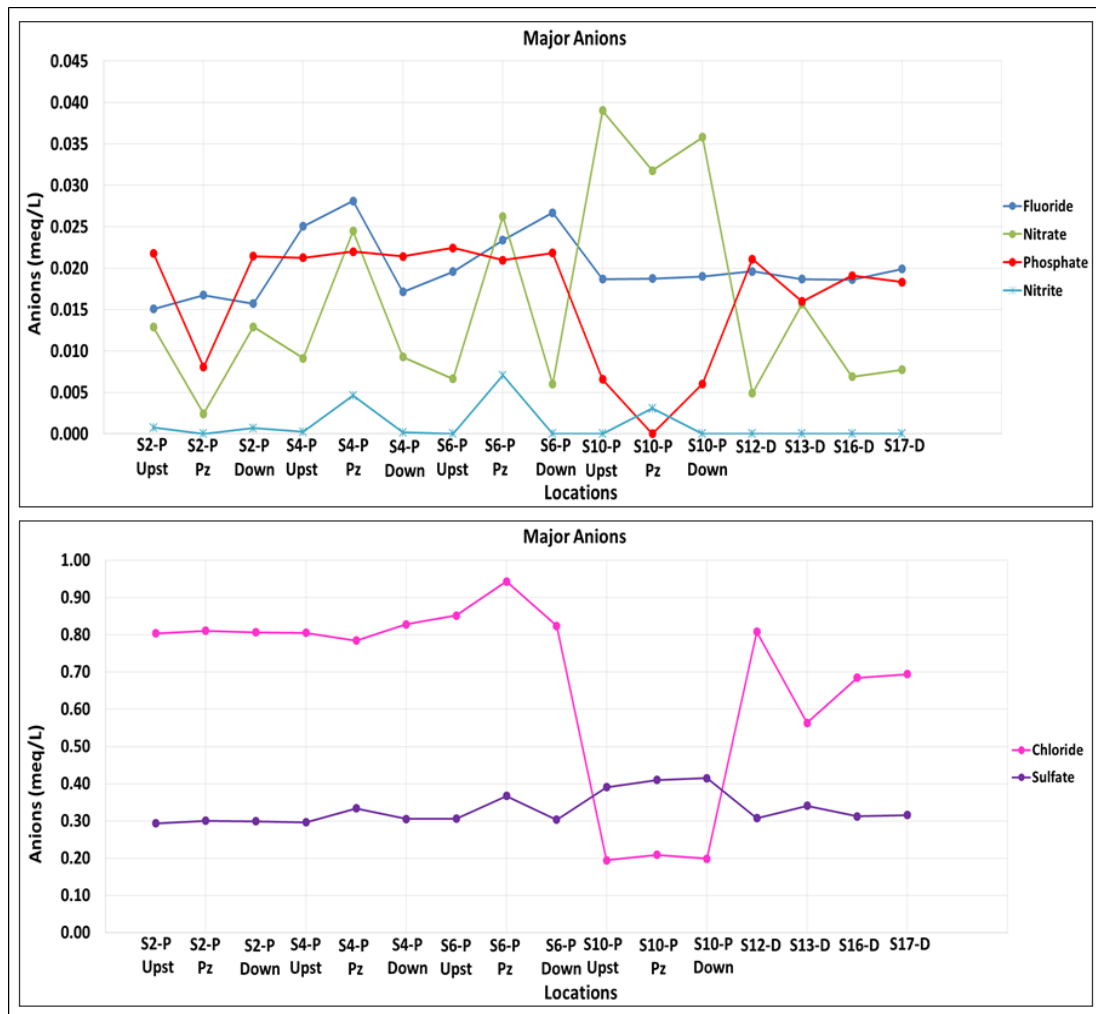


Figure 48: Major anion concentrations throughout the selected sampling locations.

When fluoride trend is examined, it can be seen that  $F^-$  concentration slightly increases towards downstream. S2-P location (upstream, piezometer and

downstream) can be noticeably separated from the other sampling locations. After this location increasing trend is observed. The relatively higher values belong to S4-P upstream, S4-P piezometer, S6-P piezometer and S6-P downstream. Starting from the monitoring location S10-P-B,  $F^-$  amount remains almost the same. The sampling locations S2-P, S4-P and S6-P have nearly the same chloride values. The highest  $Cl^-$  amount was detected in the water sample taken from S6-P piezometer. As mentioned in previous paragraph, S10-P-B shows the lowest  $Cl^-$  concentrations. Hence, the sites situated downstream of S10-P-B, except S12-D, also have lower chloride concentrations compared to upstream locations. Only S12-D has almost the same  $Cl^-$  concentrations with S2-P, S4-P and S6-P. In sites S13-D, S16-D and S17-D chloride concentrations decrease noticeably. Site S13-D is situated just downstream of groundwater discharge location S10-P-B so the anion concentrations in S13-D could be directly affected from S10-P-B. Therefore, the second lowest  $Cl^-$  concentration is observed in this location. S12-D and S13-D reaches join to form the reach where S15 is located then and flows downstream towards S16-D. As a result, relatively low chloride concentration in S13-D leads to low chloride concentrations in S16-D and S17-D. Same situation is valid for phosphate concentrations.  $PO_4^{3-}$  concentration trend throughout the sampling locations shows the same trend as chloride. Only S6-P piezometer does not have the highest value and the lowest value is observed in S2-P piezometer. Nearly all sampling locations have 0.00 meq/L nitrite amount. Only S2-P upstream – downstream and S4-P upstream – downstream have very low values within all stream water sampling locations. However, S4-P, S6-P and S10-P-B piezometers have significantly higher  $NO_2^-$  amounts. Nitrate amounts in sampling locations do not follow a trend. As mentioned in previous paragraph, the highest values are observed in S10-P-B location. Then, values in piezometers of S6-P and S4-P follow S10-P-B. All other sampling locations do not reach 1.00 mg/L nitrate amount.  $SO_4^{2-}$  variation throughout the sampling locations is more stable with respect to other trends. The sampling locations in S10-P-B show the greatest sulfate values. This site is followed by S6-P piezometer. S2-P sampling locations and S4-P upstream location have almost the same  $SO_4^{2-}$  amounts (Figure 48 and Table 20).

Sulfate ion concentration in the other locations does not vary prominently. The trend of total anion concentrations is similar to chloride concentrations (Figure 49). S10-P-B can be distinguished from the other locations in terms of total anion concentration. The other locations have significantly higher anion concentration compared to S10-P-B.

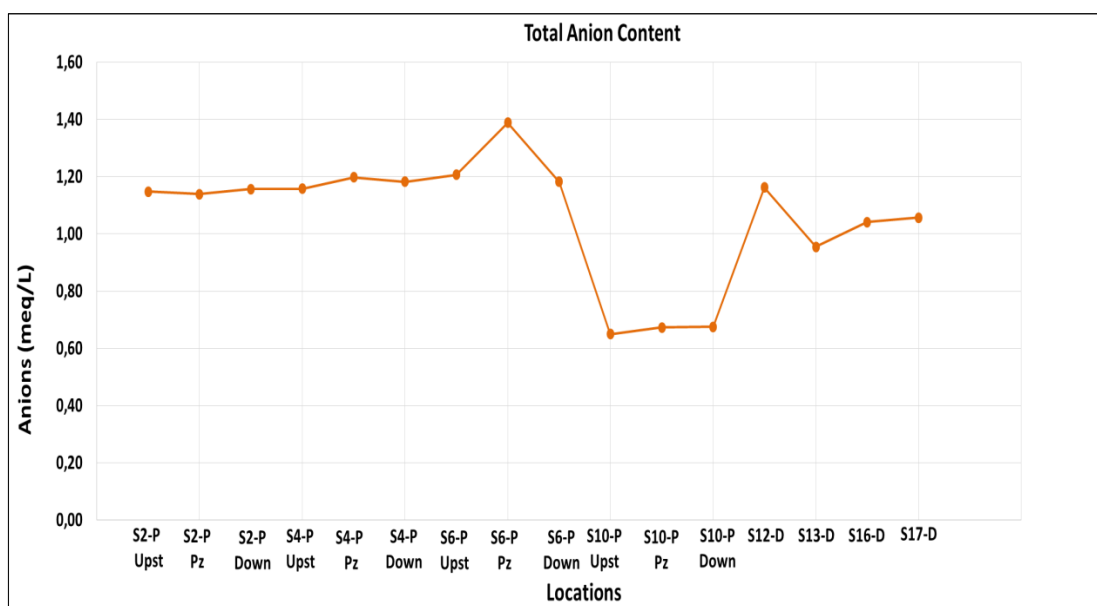


Figure 49: Change in total anion concentration through the sampling locations

Comparison of chloride concentrations in the study area with the wells and fountains

To make possible connections between the groundwater source feeding the Kirmir stream and surrounding aquifer systems, the chloride concentrations measured in the study area were compared with those measured in nearby wells and fountains. Within the scope of the study performed by Yazıcıgil et al. (2015), chloride analysis was performed in a number of wells and fountains located in the vicinity of study area. Chloride concentrations (mg/L) in the study area, wells and fountains are given in Table 21, Table 22 and Table 23 respectively.

Table 21: Chloride concentrations (mg/L) in sampling locations.

<b>Locations</b>	<b>Cl<sup>-</sup> (mg/L)</b>
S2-P Upstream	28.499
S2-P Piezometer	28.755
S2-P Downstream	28.605
S4-P Upstream	28.565
S4-P Piezometer	27.821
S4-P Downstream	29.376
S6-P Upstream	30.213
S6-P Piezometer	33.457
S6-P Downstream	29.217
S10-P-B Upstream	6.889
S10-P-B Piezometer	7.421
S10-P-B Downstream	7.057
S12-D	28.664
S13-D	19.966
S16-D	24.269
S17-D	24.623

Table 22: Chloride concentrations (mg/L) and the interacted geological units of wells around the study area.

<b>Wells</b>	<b>Interacted Unit</b>	<b>Cl<sup>-</sup> (mg/L)</b>
PW1	Volcanics	143
PW2	Çavuşlar Unit	1330
PW3	Aktepe-Kocalar Units	3.1
PW4A	Volcanics	261
PW5	Coal	5.7
PW6	Coal	<5
PW7	Alluvium - Çavuşlar Unit	45
PW8	Çavuşlar Unit	6.1
PW9	Alluvium - Çavuşlar Unit	15.5
CEL35	Çavuşlar Unit	<4
CEL36	Çavuşlar Unit	14.5
CEL44	Çavuşlar Unit	7.1
CEL47	Çavuşlar Unit	9.6
CEL47A	Coal	<5.5
CEL51	Çavuşlar Unit	7.9
CEL52	Volcanics	35.5
CEL53A	Coal	5.2
CEL59A	Coal	5.9
CEL59B	Çavuşlar Unit	5
CEL107	Çavuşlar Unit	4.63

Table 23: Chloride concentrations (mg/L) and the interacted geological units of fountain around the study area.

No	Interacted Unit	Cl <sup>-</sup> (mg/L)	No	Interacted Unit	Cl <sup>-</sup> (mg/L)
F1	Bezci Unit	3.31	F52	Volcanics	22
F2	Aktepe Unit (ve Bezci Unit?)	7.87	F53	Kocalar Unit (ve Aktepe Unit? )	8.85
F3	Aktepe Unit ve Bezci Unit	2.94	F54	Alluvium ve Volcanics	5.1
F4	Aktepe Unit ve Kocalar Unit	4.95	F55	Volcanics	3.17
F5	Kocalar Unit	1.27	F56	Volcanics	1.69
F6	Upper Çavuşlar Unit	6.48	F57	Volcanics	1.94
F7	Upper Çavuşlar Unit (ve Alluvium?)	22.48	F58	Lower Çavuşlar Unit (ve Bostantepe Unit)	<5
F8	Upper Çavuşlar Unit	6.7	F59	Lower Çavuşlar Unit	1.42
F9	Upper Çavuşlar Unit ve Volcanics	24	F61	Lower Çavuşlar Unit	2.6
F10	Alluvium ve (Upper Çavuşlar Unit?)	6.29	F63	Bostantepe Unit ( ve Volcanics?)	4.6
F11C	Upper Çavuşlar Unit	16.8	F64	Volcanics	17.8
F12	Upper Çavuşlar Unit	2.8	F65	Volcanics	4.2
F13	Upper Çavuşlar Unit	<5	F66	Volcanics	5.05
F14	Upper Çavuşlar Unit	5.4	F67	Volcanics?	1.58
F15	Upper Çavuşlar Unit, Abacı Unit, Kocalar Unit?	1.72	F68	Volcanics	2.07
F16	Plio-Quaternary (and Upper Çavuşlar Unit?, Volcanics?)	57.9	F69	Lower Çavuşlar Unit (ve Volcanics?)	6.05
F17	?	21.1	F70	Upper Çavuşlar Unit (ve Alluvium?, Abacı Unit?)	5.51
F28	?	2.53	F71	?	nm
F35B	Upper Çavuşlar Unit	3.3	F72	?	nm
F36	Abacı Unit and Alluvium	12.3	F73	Lower Çavuşlar Unit?	1.27
F36B	Abacı Unit and Alluvium	11.2	F74	Lower Çavuşlar Unit?	3.68
F37	Lower Çavuşlar Unit (and Volcanics?)	<5	F75	Lower Çavuşlar Unit?	15.5
F37B	Lower Çavuşlar Unit (and Volcanics?)	<5	F75B	Lower Çavuşlar Unit?	6.32
F38	?	10.3	F76	Lower Çavuşlar Unit?	9.7
F39	?	nm	F77	?	1.1
F40	Upper Çavuşlar Unit	-	F79	Volcanics?	1.93
F45	Upper Çavuşlar Unit ve Alluvium	7.38	F80	Volcanics?	1.71
F46	Bezci Unit	1.82	F81	?	3.56
F47	Upper Çavuşlar Unit	nm	F82	?	1.13
F49	Upper Çavuşlar Unit (ve Alluvium?)	<5	F83	Lower Çavuşlar Unit (ve Bostantepe Unit)?	nm
F51	Upper Çavuşlar Unit ve Alluvium	14.7	F84	Upper Çavuşlar Unit	4.5

\* nm denotes no measurement

The locations of wells and fountains can be examined in Figure 50 and Figure 51 respectively. The closest wells to the study area are CEL40 and CEL84 which are exploration wells. Although both of the wells are located in regions covered with volcanic units at the surface (Figure 50), different geological units also exist according to the borehole information (Yazıcıgil et al., 2015).





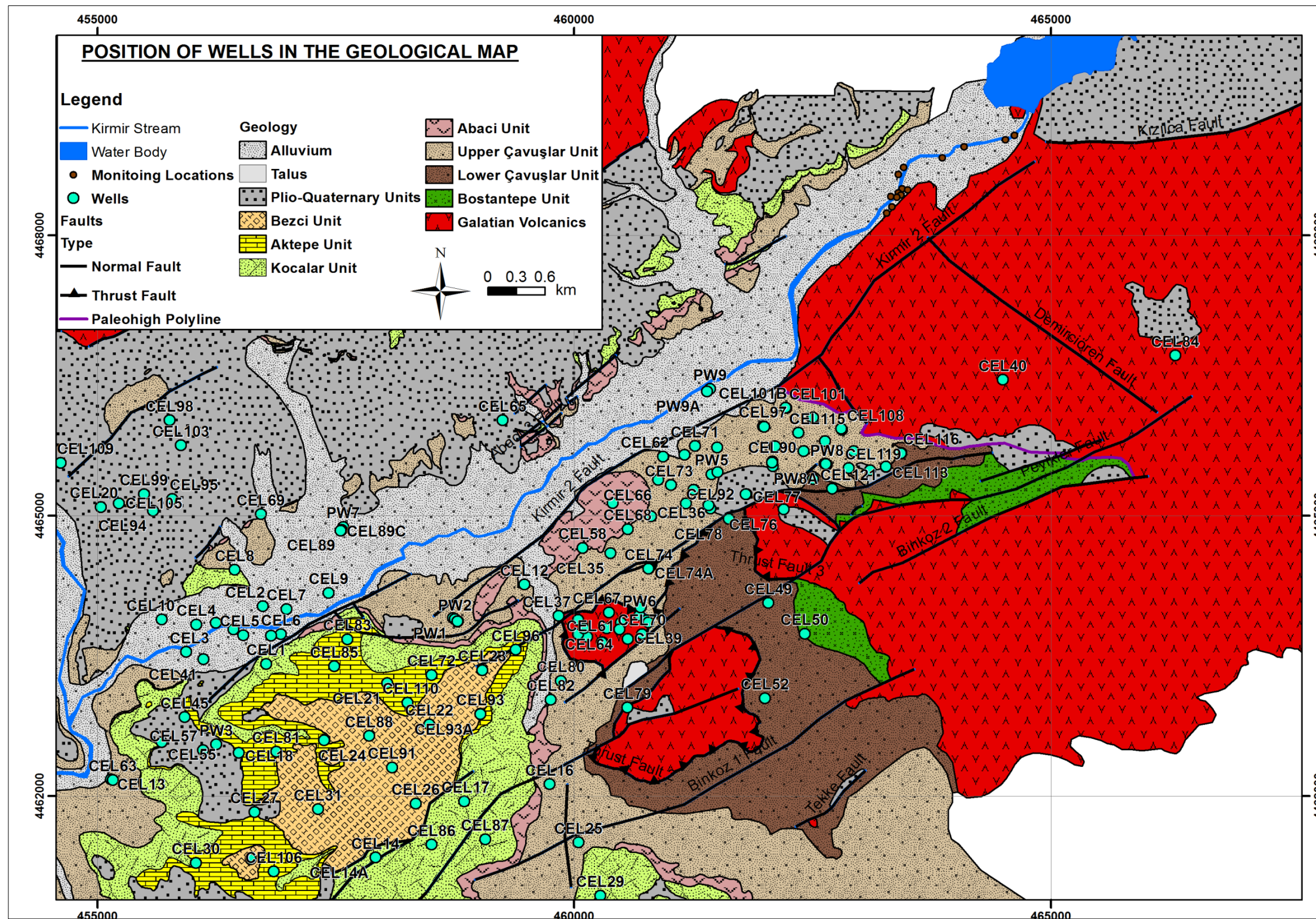


Figure 50: Position of wells in the geological map (AMM, 2015).



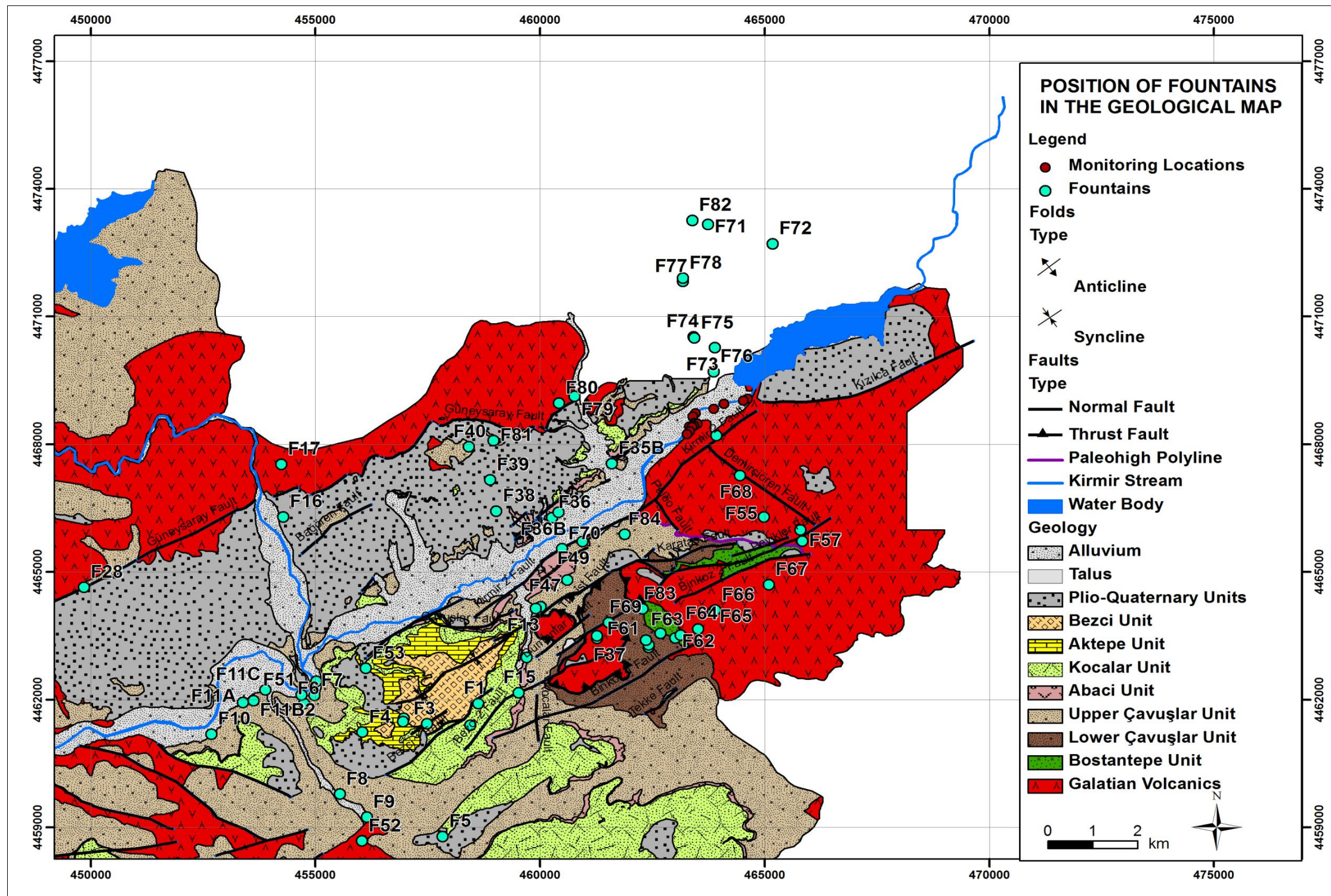


Figure 51: Position of fountains in the geological map (AMM, 2015).



In CEL40 well, the upper 46 m comprises of Çavuşlar unit. Between the depths 46 m and 114.30 m talus is present. From talus to 143.50 m depth sandstone is observed (Bostantepe Unit is characterized by sandstones deposited in fluvial environment) and this sandstone is underlain by volcanic breccia having 271.5 m thickness. The total depth of this borehole is 415 m and volcanics are situated at the bottom. In CEL 84, the top section is soil and it is underlain by volcanic unit with a thickness of 46 m. Below this, relatively thin sandstone (8.2 m) indicating Bostantepe unit is located. This sandstone overlies volcanic unit which is in 16.4 m thickness and this volcanic unit is underlain by sandstone whose thickness is 91.5 m. The bottom of the well comprises volcanics with 90.1 m thickness. The total depth of CEL 84 is 254.30 m and except volcanic units, sandstones indicating Bostantepe unit are observed as well. Although the geology of the study area includes alluvium and volcanics primarily (Figure 50) (the closer view can also be seen in section 3.5.2), borehole information show that Çavuşlar unit and Bostantepe unit also present in deeper sections.

While comparing chloride concentrations of wells and monitoring locations with each other, it was thought that these wells should be analyzed initially because of their proximity to the study area. However, chloride concentration analysis was not performed for these exploration wells. Hence, other wells representing volcanics and Bostantepe units were analyzed as the first step.

As can be understood from Table 22, there is no well representing Bostantepe unit. However, wells PW1, PW4A and CEL 52 are represent the volcanic units. The chloride concentrations of PW1 and PW4A are significantly higher compared to the chloride concentrations measured in the study area. These wells are affected from the volcanic units which are under the control of deeper flow systems (Yazıcıgil et al., 2015). As a result, the volcanic units cut by these wells are exposed to long time interactions with groundwater flow. Due to long terms interactions, they have significantly high chloride amounts. On the other hand, it can be said that concentration of CEL52 is relatively closer to the concentrations of the sampling

locations except S10-P-B and this site is distinguishable from the rest of the study area as explained in previous sections. Specifically, S6-P monitoring location has a chloride concentration similar to CEL 52 and as known this location shows both gaining and losing characteristics. Also, S2-P, S4-P and S12-D have approximate values to CEL 52. This well is represented by volcanic units characterized by shallow flow system (Yazıcıgil et al., 2015).

In the NW of the study area, Kocalar and Upper Çavuşlar units are seen additional to volcanics, alluvium and Plioquaternary units. Furthermore, the other wells affected from these units were examined as the next step. As listed in Table 22, Çavuşlar unit and Kocalar unit have lower chloride amounts than the volcanics. However, this is not valid for well PW2. Yazıcıgil et al. (2015) stated that this well is also characterized by significantly high electrical conductivity values as well. Both situations were explained by long time water-rock interactions. Due to the long residence time of groundwater, it has significantly high amount of dissolved ions. There is only one well, PW3, screened in both Aktepe and Kocalar units. Chloride concentration of this well is 3.1 mg/L (Table 22) which is noticeably low when it is compared to rest of the wells and the study area. This well also has the lowest electrical conductivity values among all wells. Low chloride concentration of PW3 can be explained by this. CEL35, CEL36, CEL44, CEL47 and CEL51 were screened in sedimentary rocks of Lower Çavuşlar units, CEL59B was filtered in sedimentary rocks of Upper Çavuşlar units and CEL 107 and PW8 cut both coal and Lower Çavuşlar units. Generally, it can be inferred that groundwater affected from sedimentary rocks in Upper Çavuşlar units (CEL59B) and coal (CEL47A, CEL53A, CEL59A) demonstrates low chloride concentrations with respect to groundwater influenced from sedimentary rocks of Lower Çavuşlar units (except CEL 35, this well has the lowest concentration). Chloride concentrations of groundwater interacted with sedimentary rocks of Lower Çavuşlar units (CEL36, CEL44, CEL47, CEL51) are similar with the chloride concentrations measured in the study area. Specifically CEL44 and CEL51 have chloride concentrations very similar to groundwater discharge location, S10-P-B. Both wells are located in the close vicinity

of Değirmenönü between the normal Faults Kirmir 2 and Karataş. In addition, there are two wells screened in Aluvium – Çavuşlar units which are PW7 and PW9. PW7 has significantly high chloride concentration compared to the study area. PW9 is located on Kirmir Stream and its chloride concentration is in the range of the concentration values of the study area. As a result, chloride amounts are different on and around Kimir stream. Because all monitoring locations are found on Kirmir stream, they have similar values with PW9.

As given in Figure 51, the closest fountains to the study area are F35B, F54, F55, F68 and F73 and they have relatively low chloride concentrations when compared to the study area. Fountains F55 and F68 are affected from volcanics, F54 is affected from both volcanics and alluvium. F35B and F73 are affected from Upper and Lower Çavuşlar units respectively. When chloride concentrations given in

Table 23 are examined, it can be seen that fountains affected from volcanic units (except F64), Lower Çavuşlar units (except F75) and Bezci units generally have lower chloride concentrations than the study area. F69, F75B and F76 interacted with Lower Çavuşlar units have relatively similar chloride concentrations with S10-P-B. The highest chloride concentration among all fountains was observed in F16 which is affected from Plio-Quaternary units and it is significantly higher than the chloride concentrations measured in the study area. F7 interacted with the Upper Çavuşlar unit follows F16 in terms of chloride concentration. It has significantly similar value with the upstream and downstream of the study area. According to

Table 23, the most similar chloride concentrations with the study area were observed in fountains interacted with Upper Çavuşlar units. Especially, F45 affected from both Upper Çavuşlar unit and alluvium shows the closest concentration with S10-P-B. In addition to Upper Çavuşlar units, F2 interacted with Aktepe units and F53 interacted with Kocalar units have also similar chloride concentrations with S10-P-B.

Also, Kirmir 2 and Demirciören Faults cut through the study area. The last monitoring location (S17-D) is in alignment of intersection of these two normal faults. Furthermore, Mahkemeağcın and Kızılca faults are in the close vicinity of the

study area. It can be said that, the study area is surrounded by normal faults (Figure 10 and Figure 50).

The faults which are around the study area can constitute pathways of groundwater to feed Kirmir Stream. Chloride concentrations measured in the study area are close to the values of groundwater affected from sedimentary rocks of Lower Çavuşlar units in terms of well information and Upper Çavuşlar units in terms of fountain information. Therefore, groundwater system affected from these units can possibly feed the Kirmir stream within the study area.

## CHAPTER 6

### CONCLUSIONS AND RECOMMENDATIONS

The purpose of this study was to characterize the interaction between surface water and adjacent groundwater in Kirmir stream - a controlled stream nearby Kizilcahamam, Ankara, Turkey. Exchange processes were investigated using water quality field parameters, major anion concentrations, in-situ and remotely sensed measurements.

#### *Thermal Images*

Thermal images from a handheld camera found to be useful to detect groundwater discharge zones into streams. Groundwater discharge zones were identified as hot (cold) spots during winter (summer) seasons both on the skin of the surface water or on the stream banks. For the thermal camera to be useful, the signature of groundwater discharge should be identifiable at the skin of the surface water, which is generally the case for shallow water depths. Moreover, during the application, reflected sunlight should be minimized as much as possible. Thermal imagery was used to quickly localize potential groundwater discharge zones within the river reach for defining the study area in addition to geological and geomorphological features. Thermal images at sites S9-P, S10-P-B, S13-D, S15-D and S17-D were investigated in the study. The most significant application of thermal imagery was detection of a significant groundwater discharge zone namely S10-P-B. Moreover, thermal imagery

was found useful in identifying different temperatures (hence other characteristics) of merging stream branches as discussed in the thesis. Also, stream temperature was measured by Solinst Model 107 TLC meter in S10-P-B and S15 on the same date when thermal images were obtained and it was found that thermal camera and Solinst Model 107 TLC meter gave almost same temperature values. Also, the influence of suspended sediments caused by the release of reservoir was not observed in this study because all thermal images were taken before the release of reservoir water.

### **Vertical Hydraulic Gradient Measurements**

Vertical hydraulic gradient values were calculated for each monitoring location using nested piezometers. According to the results, the study area was divided into two main regions which are losing and both losing – gaining regions. Losing reach includes upstream sites S1-P, S2-P, S3-P close to the Doğanözü Dam and they are characterized by positive VHG values indicating losing reach of Kirmir stream. S1-P has higher VHG values in summer than in winter. S2-P and S3-P have lower values in summer than in winter. S2-P and S3-P have lower values in summer with respect to winter.

Mid-section of the study including S4-P, S6-P, S7-P and S9-P was defined as the region having both losing and gaining characters (both positive and negative VHG) depending on the season. Absolute VHG values are higher in summer season than in winter season. Site S9-P has mostly losing character because it usually has positive VHG values.

S10-P-B monitoring location is found to be on a groundwater discharge zone and with continuous negative VHG values. This site shows the highest gradient values among all locations. Vertical hydraulic gradient values in summer season are noticeably higher in magnitude with respect to the values in winter season.

The installation of the piezometers was performed using hammering. Hence deep piezometers could not be installed in this study. Moreover, clogging of the

piezometers is possible and hence should be checked regularly. In this study, the piezometers were purged using air compressor after installation. The hydraulic connection was checked in each measurement by purging and recovery of the water levels.

### **Discharge Measurement Results**

Discharge measurements taken at regular intervals along the study area and in different times were used to estimate the contribution of groundwater to the study area. Along the study area, there is no surface water tributaries joining Kirmir stream and hence the discharge differences at relatively short distances are indicative of the groundwater gain and the loss. Also, effect of reservoir water release from Doğanözü Dam could be observed during measurement period. Measured flow amounts significantly increased with the influence of reservoir water which is found to change gaining and losing characters of the sites investigated. From most upstream discharge measurement site (S3-P) to the most downstream discharge measurement site (S17-D), Kirmir stream gained water from groundwater in the range of 28 L/sec - 68 L/sec during the study period.

In study performed by Yazıcıgil et al. (2015), groundwater flow was modeled using (FEFLOW v6.2) and according to this research Kirmir stream gains water from groundwater in the amount of 16.4 L/sec within the boundaries of present study area. This value enters the range of the discharge differences between the successive locations. However, this model is not developed for the modeling of interaction processes and also, coarser grids were used to study a much more broader research area. Therefore, some differences between the present study area and the study by Yazıcıgil et al. (2015) are expected.

### **Vertical Flux Estimation Using Temperature Loggers**

With the help of temperature loggers (ibuttons) installed at two different depths into the streambed in locations S3-P, S4-P and S16-D, temperature time series were

obtained and vertical flux values were calculated from temperature time series by using VFLUX software. It was found that losing character of S3-P caused more apparent diurnal fluctuations in the temperature profiles. In S4-P and S16-D, streambed showed similar temperature values in two different depths for all measurement periods. More stable temperature profiles and damped diurnal variations were seen in S4-P and S16-D. Among all three locations, the lowest and the highest streambed temperatures were detected in S3-P due to the fact that stream water lost into the sediments significantly change the temperature (due to changes in air temperature). Effect of reservoir water release was identified and found to cause the most significant and abrupt temperature decreases and more fluctuations in S16-D.

S3-P displayed negative vertical water flux values indicating upward water movement in March 2015, this was because of the distance between piezometer locations and the ibutton installation locations. In general downward flow was defined in this location. S4-P consistently had negative values indicating upward water movement except dates between 9 and 12 September 2015. Generally, absolute vertical flux values in S4-P were higher with respect to S3-P for all measurement periods. S16-D was investigated as segments for March – April 2015 period to eliminate the noise. Positive values indicating downward water movement were calculated between dates 11 and 20 April 2015. Except these, all values are negative and upward water movement occurred in this period. Greatest flux values were calculated in July – August 2015 period ( $-1.36 \times 10^{-5}$  –  $3.08 \times 10^{-5}$  m/sec). For a very short time, downward movement was detected in this period. All vertical flux values were negative in September 2015 and they ranged between  $-1.29 \times 10^{-5}$  and  $-1.24 \times 10^{-6}$  m/sec in magnitude.

Using VHG and vertical flux values vertical hydraulic conductivity values (m/sec) were calculated for sites S3-P and S4-P. For all overlapping dates S3-P has higher  $K_v$  values than S4-P. Geometric means for S3-P change between  $3.30 \times 10^{-5}$  m/sec and



$1.63 \times 10^{-4}$  m/sec. For S4-P, they change between  $2.54 \times 10^{-5}$  m/sec and  $2.05 \times 10^{-4}$  m/sec.

### **Chloride Mass Balance**

Chloride mass balance was performed to find the source of excess water between monitoring locations. By chloride mass balance, it was found that S10-P-B which is groundwater discharge location affected the monitoring sites in the downstream of this location (according to mass balance between S6-P, S10-P-B, S12-D and S13-D). The lowest chloride concentration was measured in S10-P-B site and this influenced the chloride concentration in S13-D (having the second lowest concentration). The chloride concentration of excess water between sites S12-D, S13-D and S16-D was equal to the concentration of water in S13-D. This indicated that there was contribution of water having relatively less chloride concentration because this water was affected from groundwater in the upstream. Also, chloride mass balance between S16-D and S17-D showed that the chloride concentration of excess water between these locations have similar values with the upstream of the study area having losing character. This means that downwelling stream water in upstream reached the surface in between S16-D and S17-D.

### **Water Quality and Major Anion Indications**

Water quality field parameters were measured in all sites and major anion concentrations were analyzed in selected locations. The most significant indications of groundwater contribution were provided by temperature, electrical conductivity and dissolved oxygen measurements. The analysis of these parameters supported the losing/gaining reaches determined by VHG measurements. Trends in losing reach (S1-P, S2-P, S3-P), in mid-section (S4-P, S6-P, S7-P and S9-P) and in S10-P-B could be distinguished clearly. S10-P-B displayed almost constant temperature values throughout the year due to groundwater contribution. Both in summer and winter seasons, dissolved oxygen decreased toward downstream due to the contribution oxygen depleted groundwater. Trends of chloride and phosphate were

same and nitrate showed exactly the reverse trend. Chloride concentrations before S10-P-B were almost the same, with a sudden and significant decrease at and downstream of S10-P-B site. Nitrate displayed the highest values in S10-P-B possibly due to the effect of oxygen depleted groundwater effect.

Chloride concentrations of the study area were also compared with the concentrations of surrounding wells and fountains to search for possible link with the geology. It was found that chloride concentrations of locations upstream of S10-P-B and the site S12-D are close to values of shallow groundwater system interacted with volcanics (CEL52). In addition, S10-P-B showed similar values with the groundwater affected from sedimentary rocks of Lower Çavuşlar units in terms of well information. Note that the top section of exploration well CEL 40 which is one of the closest wells to the study area, cuts through Çavuşlar unit in the top 46 meters. In addition, fountains interacted with Upper Çavuşlar units have similar chloride concentrations with S10-P-B.

### **Recommendations**

Characterizing groundwater – stream interaction is a growing issue and this study will shed light on the future studies for understanding the interaction processes and ensuring an effective management of water resources in Turkey.

In addition to applied methods, automatic water level and temperature recorders (e.g. pressure transducer) can be placed inside the piezometers to obtain a continuous data. By this way, variation in temperatures can be observed easily and effect of groundwater can be detected at finer time scales. Also, continuous measurement of water levels provides more information about the losing and gaining character of that location. In addition, the effect of dam (e.g.release of reservoir water) can be observed easily.

Chemistry analysis can be improved by adding the isotope and major cation analyses. Especially, isotope analysis can give direct information about the source of groundwater feeding the stream.

In this study, different methods were combined to characterize groundwater stream interaction in Kirmir Stream. Variation in streambed elevation throughout the study area (high in upstream and low in downstream) was found to control gaining/losing character of the Kirmir Stream. Moreover, water seepage from the Doğanözü Dam could possibly effect the interaction process. Therefore, it is recommended that hyporheic flow conditions and seepage through dam should be investigated in more detail. Therefore, further application of environmental tracers and numerical modeling are possible future directions of research in the study area.



## REFERENCES

- Alexander, M. D., & MacQuarrie, K. T. B. (2005). The measurement of groundwater temperature in shallow piezometers and standpipes. *Canadian Geotechnical Journal*, 42(5), 1377–1390. <http://doi.org/10.1139/t05-061>
- Anderson, M. P. (2005). Heat as a Ground Water Tracer. *Groundwater*, 43(6), 951–968. <http://doi.org/10.1111/j.1745-6584.2005.00052.x>
- Asia Minor Mining. (2015). *Geology of Çeltikçi Project Area*.
- Becker, M. W., Georgian, T., Ambrose, H., Siniscalchi, J., & Fredrick, K. (2004). Estimating flow and flux of ground water discharge using water temperature and velocity. *Journal of Hydrology*, 296(1-4), 221–233. <http://doi.org/10.1016/j.jhydrol.2004.03.025>
- Bencala, K. E. (2000). Hyporheic zone hydrological processes. *Hydrological Processes*, 14, 2797–2798. [http://doi.org/10.1002/1099-1085\(20001030\)14:15<2797::AID-HYP402>3.0.CO;2-6](http://doi.org/10.1002/1099-1085(20001030)14:15<2797::AID-HYP402>3.0.CO;2-6)
- Boulton, A. J., Findlay, S., Marmonier, P., Stanley, E. H., & Valett, H. M. (1998). The functional significance of the hyporheic zone in streams and rivers. *Ann. Rev. Ecol. Syst.*, 29(1), 59–81. <http://doi.org/10.1146/annurev.ecolsys.29.1.59>
- Buss, S. R., Cai, Z., Cardenas, B., Fleckenstein, J., Hannah, D. M., Hepell, K., ... Wood, P. (2009). *The Hyporheic Handbook A handbook on the groundwater – surface water interface and hyporheic zone for environment managers Integrated catchment science programme Science report: SC050070 The Environment Agency is the leading public body protecting and im.*
- Candela, L., & Morell, I. (2009). Basic Chemical Principles of Groundwater. In *Encyclopedia of Life Support Systems* (Vol. II, pp. 43 – 55).
- Cartwright, I., Hofman, H., Sirianos, M., Weaver, T., & Simmons, C. (2011). Geochemical and <sup>222</sup>Rn constraints on baseflow to the Murray River, Australia, and timescales for the decay of low-salinity groundwater lenses. *Journal of Hydrology*, 405, 333 – 343.

- Conant, B. (2004). Delineating and Quantifying Groundwater Discharge Zones Using streambed temperatures. *Ground Water*, 42, 243 – 257.
- Constantz, J. (1998). Interaction between stream temperature, streamflow, and groundwater exchanges in alpine streams. *Water Resources Research*, 34(7), 1609. <http://doi.org/10.1029/98WR00998>
- Constantz, J., Cox, M. H., & Su, G. W. (2003). Comparison of Heat and Bromide as Ground Water Tracers Near Streams. *Geoscience Frontiers*, 41, 647 – 656.
- Cook, P. G. (2013). Estimating groundwater discharge to rivers from river chemistry surveys. *Hydrological Processes*, 27(25), 3694–3707. <http://doi.org/10.1002/hyp.9493>
- Cook, P. G., Favreau, G., Dighton, J. C., & Tickell, S. (2003). Determining natural groundwater influx to a tropical river using radon, chlorofluorocarbons and ionic environmental tracers. *Journal of Hydrology*, 277(1-2), 74–88. [http://doi.org/10.1016/S0022-1694\(03\)00087-8](http://doi.org/10.1016/S0022-1694(03)00087-8)
- Cranswick, R. H., Cook, P. G., & Lamontagne, S. (2014). Hyporheic zone exchange fluxes and residence times inferred from riverbed temperature and radon data. *Journal of Hydrology*, 519, 1870–1881. <http://doi.org/10.1016/j.jhydrol.2014.09.059>
- Dahm, C. N., & Valett, H. M. (1996). Hyporheic Zones. In *Methods in Stream Ecology* (pp. 107–119).
- Daniluk, T. L., Lautz, L. K., Gordon, R. P., & Endreny, T. A. (2013). Surface water-groundwater interaction at restored streams and associated reference reaches. *Hydrological Processes*, 27(25), 3730–3746. <http://doi.org/10.1002/hyp.9501>
- Duque, C., Muller, S., Sebok, E., Haider, K., & Engesgaard, P. (2015). Estimating groundwater discharge to surface waters using heat as a tracer in low flux environments: the role of thermal conductivity. *Hydrological Processes*, n/a–n/a. <http://doi.org/10.1002/hyp.10568>
- Ellins, K., Roman-Mas, A., & Lee, R. (1990). Using <sup>222</sup>Rn to examine groundwater/surface discharge interaction in the Rio Grande De Manati, Puerto Rico. *Journal of Hydrology*, 115, 319–341.
- Fan, Y., Toran, L., & Schlische, R. W. (2007). Groundwater flow and groundwater-stream interaction in fractured and dipping sedimentary rocks: Insights from numerical models. *Water Resources Research*, 43(1), 1–13. <http://doi.org/10.1029/2006WR004864>

- Fanelli, R. M., & Lautz, L. K. (2008). Patterns of water, heat, and solute flux through streambeds around small dams. *Ground Water*, 46(5), 671–687. <http://doi.org/10.1111/j.1745-6584.2008.00461.x>
- Fraser, B. G., & Williams, D. D. (1998). Seasonal Boundary Dynamics of a Groundwater/ Surface-Water Ecotone. *Ecology*, 79(6), 2019–2031. [http://doi.org/10.1890/0012-9658\(1998\)079\[2019:SBDOAG\]2.0.CO;2](http://doi.org/10.1890/0012-9658(1998)079[2019:SBDOAG]2.0.CO;2)
- Freeze, R. A., & Cherry, J. A. (1979). *Groundwater*. New Jersey.
- Gardner, W., Harrington, G., Solomon, D., & Cook, P. (2011). Using terrigenic 4He to identify and quantify regional groundwater discharge to streams. *Water Resources Research*, 47. <http://doi.org/10.1029/2010WR010276>.
- Gordon, R. P., Lautz, L. K., Briggs, M. a., & McKenzie, J. M. (2012). Automated calculation of vertical pore-water flux from field temperature time series using the VFLUX method and computer program. *Journal of Hydrology*, 420-421, 142–158. <http://doi.org/10.1016/j.jhydrol.2011.11.053>
- Goto, S., Yamano, M., & Kinoshita, M. (2005). Thermal response of sediment with vertical fluid flow to periodic temperature variation at the surface. *Journal of Geophysical Research B: Solid Earth*, 110(1), 1–11. <http://doi.org/10.1029/2004JB003419>
- Guggenmos, M. R., Daughney, C. J., Jackson, B. M., & Morgenstern, U. (2011). Regional-scale identification of groundwater-surface water interaction using hydrochemistry and multivariate statistical methods, Wairarapa Valley, New Zealand. *Hydrology and Earth System Sciences*, 15(11), 3383–3398. <http://doi.org/10.5194/hess-15-3383-2011>
- Harrington, G. A., Cook, P. G., & Herczeg, A. L. (2002). Spatial and Temporal Variability of GW Recharge\_A Tracer Approach.pdf. *Ground Water*, 40, 518–528.
- Harvey, J. W., & Bencala, K. E. (1993). The Effect of Streambed Topography on Surface-Subsurface Water Exchange in Mountain Catchments. *Water Resources Research*. <http://doi.org/10.1029/92WR01960>
- Hatch, C. E., Fisher, A. T., Revenaugh, J. S., Constantz, J., & Ruehl, C. (2006). Quantifying surface water-groundwater interactions using time series analysis of streambed thermal records: Method development. *Water Resources Research*, 42(10), n/a–n/a. <http://doi.org/10.1029/2005WR004787>
- Hatch, C. E., Fisher, A. T., Ruehl, C. R., & Stemler, G. (2010). Spatial and temporal

- variations in streambed hydraulic conductivity quantified with time-series thermal methods. *Journal of Hydrology*, 389(3-4), 276–288. <http://doi.org/10.1016/j.jhydrol.2010.05.046>
- Hester, E. T., Doyle, M. W., & Poole, G. C. (2009). The influence of in-stream structures on summer water temperatures via induced hyporheic exchange. *Limnology and Oceanography*, 54(1), 355–367. <http://doi.org/10.4319/lo.2009.54.1.0355>
- Johnson, A. N., Boer, B. R., Woessner, W. W., Stanford, J. A., Poole, G. C., Thomas, S. A., & O’Daniel, S. J. (2005). Evaluation of an inexpensive small-diameter temperature logger for documenting ground water-river interactions. *Ground Water Monitoring and Remediation*, 25(4), 68–74. <http://doi.org/10.1111/j.1745-6592.2005.00049.x>
- Johnson, T. C., Slater, L. D., Ntarlagiannis, D., Day-Lewis, F. D., & Elwaseif, M. (2012). Monitoring groundwater-surface water interaction using time-series and time-frequency analysis of transient three-dimensional electrical resistivity changes. *Water Resources Research*, 48(7), 1–13. <http://doi.org/10.1029/2012WR011893>
- Kalbus, E., Reinstorf, F., & Schirmer, M. (2006). Measuring methods for groundwater, surface water and their interactions: a review. *Hydrology and Earth System Sciences Discussions*, 3(4), 1809–1850. <http://doi.org/10.5194/hessd-3-1809-2006>
- Kerry, J., Binley, A., Crook, N., & Smith, J. W. N. (2007). Temporal and Spatial Variability of groundwater - surface water fluxes: Development and application of an analytical method using temperature time series. *Journal of Hydrology*, 336, 1 – 16.
- Kikuchi, C. P., Ferré, T. P. a., & Welker, J. M. (2012). Spatially telescoping measurements for improved characterization of ground water–surface water interactions. *Journal of Hydrology*, 446-447, 1–12. <http://doi.org/10.1016/j.jhydrol.2012.04.002>
- Kimball, B. A., Runkel, R. L., & Gerner, L. J. (2001). Quantification of mine-drainage inflows to Little Cottonwood Creek, Utah, using a tracer-injection and synoptic-sampling study. *Environmental Geology*, 40(11-12), 1390–1404. <http://doi.org/10.1007/s002540100320>
- Koçyiğit, A., Winchester, J. A., Bozkurt, E., & Holland, G. (2003). Saraçköy Volcanic Suite: implications for the subductional phase or arc evolution in the



- Galatian Arc Complex, Ankara, Turkey. *Geological Journal*, 38, 1–14.
- Krause, S., Tecklenburg, C., Munz, M., & Naden, E. (2013). Streambed nitrogen cycling beyond the hyporheic zone: Flow controls on horizontal patterns and depth distribution of nitrate and dissolved oxygen in the upwelling groundwater of a lowland river. *Journal of Geophysical Research: Biogeosciences*, 118(1), 54–67. <http://doi.org/10.1029/2012JG002122>
- Kumar, M., Ramanathan, A., & Keshari, A. K. (2009). Understanding the Extent of Interactions Between Groundwater and Surface Water through Major Ion Chemistry and Multivariate Statistical Techniques. *Hydrological Processes*, 23(October 2008), 297–310. <http://doi.org/10.1002/hyp>
- Kurylyk, B. L., Moore, R. D., & MacQuarrie, K. T. B. (2015). Scientific Briefing: Quantifying streambed heat advection due to groundwater-surface water interactions. *Hydrological Processes*, 4, n/a–n/a. <http://doi.org/10.1002/hyp.10709>
- Langston, G., Hayashi, M., & Roy, J. W. (2013). Quantifying groundwater-surface water interactions in a proglacial moraine using heat and solute tracers. *Water Resources Research*, 49(October 2012), 5411–5426. <http://doi.org/10.1002/wrcr.20372>
- Lapham, W. W. (1989). *Use of temperature profiles beneath streams to determine rates of vertical ground-water flow and vertical hydraulic conductivity*. US Geological Survey Water-Supply Paper. Retrieved from <http://agris.fao.org/agris-search/search/display.do?f=1991/US/US91293.xml;US9101682><http://www.csa.com/partners/viewrecord.php?requester=gs&collection=ENV&recid=9005554>
- Lautz, L. K. (2010). Impacts of nonideal field conditions on vertical water velocity estimates from streambed temperature time series. *Water Resources Research*, 46(W01509), 1–14. <http://doi.org/10.1029/2009WR007917>
- Lee, D. R. (1977). A device for measuring seepage flux in lakes and estuaries. *Limnology and Oceanography*, 22(1), 140–147. <http://doi.org/10.4319/lo.1977.22.1.0140>
- Lee, J.-Y., Lim, H., Yoon, H., & Park, Y. (2013). Stream Water and Groundwater Interaction Revealed by Temperature Monitoring in Agricultural Areas. *Water*, 5(4), 1677–1698. <http://doi.org/10.3390/w5041677>
- Liu, W., Field, R. T., Gantt, R. G., & Klemas, V. (1987). Measurement of the Sea Surface Emissivity of Turbid Waters. *Chinese Journal of Oceanography and*

- Limnology*, 5, 363 – 369. <http://doi.org/10.1007/BF02233853>
- McCallum, J. L., Cook, P. G., Berhane, D., Rumpf, C., & McMahon, G. a. (2012). Quantifying groundwater flows to streams using differential flow gaugings and water chemistry. *Journal of Hydrology*, 416-417, 118–132. <http://doi.org/10.1016/j.jhydrol.2011.11.040>
- Menció, A., & Mas-Pla, J. (2008). Assessment by multivariate analysis of groundwater-surface water interactions in urbanized Mediterranean streams. *Journal of Hydrology*, 352, 355–366. <http://doi.org/10.1016/j.jhydrol.2008.01.014>
- Meredith, K. T., Hollins, S. E., Hughes, C. E., Cendon, D. I., Hankin, S., & Stone, D. J. M. (2009). Temporal variation in stable isotopes (O-18 and H-2) and major ion concentrations within the Darling River between Bourke and Wilcannia due to variable flows, saline groundwater influx and evaporation. *Journal of Hydrology*, 378, 313 – 324.
- Meybeck, M. (2003). Chemical characteristics of rivers. *Fresh Surface Water*, I(iii).
- Michel, R. L. (1992). Residence times in river basins as determined by analysis of long-term tritium records. *North*, 130, 367–378.
- Mullinger, N., Binley, A., Pates, J., & Crook, N. (2007). Radon in Chalk streams: spatial and temporal variation of groundwater sources in the Pang and Lambourn catchments, UK. *Journal of Hydrology*, 339, 172–182.
- Négrel, P., Petelet-Giraud, E., Barbier, J., & Gautier, E. (2003). Surface water–groundwater interactions in an alluvial plain: Chemical and isotopic systematics. *Journal of Hydrology*, 277(3-4), 248–267. [http://doi.org/10.1016/S0022-1694\(03\)00125-2](http://doi.org/10.1016/S0022-1694(03)00125-2)
- Nikanorov, A. M., Brazhnikova, L. V., & Sketchev, B. (2009). Water Chemical Composition of Rivers, Lakes and Wetlands, II(1), 1–11.
- Öngür, T. (1977). Volcanologic and petrologic study of the SW of Kızılcahamam. *Bulletin of Geological Society of Turkey*, 20(August), 1–12.
- Peterson, R., Santos, I., & Burnett, W. (2010). Evaluating groundwater discharge to tidal rivers based on a Rn-222 time-series approach. *Estuaries, Coastal and Shelf Science*, 86, 165–178.
- Prakash, a. (2000). Thermal remote sensing: concepts, issues and applications. ... *Archives of Photogrammetry and Remote Sensing*, XXXIII, 239–243. Retrieved from [http://www.isprs.org/proceedings/XXXIII/congress/part1/239\\_XXXIII-](http://www.isprs.org/proceedings/XXXIII/congress/part1/239_XXXIII-)

part1.pdf

- Rojay, B. (2013). *Structural Evolution of Çeltikçi-Gümele Area During post-Miocene*.
- Rosenberry, D. O., & Labaugh, J. W. (2008). *Field Techniques for Estimating Water Fluxes Between Surface Water and Ground Water Techniques and Methods 4 – D2*.
- Rosenberry, D. O., Labaugh, J. W., & Hunt, R. J. (2008). *Use of Monitoring Wells , Portable Piezometers , and Seepage Meters to Quantify Flow Between Surface Water and Ground Water*. Retrieved from <http://pubs.usgs.gov/tm/04d02/>
- Schmidt, C., Bayer-Raich, M., & Schirmer, M. (2006). Characterization of spatial heterogeneity of groundwater-stream water interactions using multiple depth streambed temperature measurements at the reach scale. *Hydrology and Earth System Sciences Discussions*, 3, 1419–1446. <http://doi.org/10.5194/hessd-3-1419-2006>
- Sklash, M. G., & Farvolden, R. N. (1979). The Role of Groundwater in Storm Runoff. *Journal of Hydrology*, 65(April 1979), 45–65.
- Smith, A., Pollock, D., & Palmer, D. (2010). Groundwater interaction with surface drains in the Ord River Irrigation Area, northern Australia: investigation by multiple methods. *Hydrogeology Journal*, 18, 1235–1252.
- Sophocleous, M. (2002). Interactions between groundwater and surface water: the state of the science. *Hydrogeology Journal*, 10(1), 52–67. <http://doi.org/10.1007/s10040-001-0170-8>
- Soulsby, C., Tetzlaff, D., van den Bedem, N., Malcolm, I. A., Bacon, P. J., & Youngson, A. F. (2007). Inferring groundwater influences on surface water in montane catchments from hydrochemical surveys of springs and streamwaters. *Journal of Hydrology*, 333(2-4), 199–213. <http://doi.org/10.1016/j.jhydrol.2006.08.016>
- Stallman, R. W. (1963). Methods of collecting and interpreting ground-water data. *U.S. Geological Survey Water-Supply Paper*, 36 – 46.
- Stallman, R. W. (1965). Steady One-Dimensional Fluid Flow in a Semi-Infinite Porous Medium with Sinusoidal Surface Temperature. *Journal of Geophysical Research*, 70, 2821 – 2827.
- Stonestrom, D. a., & Constantz, J. (2003). *Heat as a Tool for Studying the Movement of Ground Water Near Streams - Circular 1260*. U.S. Geological Survey

*Circular*. Retrieved from <http://pubs.water.usgs.gov/circ1260/>

- Suzuki, S. (1960). Percolation measurements based on heat flow through soil with special reference to paddy fields. *Journal of Geophysical Research*, 65(9), 2821–2827. <http://doi.org/10.1029/JZ065i009p02883>
- Toprak, V., Savaşçın, Y., Güleç, N., & Tankut, A. (1996). Structure of the Galatian volcanic province. *Int. Geology Review*, 38, 747–758.
- Tóth, J. (1963). A theoretical analysis of groundwater flow in small drainage basins. *Journal of Geophysical Research*, 68(16), 4795–4812. <http://doi.org/10.1029/JZ068i016p04795>
- Türkecan, A., Hepşen, N., Papak, İ., Akbaş, B., Dinçel, A., Karataş, S., ... Saraç, G. (1991). *Seben-Gerede (Bolu)- Gündül- Beypazarı (Ankara) ve Çerkeş- Orta-Kurşunlu (Çankırı) yörelerinin (Köroğlu Dağları) jeolojisi ve volkanik kayaların petrolojisi*, MTA Report no. 9193.
- Unland, N. P., Cartwright, I., Andersen, M. S., Rau, G. C., Reed, J., Gilfedder, B. S., ... Hofmann, H. (2013). Investigating the spatio-temporal variability in groundwater and surface water interactions: a multi-technique approach. *Hydrology and Earth System Sciences*, 17(9), 3437–3453. <http://doi.org/10.5194/hess-17-3437-2013>
- Valett, H. M., Hakenkamp, C. C., & Boulton, A. J. (1993). Perspectives on the Hyporheic Zone : Integrating Hydrology and Biology . Introduction Published by : The North American Benthological Society Perspectives on the hyporheic zone : integrating hydrology and biology . Introduction. *Journal of the North American Benthological Society*, 12(1), 94–99.
- Vogt, T., Hoehn, E., Schneider, P., Freund, A., Schirmer, M., & Cirpka, O. A. (2010). Fluctuations of electrical conductivity as a natural tracer for bank filtration in a losing stream. *Advances in Water Resources*, 33(11), 1296–1308. <http://doi.org/10.1016/j.advwatres.2010.02.007>
- Wagner, B. J., & Harvey, J. W. (1997). Experimental design for estimating parameters of rate-limited mass transfer: Analysis of stream tracer studies. *Water Resources Research*, 33(7), 1731. <http://doi.org/10.1029/97WR01067>
- Winter, T. C. (1983). The interaction of lakes with variably saturated porous media. *Water Resources Research*, 19(5), 1203. <http://doi.org/10.1029/WR019i005p01203>
- Winter, T. C. (1999). Relation of streams, lakes, and wetlands to groundwater flow

- systems. *Hydrogeology Journal*, 7(1), 28–45.  
<http://doi.org/10.1007/s100400050178>
- Winter, T. C., Harvey, J. W., Franke, O. L., & Alley, W. M. (1998). Ground Water and Surface Water A Single Resource U . S . Geological Survey Circular 1139.
- Woessner, W. W. (2000). Stream and fluvial plain ground water interactions: Rescaling hydrogeologic thought. *Groundwater*. <http://doi.org/10.1111/j.1745-6584.2000.tb00228.x>
- Woocay, A., & Walton, J. (2008). Multivariate analyses of water chemistry: surface and ground water interactions. *Ground Water*, 46(3), 437–49.  
<http://doi.org/10.1111/j.1745-6584.2007.00404.x>
- Wu, Y., Wen, X., & Zhang, Y. (2004). Analysis of the exchange of groundwater and river water by using Radon-222 in the middle Heihe Basin of northwestern China. *Environmental Geology*, (43), 647–653.
- Yang, L., Song, X., Zhang, Y., Han, D., Zhang, B., & Long, D. (2012). Characterizing interactions between surface water and groundwater in the Jialu River basin using major ion chemistry and stable isotopes. *Hydrology and Earth System Sciences*, 16(11), 4265–4277. <http://doi.org/10.5194/hess-16-4265-2012>
- Yazıcıgil, H., Çamur, Z., Süzen, M. L., Yılmaz, K. K., Peksezer Sayıt, A., & Kahraman, C. (2014). *Çeltikçi Kömür Havzasının Hidrojeolojik Etüdü ve Karakterizasyonu*.
- Yazıcıgil, H., Çamur, Z., Yılmaz, K. K., Peksezer Sayıt, A., & Kahraman, C. (2015). *Çeltikçi Kömür Havzasının Yeraltı Sularının Akım Modelinin Geliştirilmesi, Susuzlaştırma Tasarımının Yapılması ve Yeraltı Sularına Olası Etkilerin Değerlendirilmesi*. Ankara.
- Young, P. C., Pedregal, D. J., & Tych, W. (1999). DYNAMIC HARMONIC REGRESSION. *Journal of Forecasting*, 369–394.
- Younger, P. L. (2007). *Groundwater in the Environment: an introduction*. [http://doi.org/10.1007/978-0-387-84891-4\\_3](http://doi.org/10.1007/978-0-387-84891-4_3)